

2012

Free Troposphere Ozone and Carbon Monoxide over the North Atlantic for 2001-2011

Aditya Kumar
Michigan Technological University

Follow this and additional works at: <https://digitalcommons.mtu.edu/etds>


 Part of the [Environmental Engineering Commons](#)

Copyright 2012 Aditya Kumar

Recommended Citation

Kumar, Aditya, "Free Troposphere Ozone and Carbon Monoxide over the North Atlantic for 2001-2011",
Master's Thesis, Michigan Technological University, 2012.
<https://doi.org/10.37099/mtu.dc.etds/464>

Follow this and additional works at: <https://digitalcommons.mtu.edu/etds>

 Part of the [Environmental Engineering Commons](#)

**FREE TROPOSPHERE OZONE & CARBON
MONOXIDE OVER THE NORTH ATLANTIC
FOR 2001-2011**

By

Aditya Kumar

A THESIS

Submitted in partial fulfillment of the requirements for the degree of

MASTER OF SCIENCE

In Environmental Engineering

MICHIGAN TECHNOLOGICAL UNIVERSITY

2012

© 2012 Aditya Kumar

This thesis has been approved in partial fulfillment of the requirements for the Degree of
MASTER OF SCIENCE in Environmental Engineering

Department of Civil and Environmental Engineering

Signatures:

Thesis advisor: Dr. Shiliang Wu

Committee Member: Dr. Chris Owen

Committee Member: Dr. Louisa Kramer

Department Chair: Dr. David Hand

To my father, mother, brother

and

dog Rido (who is no more)

Table of Contents

List of Figures	vii
List of Tables	xii
Acknowledgements	xvii
Definitions	xviii
List of Abbreviations/Symbols	xx
Abstract	xxi
Chapter 1: Introduction	1
1.1. Atmospheric Chemistry of Carbon Monoxide and Ozone: The Role of Nitrogen Oxides	1
1.2. Inter-Continental Transport of Pollutants	3
1.3. Transport of Pollution into and out of North America	6
1.3.1. Major Pathways of Pollution Outflow from NA	7
1.3.2. Major Pathways of Pollution Inflow into NA	7
1.4. ICT of Carbon Monoxide and Ozone to/from North America	8
1.5. Motivation of this Study	9
Chapter 2: The PICO-NARE Observatory	12
2.1. Introduction	12
2.2. Importance of the Site relative to Pollution Outflow from North America	13
2.3. PICO-NARE Observations	15
Chapter 3: The GEOS-Chem Model of Atmospheric Chemistry and Composition	19
3.1. Model Description	19
3.2. GEOS-Chem NO _x -O _x -Hydrocarbon-Aerosol (a.k.a “Full Chemistry”) Simulation ..	24
3.2.1. Full Chemistry Simulation with Normal Emissions	25

3.2.2. Full Chemistry Simulation with Fixed Anthropogenic Emissions	25
3.3. Tagged CO Simulation	26
Chapter 4: Trend Analysis	31
4.1. Introduction	31
4.2. Hypothesis Testing.....	31
4.2.1. Introduction.....	31
4.2.2. Procedure for a Hypothesis Test.....	32
4.3. Regression Analysis.....	36
4.4. Non-Parametric & Parametric Tests Used in this Study.....	37
4.4.1. The Non-Parametric Mann-Kendall test.....	37
4.4.2. Time Series Analysis	47
4.4.3. Smoothing schemes applied.....	48
4.4.4. Regression Analysis.....	55
Chapter 5: Results & Discussion	58
5.1. Mann-Kendall's test.....	58
5.1.1. Application to the Daily Average Observations for PICO-NARE	58
5.1.2. Application of the Exact and Approximate Mann-Kendall Tests to the Derived Datasets	59
5.1.3. Application of the Seasonal Mann-Kendall Test.....	62
5.2. Evaluation of the 5 Day CSMA Scheme	64
5.3. Analysis of PICO-NARE Observations & GEOS-Chem Full Chemistry (with Normal Emissions) Simulation Output using the Regression Model	77
5.3.1. Regression fit to the PICO-NARE observations.....	77
5.3.2. Regression Fit to GEOS-Chem Output from the Full Chemistry Simulation with Normal Emissions.....	80

5.4. Results from Regression Analysis of the Output from GEOS-Chem Full Chemistry Simulation (with Fixed Anthropogenic Emissions).....	83
5.4.1. Trends for CO and O ₃ at PICO-NARE.....	83
5.5. Regression Analysis of output from the GEOS-Chem Tagged CO Simulation	86
5.6. Interpretation of the Trends in CO.....	93
5.6.1. Trends in Global Biogenic Emissions of VOCs	93
5.6.2. Trends in Biogenic Emissions from North America	96
5.7. Interpretation of the Trends in O ₃	99
5.7.1. Trends in Global Lightning Flashes	99
5.7.2. Trends in Global Lightning NO _x	102
5.7.3. Trends in Lightning Flashes in the Region from North America to PICO-NARE.....	105
5.7.4. Trends in Lightning NO _x in the Region from North America to PICO-NARE.....	107
5.7.5. Trends in Global NO _x from Biomass Burning	109
5.7.6. Trends in NO _x from Biomass Burning in North America	111
5.7.7. Trends in NO _x from Soils	113
5.7.8. Trends in Soil NO _x from North America.....	115
5.7.9. Trends in Humidity for the Domain Extending from North America to PICO-NARE.....	117
5.7.10. Possible reasons for the trends of O ₃ at PICO-NARE.....	122
Chapter 6: Conclusions	123
References.....	127

List of Figures

Figure 1.1: US anthropogenic emissions (in Tg/yr) for CO and NO _x from 2000 to 2011.....	10
Figure 2.1: CO produced from fossil fuel combustion in USA for June and July 2004.....	14
Figure 2.2: CO produced from fossil fuel combustion in Europe for June and July 2004.....	14
Figure 3.1: Flowchart representing the working of GEOS-Chem	20
Figure 3.2: Schematic representation of the tagged CO simulation in GEOS-Chem.....	29
Figure 3.3: Flowchart of this study.....	30
Figure 4.1: Steps of Hypothesis testing	35
Figure 4.2: Flowchart for the Exact Mann-Kendall test	40
Figure 4.3: Flowchart for the Approximate Mann-Kendall test	42
Figure 4.4: Flowchart of the Seasonal Mann-Kendall test	44
Figure 5.1: Regression model & observations V/s time for CO with no smoothing.....	66
Figure 5.2: Regression model & observations V/s time for CO with 5 day SMA scheme.....	66
Figure 5.3: Regression model & observations V/s time for CO with 10 day SMA scheme.....	67
Figure 5.4: Regression model & observations V/s time for CO with 15 day SMA scheme.....	67

Figure 5.5: Regression model & observations V/s time for CO with 5 day CSMA scheme.....	68
Figure 5.6: Regression model & observations V/s time for CO with 10 day CSMA scheme.....	68
Figure 5.7: Regression model & observations V/s time for CO with 15 day CSMA scheme.....	69
Figure 5.8: Regression model & observations V/s time for CO with 5 day CM scheme.....	69
Figure 5.9: Regression model & observations V/s time for CO with 10 day CM scheme.....	70
Figure 5.10: Regression model & observations V/s time for CO with 15 day CM scheme.....	70
Figure 5.11: Regression model & observations V/s time for O ₃ with no smoothing	71
Figure 5.12: Regression model & observations V/s time for O ₃ with 5 day SMA scheme.....	71
Figure 5.13: Regression model & observations V/st for O ₃ with 10 day SMA scheme.....	72
Figure 5.14: Regression model & observations V/s time for O ₃ with 15 day SMA scheme.....	72
Figure 5.15: Regression model & observations V/s time for O ₃ with 5 day CSMA scheme.....	73
Figure 5.16: Regression model & observations V/s time for O ₃ with 10 day CSMA scheme	73

Figure 5.17: Regression model & observations V/s time for O ₃ with 15 day CSMA scheme	74
Figure 5.18: Regression model & observations V/s time for O ₃ with 5 day CM scheme.....	74
Figure 5.19: Regression model & observations V/s time for O ₃ with 10 day CM scheme.....	75
Figure 5.20: Regression model & observations V/s time for O ₃ with 15 day CM scheme.....	75
Figure 5.21: Regression model fit to the Pico observations for CO (2001-2010)	78
Figure 5.22: Regression model fit to the Pico observations for O ₃ (2001-2011)	79
Figure 5.23: Regression model fit to the GEOS-Chem output (from full chemistry simulation with normal emissions) for CO (2001-2010).....	81
Figure 5.24: Regression model fit to the GEOS-Chem output (from full chemistry simulation with normal emissions) for O ₃ (2001-2011)	82
Figure 5.25: Regression model fit to CO (2001-2010) at Pico for full chemistry simulation with fixed anthropogenic emissions.....	85
Figure 5.26: Regression model fit to O ₃ (2001-2011) at Pico for full chemistry simulation with fixed anthropogenic emissions.....	85
Figure 5.27: Regression fit for CO at Pico from anthropogenic (fossil fuel) emissions in USA.....	89
Figure 5.28: Regression fit for CO at Pico from anthropogenic (fossil fuel) emissions in Asia	89
Figure 5.29: Regression fit for CO at Pico due to global Methane oxidation	90

Figure 5.30: Regression fit for CO at Pico due to global biofuel emissions	90
Figure 5.31: CO emissions from biofuels in January 2001	91
Figure 5.32: CO emissions from biofuels in April 2001	91
Figure 5.33: CO concentrations due to global biofuel emissions for January and February 2001	92
Figure 5.34: CO concentrations due to global biofuel emissions for March and April 2001	92
Figure 5.35: Domain including North America	97
Figure 5.36: Regression fit for global monthly means of total lightning flashes (2001-2011).....	101
Figure 5.37: Regression fit for global monthly means of cloud to ground (CG) lightning flashes (2001-2011)	102
Figure 5.38: Regression fit to the monthly means of global NO _x from lightning for 2001-2011	104
Figure 5.39: Domain extending from North America to PICO-NARE	106
Figure 5.40: Regression fit for global NO _x from biomass burning for 2001-2011.....	111
Figure 5.41: Regression fit to the monthly means of global NO _x emissions from soils for 2001-2011	115
Figure 5.42: Specific Humidity over the region extending from North America to PICO-NARE (averaged over 38°N -42°N latitude).....	120
Figure 5.43: Specific Humidity over the region extending from North America to PICO-NARE (averaged over 30°N-50°N).....	120

Figure 5.44: Specific Humidity over the region extending from North America to PICO-NARE for the summer (June-August) (averaged over 38°N-42°N)..... 121

Figure 5.45: Specific Humidity over the region extending from North America to PICO-NARE for the summer (June-August) (averaged over 30°N-50°N)..... 121

List of Tables

Table 2.1: Hourly distribution of PICO-NARE observations for CO and O ₃	16
Table 2.2: Data availability (Number of days in each month) for CO (2001-2010)	17
Table 2.3: Data availability (Number of days in each month) for O ₃ (2001-2011).....	17
Table 2.4: Monthly Mean Matrix for CO (in ppbv) (2001-2010).....	18
Table 2.5: Monthly Mean Matrix for O ₃ (in ppbv) (2001-2011).....	18
Table 3.1: List of emission inventories used in GEOS-Chem	22
Table 3.2: Tracer list for the tagged CO simulation	28
Table 4.1: Derived data sets used for performing the Mann-Kendall test	46
Table 4.2: MSE values obtained for different smoothing schemes	54
Table 5.1: Mann-Kendall test results for PICO-NARE daily average data	59
Table 5.2: Exact & approximate Mann-Kendall test results for derived datasets	60
Table 5.3: Seasons defined for the Seasonal Mann-Kendall test.....	63
Table 5.4: Seasonal Mann-Kendall test results.....	64
Table 5.5: Statistics for the regression model fit to observations for CO at PICO- NARE (2001-2010).....	76
Table 5.6: Statistics for the regression model fit to observations for O ₃ at PICO- NARE (2001-2010).....	76
Table 5.7: Statistics for the regression fit to the Pico observations for CO (2001- 2010) and O ₃ (2001-2011)	79
Table 5.8: Trends obtained for CO (2001-2010) and O ₃ (2001-2011) from observations at Pico.....	79

Table 5.9: Statistics for the regression fit to the GEOS-Chem output (full chemistry with normal emissions) for CO (2001-2010) and O ₃ (2001-2011)	81
Table 5.10: Trends obtained for CO (2001-2010) and O ₃ (2001-2011) from the GEOS-Chem output (full chemistry with normal emissions).....	81
Table 5.11: Regression statistics for CO and O ₃ at Pico for full chemistry simulation with fixed anthropogenic emissions.....	84
Table 5.12: Trends for CO and O ₃ at Pico for full chemistry simulation with fixed anthropogenic emissions	84
Table 5.13: Regression statistics for the fit to CO concentrations (from various sources) at Pico (2001-2010)	88
Table 5.14: Trends obtained for CO (from different sources) at Pico (2001-2010).....	88
Table 5.15: Biogenic VOCs incorporated in GEOS-Chem	95
Table 5.16 : Global annual total biogenic emissions	95
Table 5.17: Regression statistics for the monthly mean biogenic emissions (total) of VOCs (2001-2011)	95
Table 5.18: Trends obtained for monthly mean biogenic emissions (total) (2001-2011)	95
Table 5.19: Annual totals of biogenic emissions in North America (2001-2010).....	97
Table 5.20: Regression statistics for the monthly mean biogenic emissions (total) of VOCs in North America (2001-2011)	98
Table 5.21: Trends obtained for monthly mean biogenic emissions (total) of VOCs in North America (2001-2011).....	98

Table 5.22: Global annual totals of lightning flashes (2001-2010)	100
Table 5.23: Regression statistics for the fit to the monthly means of global lightning flashes (2001-2011)	101
Table 5.24: Trends obtained for the monthly means of global lightning flashes (2001-2011).....	101
Table 5.25: Global annual totals of NO _x emissions from lightning from 2001-2010.....	103
Table 5.26: Regression statistics for the fit to the monthly means of global NO _x from lightning for 2001-2011.....	104
Table 5.27: Trends obtained for the monthly means of global NO _x from lightning for 2001-2011	104
Table 5.28: Annual totals of lightning flashes (2001-2010) over the domain extending from North America to PICO-NARE.....	106
Table 5.29: Regression statistics for the fit to the monthly means of lightning flashes (2001-2011) over the region from North America to PICO- NARE.....	107
Table 5.30: Trends obtained for the monthly means of lightning flashes (2001- 2011) over the region from North America to PICO-NARE.....	107
Table 5.31: Annual totals of NO _x from lightning (2001-2010) for the domain extending from North America to PICO-NARE.....	108
Table 5.32: Regression statistics for the fit to the monthly means of NO _x from lightning (2001-2011) for the domain extending from North America to PICO-NARE	108

Table 5.33: Trend obtained for the monthly means of NO _x from lightning (2001-2011) for the domain extending from North America to PICO-NARE.....	108
Table 5.34: Global annual totals of NO _x from biomass burning from 2001-2010	110
Table 5.35: Regression statistics for the fit to the monthly means of global NO _x from biomass burning for 2001-2011	110
Table 5.36: Trend obtained for the monthly means of global NO _x from biomass burning for 2001-2011	110
Table 5.37: Annual totals of NO _x from biomass burning in North America from 2001-2010	112
Table 5.38: Regression statistics for the fit to the monthly means of NO _x from biomass burning in North America from 2001-2011	112
Table 5.39: Trend obtained for monthly mean NO _x from biomass burning in North America from 2001-2011.....	112
Table 5.40: Global annual totals of NO _x emissions from soils for 2001-2010.....	114
Table 5.41: Regression statistics for the fit to the monthly means of global NO _x emissions from soils for 2001-2011	114
Table 5.42: Trend obtained for the monthly means of global NO _x emissions from soils for 2001-2011	114
Table 5.43: Annual totals of NO _x emissions from soils for North America from 2001-2010	116
Table 5.44: Regression statistics for the fit to the monthly means of NO _x emissions from soils in North America for 2001-2011.....	117

Table 5.45: Trend obtained for the monthly means of NO_x emissions from soils in
North America for 2001-2011..... 117

Acknowledgements

I would like to thank my advisor Dr. Shiliang Wu for his support and guidance throughout this work. Working with him over the past one and a half years has been a great experience. I would also like to thank Dr. Chris Owen and Dr. Louisa Kramer for agreeing to be a part of the MS defense committee and providing valuable feedback which has aided in improving this document significantly. The help of Dr. Detlev Helmig (University of Colorado, Boulder) with the statistical part of this work and Ms. Pei Hou in preparing the specific humidity plots is greatly appreciated. I also acknowledge the contribution of faculty members and research group members at Michigan Tech and friends in Houghton.

Definitions

- Airstream.** An airstream is essentially an air mass moving away from its place of origin in a coherent flow, with chemical and meteorological characteristics imparted on it by both the place of origin and the subsequent transport processes [*Cooper et al.*, 2001].
- Cyclone.** A cyclone is a weather system characterized by a low pressure center as compared to the surrounding air. Movement of air is counter-clockwise around the center in the Northern Hemisphere (clockwise in the Southern Hemisphere). The movement results in clouds and precipitation.
- Jet Streams.** Jet Streams are fast flowing, narrow air currents found near the tropopause in the earth's atmosphere.
- Mid-Lat Cyclones.** Mid-lat cyclones are also known as extra-tropical cyclones. They are found in the middle latitudes and are connected with weather fronts. They drive the weather over most of the earth and produce cloudiness as well as thunderstorms.
- Normal emissions.** Normal emissions imply that the emissions used in the simulation for a particular year represent the real emissions for that year as closely as possible.

- Offline simulation.** An offline simulation uses previously archived data for certain species (e.g. OH radical concentrations) while performing chemistry. It does not use the chemistry solvers.
- Online simulation.** An online simulation would perform concentration calculations for each species at every chemistry time-step using the chemistry solvers.
- Pearson's r.** Pearson's r provides a measure of the correlation between two variables. It can take values between -1 and 1.
- R-squared.** R-squared is known as the coefficient of determination and commonly denoted as R^2 . It is a standard measure of the closeness of the data points to the regression curve and takes values between 0 and 1.
- Weather Front.** A weather front is a boundary separating two masses of air of different densities. The air masses generally differ in temperature and humidity.
- WCBs.** WCBs are airstreams of mid latitude cyclones that can rise from the atmospheric boundary layer to the upper troposphere [Eckhardt *et al.*, 2004].

List of Abbreviations/Symbols

α	Significance Level
BUF	Buoyant Upslope Flows
CCB	Cold Conveyor Belt
CH ₄	Methane
CO	Carbon Monoxide
CO ₂	Carbon Dioxide
CM	Centered Median scheme
CSMA	Centered Simple Moving Average scheme
DA	Dry Airstream
FT	Free Troposphere
h ν	Energy of photons from sunlight
H	Hydrogen atom
HO ₂	Peroxy radical
H ₂ O ₂	Hydrogen Peroxide
ICT	Inter-Continental Transport
M	Species such as Nitrogen or Oxygen present in air
MFU	Mechanically Forced Upslope Flows
NA	North America
NMVOCs	Non Methane Volatile Organic Compounds
NO	Nitrogen Monoxide
NO ₂	Nitrogen Dioxide
NO _x	Family species of NO and NO ₂
O	Oxygen atom
O(¹ D)	Oxygen atom in excited state
O ₂	Oxygen
O ₃	Ozone
OH	Hydroxyl radical
PAN	Peroxyacyl Nitrate
PCFA	Post Cold Front Airstream
SMA	Simple Moving Average scheme
U.S. EPA	United States Environmental Protection Agency
VOCs	Volatile Organic Compounds
WCB	Warm Conveyor Belt

Abstract

Carbon Monoxide (CO) and Ozone (O₃) are considered to be one of the most important atmospheric pollutants in the troposphere with both having significant effects on human health. Both are included in the U.S. E.P.A list of criteria pollutants. CO is primarily emitted in the source region whereas O₃ can be formed near the source, during transport of the pollution plumes containing O₃ precursors or in a receptor region as the plumes subside. The long chemical lifetimes of both CO and O₃ enable them to be transported over long distances. This transport is important on continental scales as well, commonly referred to as inter-continental transport and affects the concentrations of both CO and O₃ in downwind receptor regions, thereby having significant implications for their air quality standards. Over the period 2001-2011, there have been decreases in the anthropogenic emissions of CO and NO_x in North America and Europe whereas the emissions over Asia have increased. How these emission trends have affected concentrations at remote sites located downwind of these continents is an important question. The PICO-NARE observatory located on the Pico Mountain in Azores, Portugal is frequently impacted by North American pollution outflow (both anthropogenic and biomass burning) and is a unique site to investigate long range transport from North America. This study uses in-situ observations of CO and O₃ for the period 2001-2011 at PICO-NARE coupled with output from the full chemistry (with normal and fixed anthropogenic emissions) and tagged CO simulations in GEOS-Chem, a global 3-D chemical transport model of atmospheric composition driven by meteorological input from the Goddard Earth Observing System (GEOS) of the NASA

Global Modeling and Assimilation Office, to determine and interpret the trends in CO and O₃ concentrations over the past decade. These trends would be useful in ascertaining the impacts emission reductions in the United States have had over Pico and in general over the North Atlantic. A regression model with sinusoidal functions and a linear trend term was fit to the in-situ observations and the GEOS-Chem output for CO and O₃ at Pico respectively. The regression model yielded decreasing trends for CO and O₃ with the observations (-0.314 ppbv/year & -0.208 ppbv/year respectively) and the full chemistry simulation with normal emissions (-0.343 ppbv/year & -0.526 ppbv/year respectively). Based on analysis of the results from the full chemistry simulation with fixed anthropogenic emissions and the tagged CO simulation it was concluded that the decreasing trends in CO were a consequence of the anthropogenic emission changes in regions such as USA and Asia. The emission reductions in USA are countered by Asian increases but the former have a greater impact resulting in decreasing trends for CO at PICO-NARE. For O₃ however, it is the increase in water vapor content (which increases O₃ destruction) along the pathways of transport from North America to PICO-NARE as well as around the site that has resulted in decreasing trends over this period. This decrease is offset by increase in O₃ concentrations due to anthropogenic influence which could be due to increasing Asian emissions of O₃ precursors as these emissions have decreased over the US. However, the anthropogenic influence does not change the final direction of the trend. It can thus be concluded that CO and O₃ concentrations at PICO-NARE have decreased over 2001-2011.

Chapter 1 : Introduction

1.1. Atmospheric Chemistry of Carbon Monoxide and Ozone: The Role of Nitrogen Oxides

Carbon Monoxide (CO) and Ozone (O₃) are considered to be one of the most important atmospheric pollutants in the troposphere. CO once inhaled by human beings can reduce the oxygen (O₂) supply to the body organs whereas even low levels of O₃ are known to cause respiratory problems. Hence, both can be found in the U.S. E.P.A criteria pollutants list alongside Nitrogen Dioxide (NO₂), Particulate Matter (PM), Sulfur Dioxide (SO₂) & Lead (Pb). CO is emitted into the atmosphere as a result of incomplete combustion with the predominant sources being fossil fuels and biomass burning. It is also formed due to the oxidation of Methane (CH₄) by the Hydroxyl (OH) radical as well as by the oxidation of Non-Methane Volatile Hydrocarbons (NMVOCs). O₃ on the other hand, is not emitted directly into the atmosphere but is formed as a result of chemical reactions/transformations of species commonly referred to as “Ozone Precursors”. In the troposphere, Volatile Organic Compounds (VOCs) and NO_x are the precursors undergoing a series of reactions resulting in the formation of O₃. These reactions are part of a complex reaction chain which is triggered once the precursors are emitted into the atmosphere and favorable conditions (e.g. presence of sunlight) exist. The most significant reaction to which O₃ formation in the troposphere can be attributed is reaction (1.2) in the following chain:

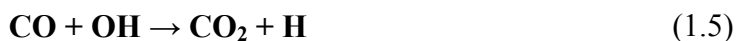




In addition, oxidation of CO by Hydroxyl (OH) radicals is another pathway which leads to the formation of O₃ in the presence of NO_x. OH radicals are themselves produced by the photolysis of O₃ in the presence of water vapor by the following reactions`:



The oxidation of CO by OH radicals can be represented by the following reactions:



The NO₂ formed initiates reactions (1.1)-(1.2) resulting in the formation of O₃. Thus, combining reactions (1.5-1.7) with (1.1 & 1.2) would provide the following net O₃ formation reaction:



Reaction (1.7) can also proceed with similar peroxy radicals that are formed due to the oxidation of more complex hydrocarbons. For example, oxidation of CH₄ results in the formation of Methoxy (CH₃O₂) radical which could react with NO_x to form NO₂. As can be seen, the presence of NO_x is essential for reaction (1.7) to occur. Thus, it is the

presence of NO_x which determines whether the HO₂ radical formed leads to O₃ formation or not. In the absence of NO_x, HO₂ can be destroyed by the pathways listed below:



Reaction (1.10) leads to the destruction of O₃ and it is the ratio of the rates of reactions (1.7) and (1.10) that determine whether a particular region will have a net production/loss of O₃. Combining reactions 1.5, 1.6 and 1.10 we get the following O₃ destroying reaction:



1.2. Inter-Continental Transport of Pollutants

It has been well established that air pollutants (both primary and secondary) can be transported over long distances. The first detailed study of long-range transport of air pollution was related to acid rain in Scandinavia and North America [*Calvert, 1983*]. Since then there have been a plethora of studies that have presented evidence of inter-continental long-range transport of air pollution. *Kallos et al.* [1998] showed that polluted air masses could be transported from Southern Europe to North Africa whereas *Jaffe et al.* [1999] used observations at the Cheeka Peak Observatory in Northwestern Washington state in 1997 to show that pollution outflow from East Asia could affect North America as well. Similar findings were reported by *Jacob et al.* [1999] and *Yienger et al.* [2000]. The Arctic haze is also believed to be caused due to pollutant transport from southern latitudes.

Inter-Continental Transport (ICT) of a pollutant can occur as a result of an increase in the background concentration of the pollutant due to excessive emissions and/or meteorological conditions that result in stagnation, followed by subsequent advection of the pollutant in the boundary layer or the free troposphere. Once emitted, a pollutant is subjected to the dynamics of the atmosphere which cause it to be transported over long distances. The following rules apply to the direction and time of transport in the atmosphere:

- 1.) ICT primarily occurs from west to east in the mid-latitudes as the mid-latitude zonal mean winds are westerly throughout the troposphere.
- 2.) In the tropics, the transport occurs from east to west with easterlies blowing in the lower and mid-troposphere.
- 3.) Pollutant transport is faster at higher altitudes due to the higher wind speeds.
- 4.) More rapid ICT can be expected in the winter due to the winds being stronger during winter than in summer.
- 5.) Pollutants tend to be transported zonally as the meridional winds are generally weaker than zonal winds.

[Cooper *et al.*]

Multiple mechanisms are at play in the atmosphere which can cause pollutants to be transported from one continent to another. These are listed and described next.

1.) Mid-Latitude Cyclone Airstreams: These cyclones are generally composed of four airstreams [Cooper *et al.*]. These are namely, the Warm Conveyor Belt (WCB), the Cold Conveyor belt (CCB), the Dry airstream (DA) and the Post cold front airstream (PCFA). The WCB is considered to be the most relevant as regards to ICT as it can lift an air mass

from the atmospheric boundary layer to the upper troposphere from where the air mass can be transported downwind by the jet streams. It is formed in the warm sector of the cyclone and flows towards the poles in a direction parallel to the cold front.

2.) Deep Convection: Deep convection occurs when the air near the surface of the Earth is much warmer than that lying above resulting in enhanced vertical movement and transport of air into the middle and upper regions of the troposphere. The high wind speeds in these upper regions transport the pollutants downwind, over long distances.

3.) Low Altitude Zonal Flow: This involves the flow of pollutants without being lifted above the boundary layer. It occurs when during the transition of the boundary layer from day to night a residual layer is formed, which experiences higher air speeds as compared to the air in the boundary layer.

ICT typically involves transport times ranging from days to weeks. Hence, it can be stated that the pollutants having chemical lifetimes similar to or greater than these time scales are the only ones that can be transported over long distances and across continents. Appropriate examples would be CO, O₃ etc. ICT is expected to influence the background concentrations of several trace gases in the receptor continent. Transport of particulates/aerosols can have health effects as well as alter the formation of clouds and incoming radiation. For example, The South Asian brown clouds which are a result of long-range transport of aerosols from Asia, form a haze layer over a major part of Southern Asia and decrease the incoming solar radiation [*Crutzen and Ramanathan, 2003; Ramana and Ramanathan, 2006; Ramanathan et al., 2001*]. Observational evidence, model results and the potential influences of ICT have made it an issue to be considered while formulating environmental policies and air quality standards for

nations. Uncertainties such as lack of complete knowledge of the transport paths for pollutants, limited observations for certain regions such as Asia, variations in the pathways by which ICT takes place still exist and make this an important area of current research.

1.3. Transport of Pollution into and out of North America

The continent of North America (NA) is bounded by the Pacific Ocean in the west and the Atlantic Ocean in the east. Predominantly, pollution outflow from the continent occurs towards Europe across the Atlantic Ocean whereas pollution inflow to it occurs from Eastern Asia across the Pacific Ocean. This movement of pollution into and out of NA is caused by two of all the possible mechanisms discussed earlier:

1.) Deep Convection: It results in lofting the polluted air above the North American boundary layer to the mid and upper troposphere where the higher wind speeds facilitate transportation across the Atlantic Ocean. The pollution entering NA is also transported via the same mechanism.

2.) Mid-Latitude Cyclone: The mid-latitude cyclones are responsible for a major part of pollution transport to and from NA [Owen *et al.*, 2006] . These cyclones when travelling west to east export pollutants from NA to Europe. Of the four airstreams a mid-latitude cyclone is composed of, the WCB is considered to be the most important in contributing to this transport [Cooper and Parrish, 2004] as it can facilitate lifting of the air mass being carried by the cyclone to the mid and high troposphere. The WCBs form on the western sides of the Atlantic and Pacific Oceans and decay on the eastern sides which

explains the export of pollution from Eastern NA and import of Asian pollution into Western NA [*Cooper and Parrish, 2004*].

1.3.1. Major Pathways of Pollution Outflow from NA

Most of the pollution export from NA occurs across the North Atlantic Ocean. This is the more commonly studied and well known pathway. Pollution transported via this pathway reaches the European mid and upper troposphere and is also transported to the North Pole before returning back in the form of air masses that break off from the tropospheric Arctic vortex [*Cooper and Parrish, 2004*].

1.3.2. Major Pathways of Pollution Inflow into NA

The most important pathway along which ICT of pollutant occurs into NA is across the Pacific Ocean. This pathway brings in pollution originating in East Asia and has been the focus of several studies over the past 10-12 years. Measurements from multiple aircraft campaigns provide evidence that Asian pollution plumes are transported over the North Pacific [*Zhang, 2010*]. WCBs play a major role in this export as well with deep convection becoming important only during the summer. [*Bey et al., 2001a; Chatfield and Baumgardner, 1997; Zhang, 2010*]. These mechanisms lift the polluted air into the free troposphere where it is transported across the Pacific by the westerly winds [*Zhang, 2010*].

1.4. ICT of Carbon Monoxide and Ozone to/from North America

CO has a chemical lifetime ranging from 30-90 days [Seinfeld and Pandis, 1998] which makes it a sufficiently long lived species to be transported over long distances. Similarly, O₃ also has a long enough chemical lifetime of 2-4 weeks in the troposphere [Law, 2010] to undergo long range transport. CO directly emitted by anthropogenic sources and biomass burning can be transported in pollution plumes produced by these sources. O₃, unlike CO may be formed near the source, in the pollution plumes that contain its precursor compounds such as NO_x, CO, CH₄ and other VOCs or at receptor sites. Hence, a general mechanism for long range transport of O₃ would involve emission of its precursors from anthropogenic/natural sources, formation of O₃ in the plume according to the chemistry in section 1.1 and transport of the plume downwind by meteorological processes as discussed earlier (section 1.2). The emitted precursors including CO and NO_x are also transported with the plume. Export of NO_x can occur as PAN as well which acts as a reservoir and undergoes thermal decomposition producing NO_x in the receptor region. This transport of NO_x can result in O₃ formation in the downwind region as well, resulting in enhanced concentrations. Cooper *et al.* [2010] reported an increase in springtime O₃ concentrations from 1995-2008 at many sites across western NA which they attributed to pollution plumes originating in Asia. Similar attribution was also made by Yang *et al.* [2010] for high tropospheric O₃ columns over coastal California, near Santa Barbara. Huntrieser *et al.* [2005] provided evidence of two North American pollution events leading to pollution plumes containing O₃ formed at the

source region being transported all the way to Europe whereas *Val Martin et al.* [2006] observed enhanced CO and O₃ levels at the PICO-NARE station in the Azores during North American boreal wild fire emission events and also acknowledge the role of PAN as a reservoir species which results in formation of NO_x as the pollution plumes subside. It can thus be seen how continental CO and NO_x may result in formation of O₃ in the pollution plumes as well as at a receptor site located far away downwind.

1.5. Motivation of this Study

The discussion in the previous sections clearly indicates that the emission of pollutants from one continent can affect the air quality at sites downwind. Countries now have to take this long-range transport into account while deciding Ambient Air Quality Standards (AAQS) and other environmental policies. Hence, it becomes imperative to understand the processes contributing to this transport, general pathways of transport and to quantify its effects on the background concentrations at the receptor continents. Several measurement stations, aircraft campaigns, satellites and modeling studies have been used to better understand ICT of pollutants. Over the past decade, there has been a decrease in the NO_x and CO emissions over NA (Figure 1.1) owing to the active measures taken by the U.S. E.P.A and the state and federal governments. Similar decreases have been registered over Europe, whereas emissions in Asia have shown an increase. How these emission trends have affected the background concentrations at remote sites located downwind of these continents is an important question. Such sites if impacted by transport from source continents not only help us identify potential pathways of pollution transport, but also aid in ascertaining whether concentrations of species such

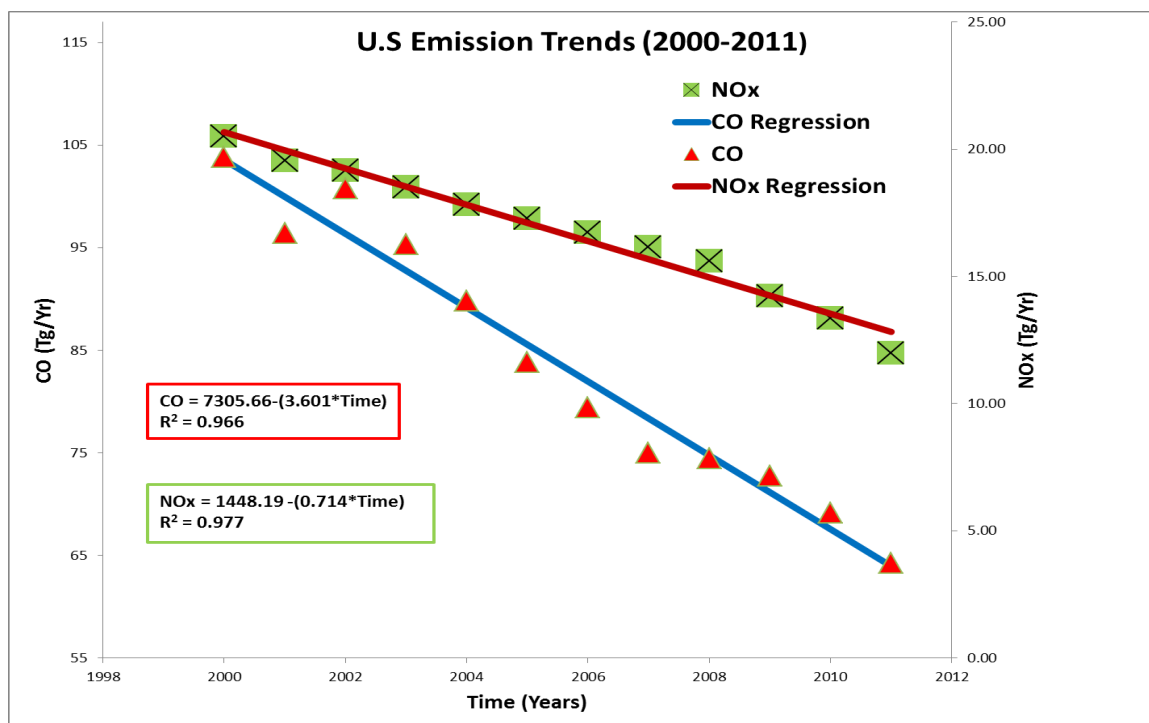


Figure 1.1: US anthropogenic emissions (in Tg/yr) for CO and NO_x from 2000 to 2011.

(Data available at: <http://www.epa.gov/ttnchie1/trends/>)

as O₃, CO, NO_x, NMHCs etc. at these sites are significantly affected by anthropogenic influence. Several such sites are located across the globe (e.g. Mauna Loa, Hawaii [Keeling *et al.*, 1976]). One such site, the PICO-NARE observatory has been established on the Pico island in Portugal [Honrath *et al.*, 2004]. This site is known to be impacted by North American pollution outflow and hence is useful in monitoring the pollution transport from NA and sampling the free troposphere. This study involves trend analysis of observations of O₃ and CO made at the PICO-NARE observatory for the period 2001-2010 (For CO) and 2001-2011 (For O₃) coupled with corresponding output from GEOS-Chem model of atmospheric chemistry and transport [Bey *et al.*, 2001b]. The goal is to ascertain whether the decreases in CO and NO_x emissions over NA have had an impact on the observed values of O₃ and CO at the station. Significant increases/decreases in the

concentrations would imply a corresponding increase/decrease in the pollutants being transported. Also, the tagged CO simulation in GEOS-Chem is employed to study the impact of CO emissions from various sources. This simulation could provide estimates of the magnitude of pollution from a particular continent that reaches the PICO-NARE observatory and would thereby help in determining the contribution of different regions to the CO concentrations at PICO-NARE. The results from tagged simulations would also help in ascertaining how the respective contributions from the different continents have varied over the period of study which would assist in explaining the cause of the trends observed at the site. In addition, the GEOS-Chem full chemistry simulation was also used with fixed anthropogenic emissions to determine whether the trends could be a result of changes in factors other than the anthropogenic emissions.

Chapter 2: The PICO-NARE Observatory

2.1. Introduction

The PICO-NARE observatory is located on the Pico Mountain, an inactive volcano on Pico island in the Azores, Portugal ($38^{\circ} 28.226'N$, $28^{\circ} 24.235'W$) at an altitude of 2225 m [Honrath *et al.*, 2004]. The station is located in the lower free troposphere (FT) and is well above the Marine Boundary Layer (MBL) during summertime. The island population is low (around 15,000) and is concentrated near sites much lower than the station (about 1200 m) which implies that the site has negligible anthropogenic influence and is an ideal location to sample the FT as well as study the impact of transport of NA pollution on the North Atlantic. Mountaintop observatories are prone to upslope transport of air (e.g. Mauna Loa observatory) which could result in air from lower altitudes (which could be cleaner/more polluted relative to the FT air) being carried to the station resulting in a significant bias in the measurements. However, upslope flow is found to be less important at Pico [Kleissl *et al.*, 2007]. The station is affected by both Buoyant and Mechanically Forced Upslope flows (BUF & MFU respectively) with the former dominating in the summer and the latter in the winter. Observations of such flows on the island have been limited with the probability of sampling MBL air being 35-60% in October-April, when MFU dominates and only 27% of the studied days showing occurrence of buoyant uplift [Kleissl *et al.*, 2007]. This is in contrast to other mountaintop observatories (e.g. Mauna Loa, Izana [Kleissl *et al.*, 2007]) and can be attributed to the smaller size and high latitude of the island as well as the small width and steep sides of the mountain, leading to the conclusion that the latitude,

size and topography of the island prevent frequent transport of air from low-altitudes to the mountaintop [Kleissl *et al.*, 2007].

2.2. Importance of the Site relative to Pollution Outflow from North America

In addition to being an ideal location to sample FT air, the PICO-NARE observatory is also frequently impacted by export of NA pollution during summertime and outflow from arctic and subarctic regions resulting in transport of biomass burning emissions from Canada, Alaska and Siberia [Honrath *et al.*, 2004]. Val Martin *et al.* [2006] reported that North American boreal wildfires contributed significantly to enhancements in CO and O₃ background concentrations during the summer of 2004. Honrath *et al.* [2004] also observed frequent enhancements in the CO levels above the marine background levels during the summertime in 2001-2003 which they attributed to North American pollution outflow or long-range transport of biomass burning emissions. High levels of both CO & O₃ were observed during the periods of biomass burning. Figure 2.1 shows the monthly mean concentrations of CO produced from fossil fuel combustion in the USA for June and July 2004 (level 1 is the surface layer and level 5 corresponds to the altitude of Pico in the GEOS-4 vertical grid) obtained from the tagged CO simulation in GEOS-Chem. Figure 2.2 shows the same plots for CO produced in Europe. It can be seen that the CO produced in these regions is transported to the North Atlantic.

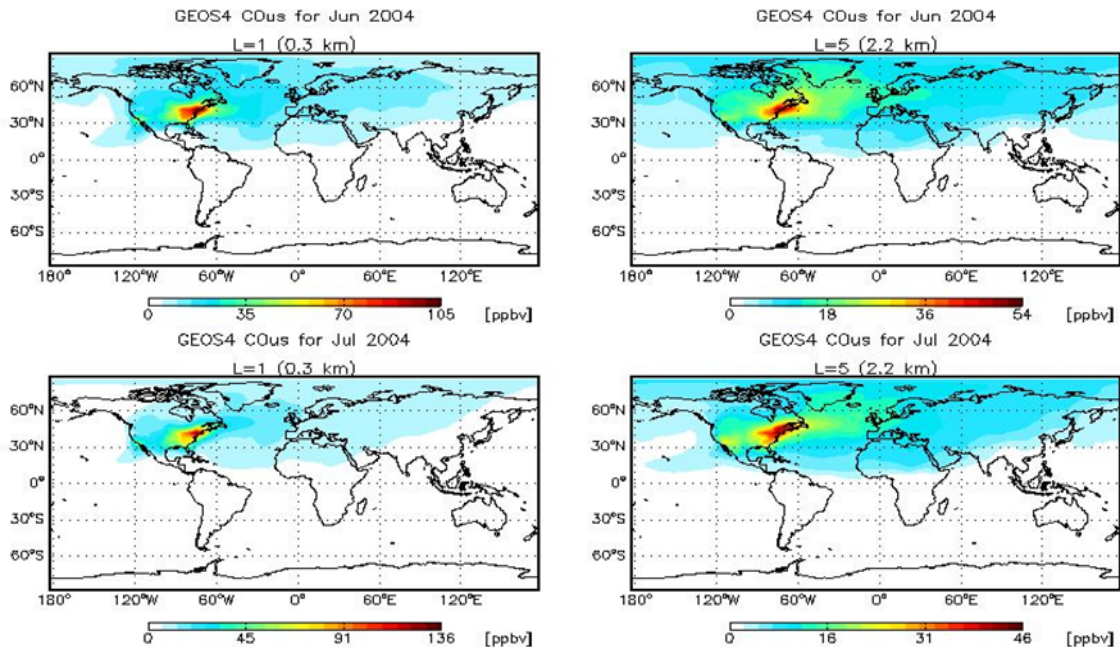


Figure 2.1: CO₂ produced from fossil fuel combustion in USA for June and July 2004

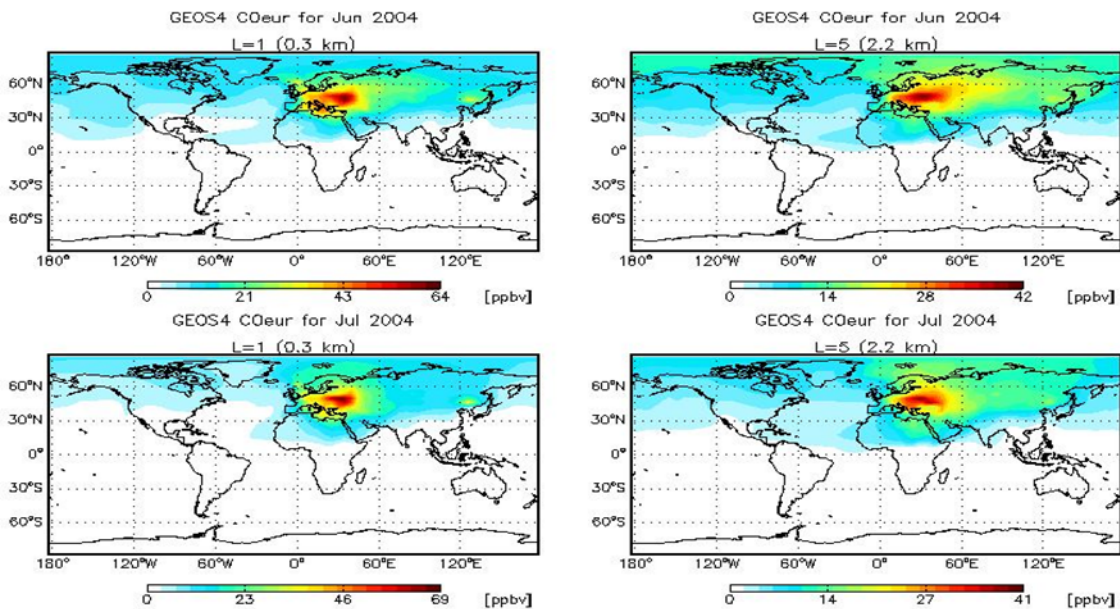


Figure 2.2: CO₂ produced from fossil fuel combustion in Europe for June and July 2004

Most of the pollution transport from NA to the North Atlantic occurs due to the WCBs of the mid latitude cyclones which move eastwards across the US. However, during summertime transport at low altitudes (< 3 km) has also been observed [*Owen et al.*, 2006]. Pollution events caused by similar transport mechanisms were analyzed by *Owen et al.* [2006] and they observed O₃ enhancements which corresponded to CO in most cases. These studies clearly point to the fact that measurements at PICO NARE can be used to understand and ascertain the impact of North American pollution transport on the North Atlantic. With the North Atlantic being a potential pathway for pollution transport from NA to Europe, these measurements aid in monitoring the ICT from NA as well.

2.3. PICO-NARE Observations

The observation data for CO and O₃ at PICO used in this study covers different time spans. For CO, the data availability is from 2001-2010, with measurements using the instrument described in *Honrath et al.* [2004]. The O₃ data for 2001-2011 was measured using the instrument again described in *Honrath et al.* [2004]. So in totality, the data for CO covers the period 2001-2010 and that for O₃ spans 2001-2011. However, the data availability during these years is not uniform, with multiple years that do not have data for several months (especially winter time), months that do not have data for many days and days that do not have data for full 24 hours. This analysis utilizes data for only those days that have full 24 hours availability. This 24 hour filter resulted in the use of 75.71% data points for CO and 86.62% for O₃. Table 2.1 lists the hourly distribution of the data for CO and O₃ whereas Tables 2.2 & 2.3 show the data availability (in number of days) in

each of the months throughout the period 2001-2011 for CO and O₃ respectively after the 24 hour filter has been applied. It can be seen that most of the years have most data available for the months of May through September with 2004 being the only year that has data for almost the whole year (both CO & O₃). The monthly and annual means of CO and O₃ are tabulated in tables 2.4 & 2.5 respectively with the months of July and August which have data for all years being highlighted.

Table 2.1: Hourly distribution of PICO-NARE observations for CO and O₃

CO (2001-2010)		O ₃ (2001-2011)	
Number of hours	Number of days	Number of hours	Number of days
24	901	24	1172
23	19	23	17
22	30	22	20
21	17	21	10
20	13	20	12
19	17	19	10
18	11	18	06
17	10	17	07
16	11	16	05
15	09	15	05
14	03	14	05
13	33	13	07
12	20	12	11
11	13	11	07
10	11	10	16
09	08	09	09
08	15	08	08
07	12	07	05
06	11	06	03
05	07	05	05
04	05	04	01
03	06	03	02
02	06	02	05
01	02	01	05

Table 2.2: Data availability (Number of days in each month) for CO (2001-2010)

Y→ M ↓	2001	2002	2003	2004	2005	2006	2007	2008	2009	2010	2011
Jan			11	05	18						
Feb					21						
Mar			08		02						
Apr		15		10	26						
May		06	12	18	26	08				23	
Jun		01	02	16	21	29			15	24	
Jul	14	16	09	20	30	23			25	18	
Aug	18	18	08	27	25	24			08	11	
Sep	11	07		12		20			15	25	
Oct	19	22	20	22		06					
Nov	24	07	05	24							
Dec	07	14	05	25							

Table 2.3: Data availability (Number of days in each month) for O₃ (2001-2011)

Y→ M ↓	2001	2002	2003	2004	2005	2006	2007	2008	2009	2010	2011
Jan				05	18						
Feb					21						
Mar			10		03				09		
Apr				16	28			08	20	02	
May				26	31	19		21	26	26	
Jun				19	24	27		29	24	28	13
Jul	14		06	20	30	30		11	25	20	27
Aug	28		08	27	26	24		24	08	11	22
Sep	11		06	13		20		15	15	25	15
Oct	25		29	26		06		01			30
Nov	27		05	24							19
Dec	12		06	28							

Table 2.4: Monthly Mean Matrix for CO (in ppbv) (2001-2010)

Y → M ↓	2001	2002	2003	2004	2005	2006	2009	2010	Monthly Mean
JAN			120.98	108.41	123.24				117.54
FEB					130.89				130.89
MAR			146.10		138.02				142.06
APR		119.76		132.30	131.50				127.85
MAY		100.23	119.04	114.59	122.77	103.05		113.62	112.22
JUN		97.32	119.80	93.36	104.07	104.36	86.83	93.64	99.91
JUL	71.38	83.20	99.66	94.76	93.12	91.52	81.34	84.52	87.44
AUG	69.82	82.47	109.74	94.90	94.20	86.34	73.04	88.42	87.36
SEP	84.55	99.72		93.97		93.88	76.96	102.09	91.86
OCT	101.67	119.16	109.06	93.14		96.62			103.93
NOV	101.29	101.29	103.65	98.32					101.14
DEC	103.01	120.95	105.70	104.31					108.49
Annual Mean	88.62	102.68	114.86	102.81	117.23	95.96	79.54	96.46	

Table 2.5: Monthly Mean Matrix for O₃ (in ppbv) (2001-2011)

Y → M ↓	2001	2003	2004	2005	2006	2008	2009	2010	2011	Monthly Mean
JAN			37.48	42.44						39.96
FEB				47.48						47.48
MAR		52.38		48.97			53.17			51.51
APR			53.07	47.48		41.42	47.03	50.25		47.85
MAY			44.14	46.92	44.59	41.62	45.19	43.30		44.29
JUN			42.24	43.84	42.01	37.56	40.72	39.01	40.13	40.79
JUL	30.88	42.24	38.93	38.78	37.63	41.21	37.31	41.01	33.30	37.92
AUG	34.48	40.84	38.93	41.52	41.21	36.77	30.86	39.30	31.79	37.30
SEP	39.59	42.97	43.55		37.77	39.86	31.27	44.36	38.46	39.73
OCT	45.86	45.20	40.03		42.35	51.98			39.98	44.23
NOV	44.06	41.80	41.96						42.83	42.66
DEC	42.28	39.84	43.69							41.94
Annual Mean	39.53	43.61	42.40	44.68	40.93	41.49	40.79	42.87	37.75	

Chapter 3: The GEOS-Chem Model of Atmospheric Chemistry and Composition

3.1. Model Description

GEOS-Chem is a global three-dimensional model of tropospheric chemistry driven by assimilated meteorological observations from the Goddard Earth Observing System (GEOS) of the NASA Global Modeling Assimilation Office [Bey *et al.*, 2001b]. It uses data for meteorology and multiple emission inventories coupled with various convection & chemistry schemes to simulate the formation, chemistry and transport of pollutants around the globe. It also simulates meteorological processes by including appropriate schemes for convection, transport (advection & dispersion), atmospheric boundary layer whereas processes such as dry and wet deposition have been included as well. The emissions and meteorology processes are activated at pre-defined time-steps which depend on the horizontal grid resolution being used. Figure 3.1 shows a flowchart representing the working of GEOS-Chem.

The meteorology files are available at a global resolution of 0.5° (latitude) x 0.667° (longitude) and are labeled as GEOS-3, GEOS-4 & GEOS-5 with each spanning different periods. GEOS-5 is the latest version (as in v9-01-02) covering the period 2004-2011. The model involves division of the world and the atmosphere into horizontal and vertical grids respectively. The horizontal grids available are $4^{\circ} \times 5^{\circ}$, $2^{\circ} \times 2.5^{\circ}$ & $0.5^{\circ} \times 0.667^{\circ}$ (latitude x longitude) while the vertical grids span 30 (GEOS-4), 47 (GEOS-5 reduced grid) & 72 (GEOS-5) layers. Emission inventories in GEOS-Chem have been

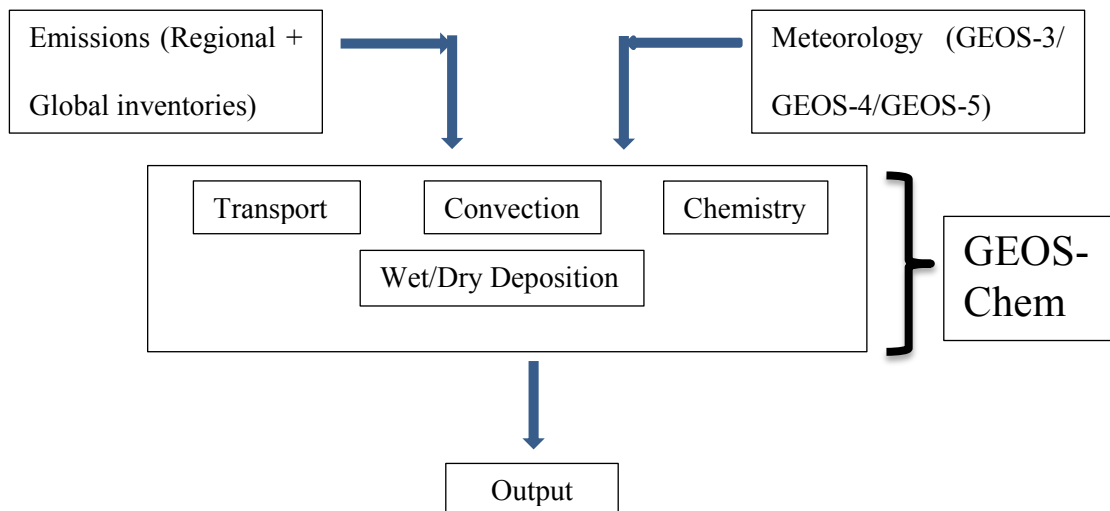


Figure 3.1: Flowchart representing the working of GEOS-Chem

derived from literature as well as from various research programs and government sources (e.g. ARCTAS, US EPA etc.). These inventories mainly provide estimates of the anthropogenic, biomass burning, biofuel and biogenic emissions and can be divided into two categories namely, the global emission inventories and the regional emission inventories. The regional inventories can overwrite the global ones if turned on over the concerned region. Emissions from other natural sources (e.g. NO_x from lightning, soil & volcanic emissions) are also included, in addition to source specific emission inventories (emissions from ships). For each inventory, the emission estimates have been compiled for a base year or a particular number of years. If a particular inventory has no data available for a year, the latest year of data available is used. However, in case of NO_x , CO and SO_x , the emission estimates are scaled using appropriate scale factors to obtain emissions for the simulated year. These scale factors for the regions of Canada, United States, Europe and Asia are based on trend data for the respective species in these

regions. For other regions, the scaling is according to changes in total CO₂ emissions (for NO_x), solid fuel CO₂ emissions (for SO_x) and liquid fuel CO₂ emissions (for CO). Table 3.1 lists these emission inventories along with relevant details. GEOS-Chem uses the KPP and SMVGEAR chemistry solvers for the troposphere. KPP stands for Kinetic Pre-Processor and is a software tool to assist computer simulations of chemical kinetic systems [Eller *et al.*, 2009; Sandu and Sander, 2006]. The SPARSE MATRIX VECTORIZED GEAR 2 (SMVGEAR 2) code is the native chemistry solver in GEOS-Chem [Eller *et al.*, 2009]. Either of these can be used in a GEOS-Chem simulation. Although GEOS-Chem is a tropospheric chemistry model the influence of the stratospheric species on the troposphere necessitates the inclusion of a stratospheric chemistry mechanism. Current model versions use the Linearized Ozone (LINOZ) mechanism for stratospheric O₃ with the latest version (v9-01-03) having an updated linearized stratospheric chemistry scheme in addition to LINOZ. LINOZ involves expressing the rate of change of O₃ as a function of the O₃ mixing ratio, temperature and the column O₃ above the point under consideration. It produces a realistic and interactive O₃ field that allows for on-line calculation of O₃ columns and photolysis rates. The earlier mechanism called Synthetic Ozone (SYNOZ) used a fixed stratosphere to troposphere flux of O₃ which was considered to be unrealistic and hence is seldom used. The convection scheme used depends on the meteorology fields being used by the model. For GEOS-4, the Hack and Zhang-McFarlane scheme [Hack, 1994; Zhang and McFarlane, 1995] is used whereas for GEOS-3 & GEOS-5, the Relaxed Arakuwa-Schubert scheme [Moorthi and Suarez, 1992] is used. The model uses two different schemes to simulate

Table 3.1: List of emission inventories used in GEOS-Chem

Emission inventory	Region	Type	Base Year	Reference
EDGAR	Global	Anthro+Ship	2000	[<i>Olivier and Berdowski, 2001</i>]
RETRO	Global	Anthro	2000	[<i>Pulles et al., 2007</i>]
GEIA/PICCOT	Global	Anthro		[<i>Piccot et al., 1992; Wang et al., 1998</i>]
CAC	Canada	Anthro	2002,2005	
EMEP	Europe	Anthro +Ship	1980-2005	
EPA/NEI99	USA	Anthro+Biofuel	1999	
EPA/NEI05	USA	Anthro	2004	
VISTAS	USA		2002	
BRAVO	Mexico	Anthro	1999	
STREETS 2000(2004)	S.E Asia	Anthro	2000(2004)	[<i>Streets et al., 2006; Streets et al., 2003</i>]
STREETS 2006	S.E Asia	Anthro+Biofuel	2006	[<i>Zhang et al., 2009</i>]
COOKE	N.America		1996	
YEVICH & LOGAN (2003)	Asia, Africa, Latin America	Biofuel	1985, 1995	[<i>Yevich and Logan, 2003</i>]
GFED v3	Global	Biomass	1997-2010	[<i>Van Der Werf et al., 2010</i>]
GFED v2	Global	Biomass	1997-2008	[<i>Van Der Werf et al., 2006</i>], [<i>Giglio et al., 2005</i>]
ARCTAS	Global	Ship		
Corbett	Global	Ship	1993	[<i>Corbett et al., 1999</i>]
ICOADS	Global	Ship		[<i>Wang et al., 2007</i>]

mixing in the boundary layer one of which (the TURBDAY scheme [*Wu et al., 2007b*]) involves instantaneous & uniform mixing throughout the boundary layer while the other (the VIDFF scheme [*Holtslag and Boville, 1993*]) uses static instability as a criteria and

incorporates different states of mixing accordingly. The mixing states vary from the full mixing scheme, with farthest deviation in the case of a stable planetary boundary layer (PBL) when the mixing is much weaker than full mixing and resembling it in the case of extremely unstable conditions. The intermediate mixing state represents unstable conditions and accounts for mixing due to eddies. This scheme uses the PBL depth and the eddy diffusivity for the different species to simulate mixing. GEOS-Chem, by default, uses PBL depth from the meteorology data but provides options to calculate the PBL depth while performing simulations. The model uses a dynamic tropopause, the location of which is computed at each time step by comparing the pressure at the bottom of every grid box to the pressure at the tropopause (obtained from the GEOS met fields). Multiple simulations can be performed using GEOS-Chem: global, for specific regions (e.g. Nested Grid simulations) or for specific species (e.g. Tagged simulations, Mercury or Radon simulations), with coarse ($4^{\circ} \times 5^{\circ}$) or fine ($0.5^{\circ} \times 0.667^{\circ}$) resolutions. The standard simulation is the NO_x - O_x -hydrocarbon-aerosol (a.k.a “Full Chemistry”) simulation which covers most of the important atmospheric species including aerosols. This study uses the standard full chemistry simulation and the tagged simulation for CO, which have been described in detail in the subsequent sections.

3.2. GEOS-Chem NO_x-O_x-Hydrocarbon-Aerosol (a.k.a “Full Chemistry”) Simulation

This is the default simulation in GEOS-Chem and can be used to archive a number of species of atmospheric relevance. It is a global simulation and uses a detailed chemistry mechanism in the troposphere (with over 200 reactions) to simulate the fate and transport of more than 80 species. It can be used to save tracers which consist of both atmospheric gases and aerosol species. The available resolutions for the global simulation are $4^0 \times 5^0$ and $2^0 \times 2.5^0$ (latitude x longitude). This study uses version v8-03-01 of the model with a $4^0 \times 5^0$ resolution. The EDGAR emissions inventory was used for global anthropogenic emissions, whereas the CAC, BRAVO, NEI2005, EMEP and STREETS inventories were used for regional anthropogenic emissions. Biofuel emissions over North America were taken from the EPA/NEI99 inventory, biogenic VOC emissions were taken from MEGAN and the monthly GFEDv2 inventory was used for the emissions from biomass burning. NO_x emissions from natural sources such as lightning, aircraft and soil were also included. The species in the simulation were emitted every 60 minutes, transported at a time-step of 30 minutes and underwent chemistry every 60 minutes. Convection was set to occur every 30 minutes. The simulation was used with two different emission settings to facilitate better interpretation of the results obtained. One of them involved using normal emission settings, implying that the anthropogenic emissions used were for the same year as the simulation whereas the other used fixed anthropogenic emissions (2001 emissions) for all the simulations from 2001-2011.

3.2.1. Full Chemistry Simulation with Normal Emissions

As mentioned in section 3.1, the emission inventories in GEOS-Chem may have data for years that are different than the simulation year or they might have data for just one year. Appropriate scaling factors are then applied to scale the emissions to the simulation year in order to yield a more realistic emission scenario. The full chemistry simulation with normal emissions includes this behavior of the model. GEOS-5 meteorology was used for the runs. The time-series of instantaneous concentrations of CO and O₃ was archived at every 240 minutes for the period September 2010-December 2010 (CO) and September 2010-November 2011 (O₃). The data for earlier years was used from Mr. M.F Weise's work with the same simulation and settings [*Mark F. Weise, Tropospheric Ozone and CO over the North Atlantic for the Past Decade: A comparison study using modeling, satellite and ground-based measurement, 2011*]. Restart files generated by Mr. Weise for July 2010 were used with a two month spin up to run the model from September 2010 onwards.

3.2.2. Full Chemistry Simulation with Fixed Anthropogenic Emissions

This simulation used similar settings as regards to emission inventories, atmospheric dynamics & chemistry to the one in section 3.2.1. The major difference was in the use of fixed anthropogenic emissions for the period of run (2001-2011). A standard full chemistry simulation in GEOS-Chem employs the use of scale factors as mentioned earlier to scale the anthropogenic emissions from the base year of an emission inventory to the year for which the simulation is to be run. In this simulation this setting in the model was overwritten by using anthropogenic emissions corresponding to 2001 for all

the runs. GEOS-4 meteorology was used from 2001-2004 whereas GEOS-5 was used from 2005-2011. The motivation behind using fixed emissions is to eliminate the anthropogenic contribution to changes in the CO and O₃ concentrations at Pico and obtain trends that are purely due to changes in emissions from natural sources or changes in meteorological conditions over these years. Restart files for the starting year 2001 were generated from an 11 month spin up of the model using a previously generated restart file for February 2000. The spin up run used normal emissions in order to have the appropriate initial conditions for 2001. All subsequent runs used the anthropogenic emissions for 2001. The time-series for concentrations of CO, O₃ as well as meteorological parameters of interest such as relative humidity and temperature were archived over Pico for the period 2001-2011. In addition, monthly means of biogenic emissions and NO_x emissions from sources such as lightning, biomass burning etc. were also archived over the period 2001-2011.

3.3. Tagged CO Simulation

The tagged CO simulation is one of the multiple offline simulations (aerosol, tagged Methane etc.) included in GEOS-Chem. It consists of source-specific CO tracers which can be used to study the contribution of various geographical regions (e.g. Asia, North America) as well as different CO sources (e.g. biomass burning, biofuels) at locations across the globe and also in understanding the potential transport pathways of CO which could be useful when studying ICT. Table 3.2 lists the CO tracers in the simulation. Being a linear simulation, the total CO tracer equals the sum of CO from all the other sources/tracers. The CO sources accounted for include

fossil fuels, biofuels, biomass burning, anthropogenic and biogenic VOCs. The contribution of VOCs to CO production is estimated either as percentages of the regularly emitted sources as in case of anthropogenic VOCs or as percentage yield from the concerned VOC in case of biogenic VOCs. Anthropogenic VOCs contribute to 19%, 19% and 11% of the direct emission of CO from the fossil fuels, biofuels and biomass burning respectively [Duncan *et al.*, 2007]. For biogenic VOCs, the yield of CO from Isoprene is 20% (average value based on maximum and minimum values obtained with NO_x) with different values for polluted regions (40%) and clean regions (< 20%), from Monoterpene it is 24% based on Hatakeyama *et al.* [1991] & [Vinckier *et al.*, 1998], Acetone yields 66% whereas the CO from Methanol is 43 Tg C/a which are distributed according to the emissions of isoprene [Duncan *et al.*, 2007]. Oxidation of CH₄ by OH radical is also included as a source with a yield of 100%. Annual mean CH₄ concentrations from 1988-1997 used are based on NOAA/GMD measurements from remote sites. The reaction of CO with the hydroxyl radical (OH) is the only sink considered in the reaction mechanism. The destruction of CO by micro-organisms is not considered due to its uncertainty and likelihood of being counterbalanced by the degradation of plant matter [Duncan *et al.*, 2007]. The simulation can be run at a global resolution of 4° x 5° & 2° x 2.5° (latitude x longitude). This study uses the coarser (4° x 5°) grid resolution to archive the tracer values for the grid box corresponding to the PICO-NARE observatory. Emission inventories included to account for anthropogenic CO production were the global EDGAR, CAC over Canada, BRAVO over Mexico, EPA/NEI99 over North America, STREETS over South-East Asia and RETRO global anthropogenic VOC inventories. Monthly GFED3 emissions accounted for the CO production from biomass

burning. The OH concentrations are archived from a previous full chemistry simulation and in this case were obtained using version 05-07-08 of the model with GEOS-3 meteorology. Other settings are typical of a $4^0 \times 5^0$ simulation. Restart files for the simulation were self-generated with zero initial concentrations for all the tracers and model spin up was performed until steady state concentrations were reached. The data archived consists of the time-series of instantaneous values of all the tracers at a time step of 240 minutes from 2001-2010 corresponding to the grid box containing Pico and their monthly mean mixing ratios from 2001-2010. Based on availability, GEOS-4 meteorology was used from 2001-2004 and GEOS-5 from 2005-2010.

Table 3.2: Tracer list for the tagged CO simulation

Tracer List	Tracer List
CO (total)	CO _{bbeu} (CO from bb in Europe)
CO _{US} (CO from fossil fuel in USA)	CO _{bbna} (CO from North America)
CO _{Eur} (CO from fossil fuel in Europe)	CO _{CH4} (CO from CH ₄)
CO _{asia} (CO from fossil fuel in Asia)	CO _{biof} (CO from Biofuels)
CO _{Oth} (CO from rest of the world)	CO _{isop} (CO from Isoprene)
CO _{bbam} (CO from bb in South America)	CO _{mono} (CO from Monoterpenes)
CO _{bbaf} (CO from bb in Africa)	CO _{methanol} (CO from Methanol)
CO _{bbas} (CO from bb in South-East Asia)	CO _{acet} (CO from Acetone)
CO _{bboc} (CO from bb in Oceania)	

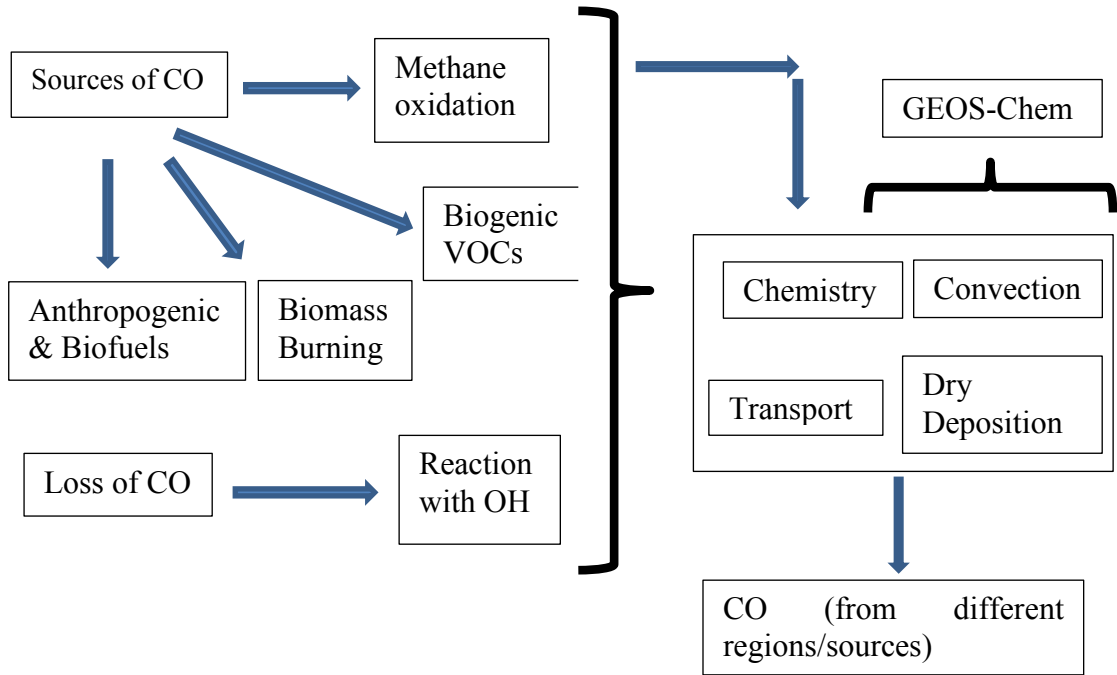


Figure 3.2: Schematic representation of the tagged CO simulation in GEOS-Chem

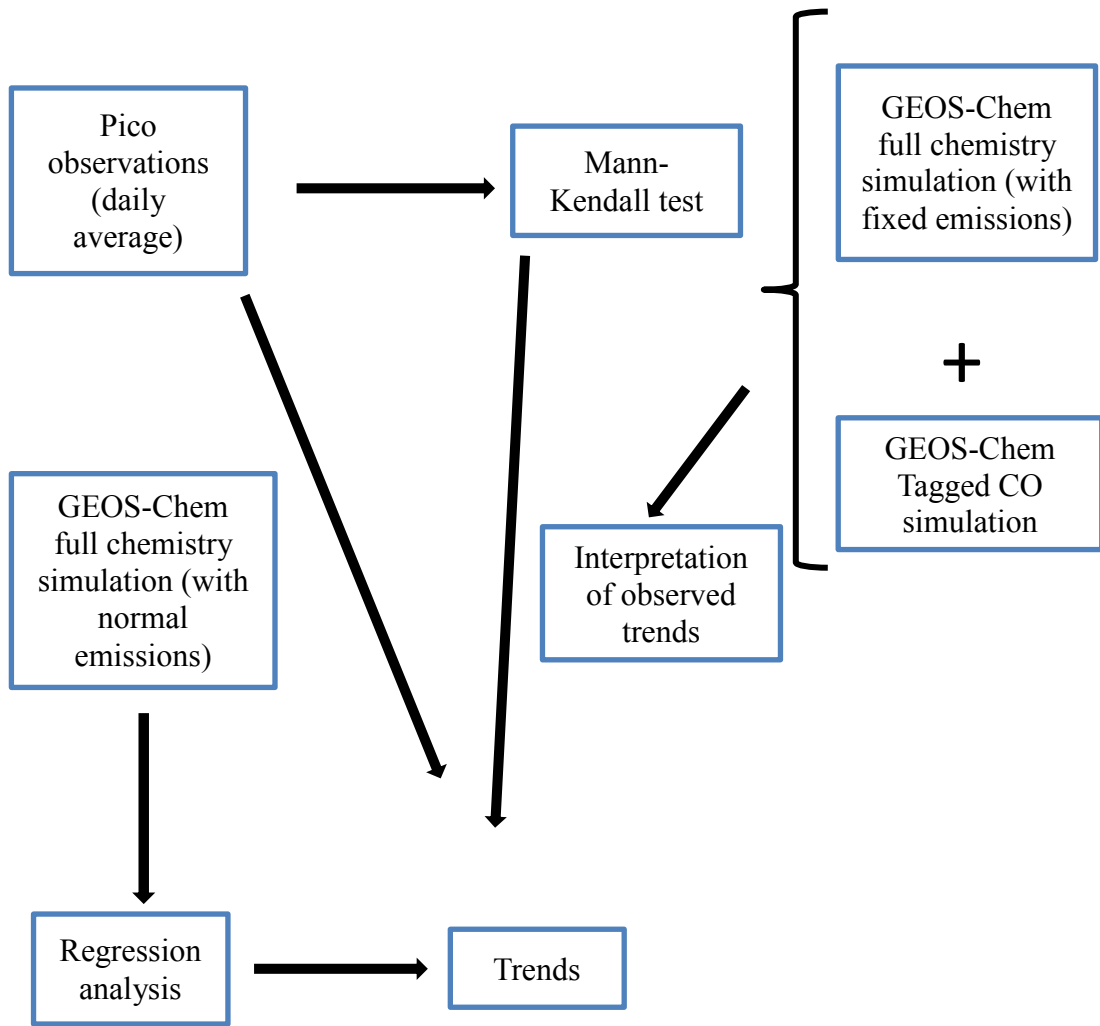


Figure 3.3: Flowchart of this study

Chapter 4: Trend Analysis

4.1. Introduction

Trend analysis refers to analyzing a dataset at hand in order to ascertain whether it exhibits a trend over the time period of study. A trend in statistics and scientific analysis can be defined as the tendency shown by the data which can be assumed to continue in the future when more data becomes available [Wu *et al.*, 2007a]. It can also be defined as the long-term change in a parameter of interest. A trend can be either with respect to time or other parameters such as distance, height etc. Trend analysis consists of a procedure which either includes the steps of hypothesis testing alone or both hypothesis testing and regression analysis. If a trend with respect to time is required, the analysis would involve using a time series of the variable of interest. Before moving on to the use of time series in trend analysis and the techniques applied in this study a brief description of hypothesis testing and regression analysis is provided in the following sections.

4.2. Hypothesis Testing

4.2.1. Introduction

A hypothesis in statistics is a statement about the behavior of the data being analyzed and hypothesis testing as the name suggests is usually applied to test this statement. Thus, it can be used to subject a hypothesis to the test of statistical significance. A hypothesis test involves two complementary hypotheses which are called the null and alternative hypothesis respectively. These tests can be classified depending

on whether the test involves assumptions about the distribution of the data or not. The division leads to:

1.) **Parametric Tests:** These tests assume that the data being considered obeys a certain distribution. They are called Parametric because they represent the data in the form of parameters such as Mean, Standard Deviation etc. and subsequently use them to compute the test-statistic which is to be used to test the hypothesis. Examples of such methods would be single step regression and multiple step regression.

2.) **Non-Parametric Tests:** Unlike the parametric tests, tests of this type do not involve assumptions regarding the distribution of the data and follow a procedure based on ranking the data points by comparing each data point with the others. An example of non-parametric tests would be the Mann-Kendall test.

4.2.2. Procedure for a Hypothesis Test

A hypothesis test consists of the following steps:

1.) **Choosing the appropriate test:** The appropriate test should be selected after carefully considering the characteristics of the dataset at hand, the test objective and the expected distribution of the data. If the parametric tests are employed it should be ensured that the assumptions incorporated in the test are satisfied. Otherwise the non-parametric tests should be used.

2.) **Defining the Null & Alternate Hypotheses:** Before performing either of the hypothesis tests, the null and alternate hypotheses should be stated clearly. The null hypothesis generally states the null situation, no relation between variables or no trend and is either negated or supported by the results of the test. The alternate hypothesis is the

conclusion assumed to be true once the test has resulted in rejecting the null hypothesis.

The alternate hypothesis can be divided into two groups:

1.) One-Sided: The one-sided alternate hypothesis states that there is variation from the null hypothesis in a single direction. A test-statistic providing evidence of such variation would result in rejection of the null hypothesis. For example, suppose the null hypothesis is that the concentration of a particular pollutant shows no trend with time. Then a one-sided alternate hypothesis would state that either the concentration has increased or decreased with time. In case of a one-sided hypothesis, the test performed is said to be a one-sided hypothesis test.

2.) Two-Sided: The two-sided alternate hypothesis states that there can be variation in either direction from the null hypothesis statement. A test-statistic providing evidence of any significant variation from the null hypothesis would result in rejection of the null hypothesis. For example, if the null hypothesis states that there is no trend observed in the concentrations of a pollutant at a particular site then any test statistic that shows an increasing or a decreasing trend will result in rejection of the null hypothesis. In case of a two-sided hypothesis, the test performed is said to be a two-sided hypothesis test. So, when the direction of variation in the alternate hypothesis cannot be ascertained it is better to perform the two-sided test.

3.) Deciding on an acceptable level of significance (α): The significance level (or α value) represents the probability below which the null hypothesis can be rejected. It represents the assumed probability that the null hypothesis is true or in other words any trend that is observed is due to random variations in the dataset. The choice of α would depend on the data availability as well as the subjective choice of the analyst. Commonly

used values in literature are 0.05, 0.1 with 0.05 (or 5%) being the most commonly used value for determining statistical significance [Cowles and Davis, 1982].

4.) Computation of the test statistic: The test statistic represents how the data being considered behaves. If a high positive correlation coefficient is obtained between two sets of data then they are said to be positively correlated and vice versa. The test statistic is used to decide whether the null hypothesis should be rejected or not at a particular significance level. If the statistic obtained is significantly different from one that would be obtained if the null hypothesis were true then the null hypothesis can be safely rejected.

5.) Finding the p-value: The p-value (probability value) represents the actual probability of observing the computed test statistic or an even more extreme one with the null hypothesis being true. It provides evidence against the null hypothesis and is read from statistical tables corresponding to the test statistic.

6.) Rejection or accepting the Null Hypothesis: The null hypothesis is rejected when the obtained p-value is less than the assumed significance level (α). If the p-value is greater than α , the null hypothesis is not rejected. Rejection of the null hypothesis implies that the evidence at hand is sufficient to conclude that there exists a trend in the dataset whereas failure to reject it would mean that there is no sufficient evidence to support the alternate hypothesis of an existing trend.

Figure 4.1 shows the steps of hypothesis testing.

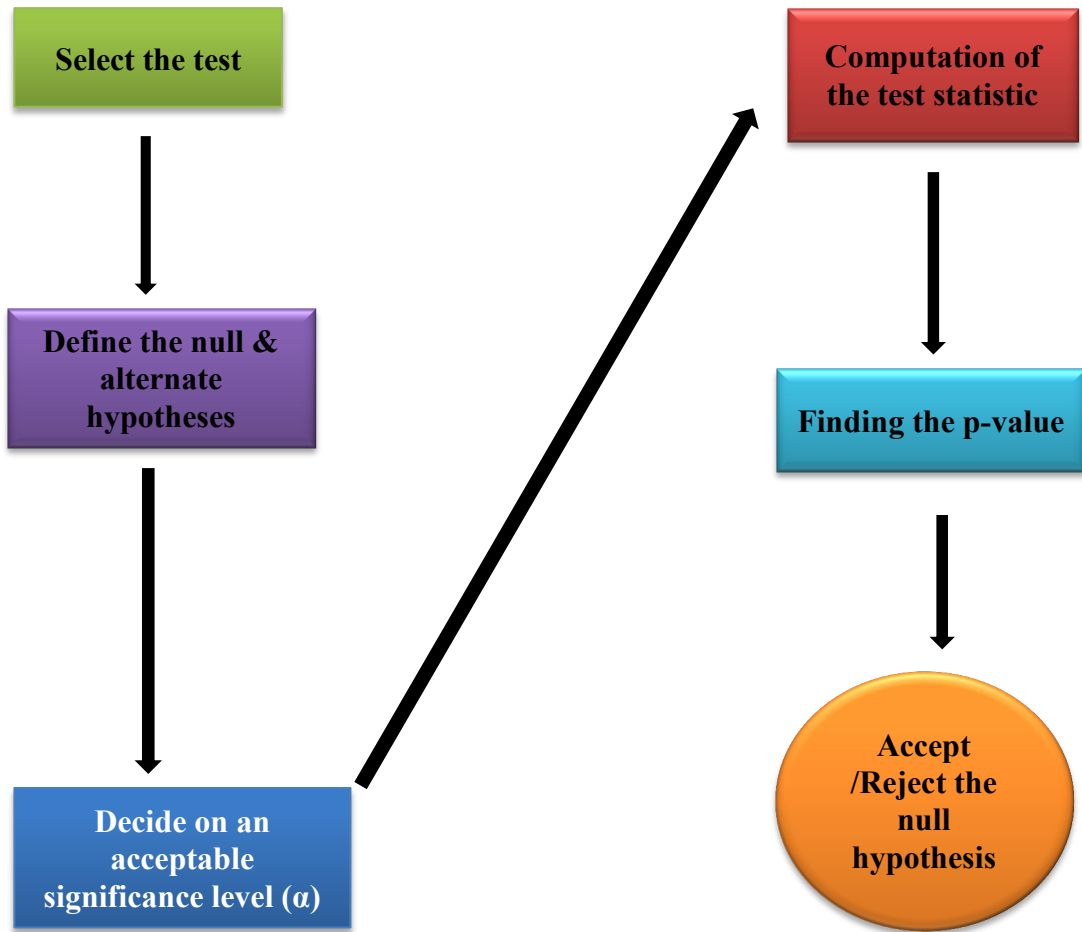


Figure 4.1: Steps of Hypothesis testing

4.3. Regression Analysis

Regression analysis in statistics is used to establish a relationship between one or more variables. The relationship is expressed as a mathematical equation which could include linear, quadratic, sinusoidal or other mathematical functions or a combination of them. These functions are expressed in terms of the variables to be included on the right hand side (RHS) of the regression equation with the variable with which the relationship is to be established being on the left hand side (LHS). The RHS also consists of coefficients corresponding to each mathematical function and a constant term. In Eq. (4.1) X_1 & X_2 can be any mathematical functions whereas Y is the variable with which the relationship of X_1 & X_2 is to be established. a_0 , a_1 , & a_2 are the coefficients.

$$Y = a_0 + a_1X_1 + a_2X_2 + \varepsilon \quad \text{Eq. (4.1)}$$

The exercise of performing a regression analysis involves determining each of these coefficients by using the ordinary least squares method [*Dismuke and Lindrooth, 2006*]. This method involves minimizing the sum of the squares of the differences between the observed and the model predicted values of the independent variable. The idea behind the method is to minimize the distance between the data points and the curve represented by the regression equation. To assess the extent to which the model fits the data, the Karl Pearson's correlation coefficient (r) can be used for a one LHS variable linear regression whereas for regression with multiple LHS variables, the coefficient of determination (R-Square) is used. Also, the statistical significance of the various coefficients can be determined by comparing the p-value corresponding to the t-statistic obtained for each of the coefficients to the assumed α . If the p-value for a coefficient is less than α then the

coefficient is said to be statistically significant otherwise it is insignificant. Another way to test the significance of the coefficient would be to read the t-statistic for probability equal to α and compare it with the one obtained for the regression. If the t-statistic read from the table is more extreme than that obtained, the corresponding coefficient is statistically insignificant. The test of statistical significance related to the regression parameters is carried out to reject/accept the null hypothesis that the parameter is equal to zero or a particular value. Of course, the alternative hypotheses can be one-sided or two-sided depending on the objective of the study.

4.4. Non-Parametric & Parametric Tests Used in this Study

This study makes use of both the non-parametric and parametric tests to determine whether statistically significant trends for CO and O₃ exist at PICO-NARE. The non-parametric Mann-Kendall test and a multiple regression model (with sinusoidal (to represent seasonal variation) and linear terms (to represent trend)) were used to test the Pico observations and GEOS-Chem output respectively for trend. While setting up the Mann-Kendall test involved following the test procedure, the formulation of the regression model was based on relevant principles of time-series analysis (described later). These principles and descriptions of the Mann-Kendall test and regression model are provided in the following sections.

4.4.1. The Non-Parametric Mann-Kendall test

The Mann-Kendall test [Kendall, 1955; Mann, 1945] is one of the most widely used tests to determine trends. It is a non-parametric test of hypothesis testing and hence does not involve assumptions regarding the data being analyzed in contrast to the

parametric tests. The test is derived from a rank correlation test for two groups of observations and takes into account the correlation between the rank order of the observed values and their order in time [*Hamed and Rao, 1998*], thereby using the procedure of computation of Kendall tau (τ) [*Kendall, 1970*] and the corresponding test of significance. Rank correlation is the first step in the method and has been commonly used in testing trends and correlation [*Alvo and Cabilio, 1995*]. The Mann-Kendall statistic (S) obtained from rank correlation is used in different ways depending on the number of data points (n). If $n \leq 10$, the exact Mann-Kendall test [*Helsel and Hirsch, 2002*] is performed which involves the computation of τ and tests its significance. For $n > 10$, an approximate test [*Helsel and Hirsch, 2002*] is carried out in which S-statistic is used to compute a normalized test statistic (Z) which is checked for statistical significance. The approximate test is also used in the Seasonal Mann-Kendall test when the test is carried out for each of the defined seasons in order to account for seasonal variations in the data being used. These tests have been described below:

1.) Exact test

For this section we will denote by Y the variable for which the trend is to be determined and X would be the other variable. Figure 4.2 shows the flowchart for this test and a brief description of the steps involved is provided below:

- 1.) Step 1: List the two datasets (containing values for X & Y) and arrange them such that X is in an ascending order. In other words, construct a dataset with X in increasing order and another with corresponding values of Y.
- 2.) Step 2: Compare each value of Y to all the subsequent values. If there is an increase a

plus sign or plus one value is written against that pair (Concordant pairs). In the other case if there is a decrease a minus sign or minus one value is written (Discordant pairs). A tie would result in a zero value.

3.) Step 3: Compute Kendall's S statistic which measures the monotonic dependence of Y on X. It is equal to the difference between the number of concordant and the number of discordant pairs.

$$S = P - M \quad \text{Eq. (4.2)}$$

P = Number of times Y values increase as the values of X increase or $Y_i < Y_j$ for $i < j$

M = Number of times Y values decrease as the values of X increase or $Y_i > Y_j$ for $i < j$

(for all $i = 1 \dots (n-1)$ and $j = (i+1) \dots n$)

So the total number of comparisons would be $\frac{n(n-1)}{2}$ where n is the number of data points. The maximum value of S could be $\frac{n(n-1)}{2}$ which will be the case when y increases all the time with X and the minimum value would be $-\frac{n(n-1)}{2}$ which occurs when Y decreases all the time with X. In the former case τ would be equal to 1 and -1 in the latter.

4.) Step 4: Compute the Kendall's tau which can be defined as:

$$\tau = \frac{S}{\left(\frac{n(n-1)}{2}\right)} \quad \text{Eq. (4.3)}$$

5.) Step 5: Test the significance of the S-statistic from the statistical tables

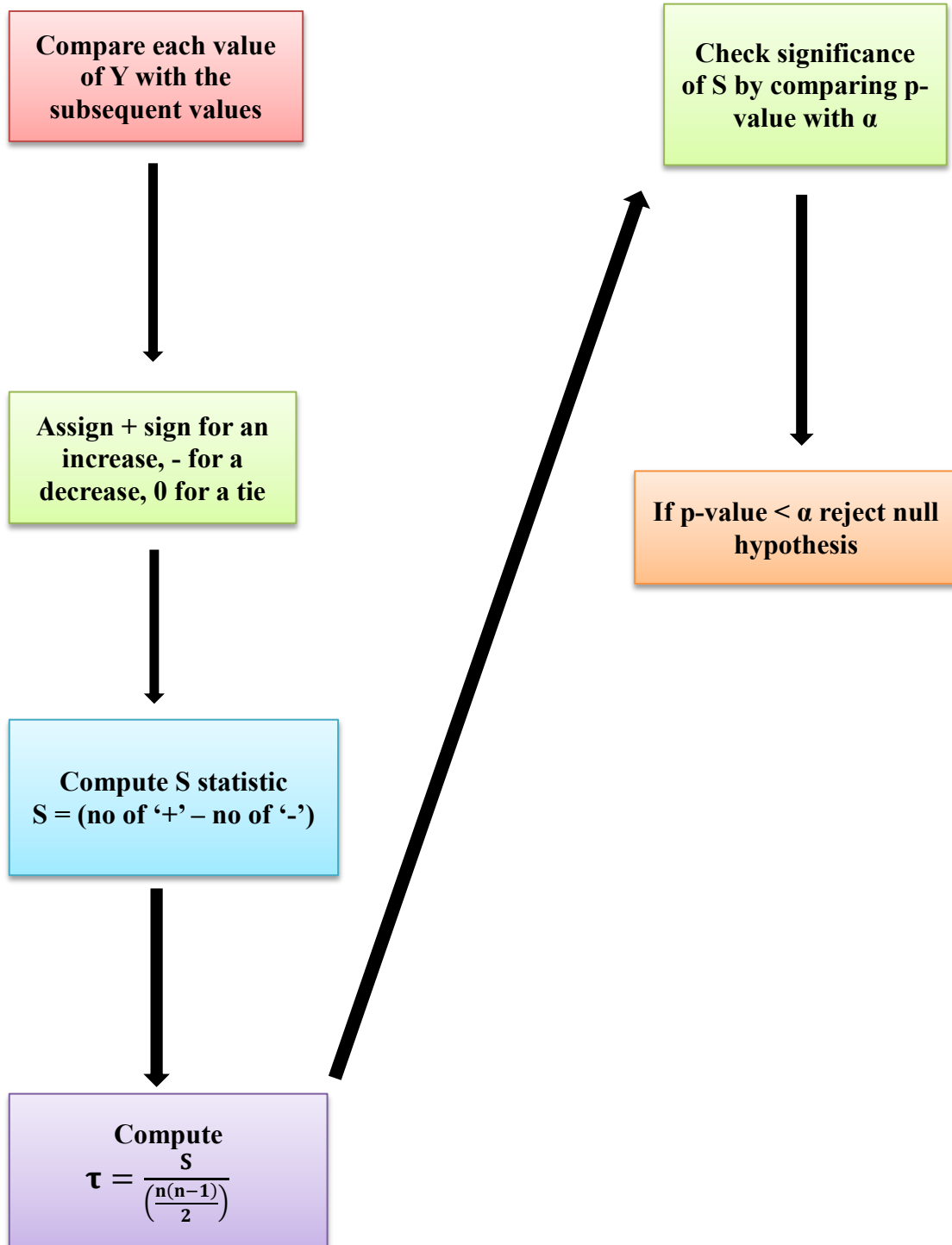


Figure 4.2: Flowchart for the Exact Mann-Kendall test

2.) Approximate test:

Figure 4.3 shows a flowchart for this test. This test involves a similar procedure to the exact test except that instead of τ , it uses a modified statistic (Z_s) which closely approximates a normal distribution. So, post the application of the rank correlation method to compute the Kendall's S statistic, Z_s can be computed as:

$$Z_s = \begin{cases} \frac{S - 1}{\sigma} & \text{if } S > 0 \\ 0 & \text{if } S = 0 \\ \frac{S + 1}{\sigma} & \text{if } S < 0 \end{cases} \quad \text{Eq. (4.4)}$$

Where:

$$\sigma = \sqrt{\left(\frac{n}{18}\right)(n - 1)(2n + 5)}, \quad n = \text{number of data points}$$

For the two-sided test, the null hypothesis can be rejected when the p-value obtained from the normal distribution table corresponding to the calculated Z statistic is less than $\alpha/2$. It means that if a value of the Z-statistic is obtained such that the probability of finding a value greater than or less than it (with the null hypothesis being true) is less than $\alpha/2$ it means that there is a trend present and the null hypothesis can be safely rejected. Similarly for the one-sided test, the null hypothesis will be rejected when the p-value obtained is less than α .

If there are repeated values in either of the datasets then there are certain modifications to be incorporated in the two tests. In the Exact test, the only modification is to assign a zero value to a comparison involving tied values and there is no change in the computation of the S-statistic. For the approximate test, the extent of the tied values is computed as the

number of times the particular value is repeated and an additional term is added to the expression used to compute the value of σ .

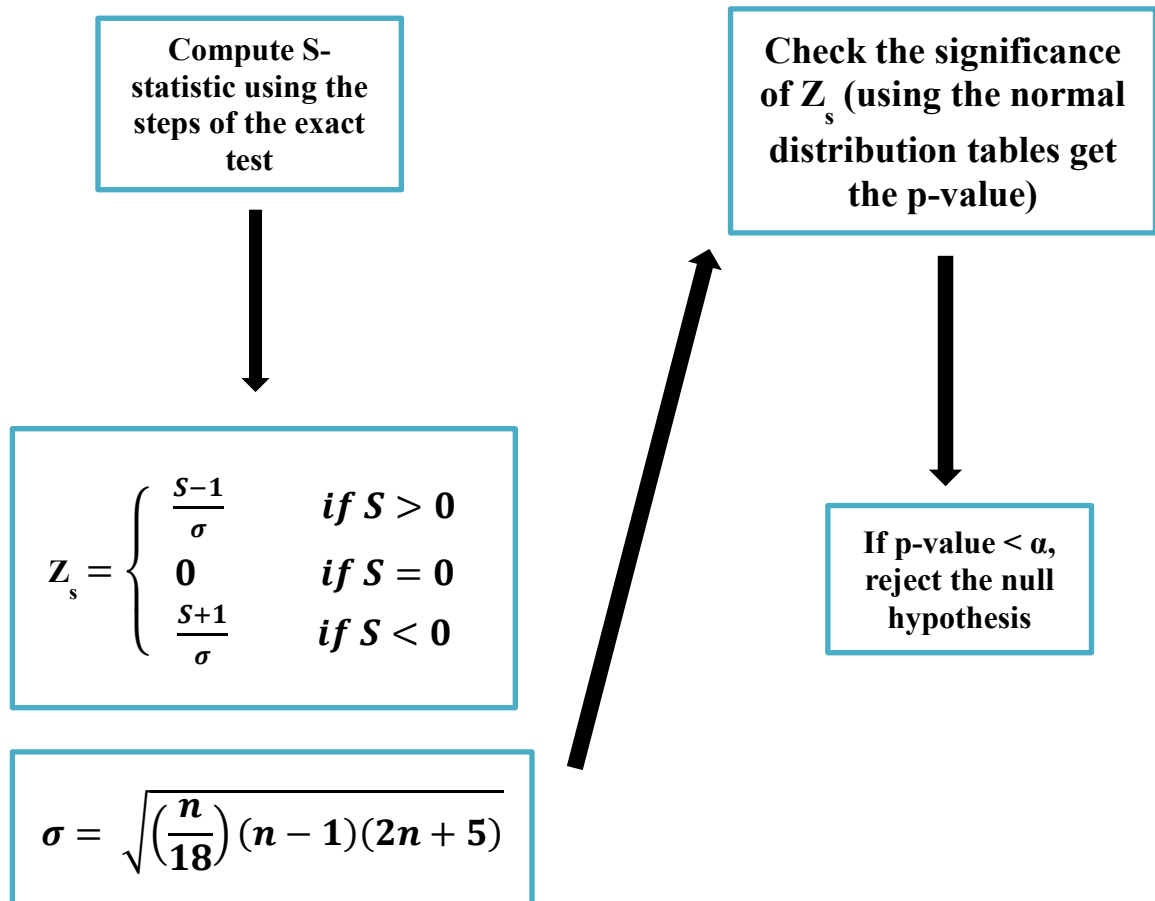


Figure 4.3: Flowchart for the Approximate Mann-Kendall test

The expression now becomes:

$$\sigma = \sqrt{\frac{n(n-1)(2n+5) - \sum_{i=1}^n t_i * i(i-1)(2i+5)}{18}} \quad \text{Eq. (4.5)}$$

Where:

i = Number of times a particular value of Y or X appears in the dataset

t_i = Number of times a tie of the extent of i occurs

3.) Seasonal Mann-Kendall Test

Figure 4.4 shows the flowchart for this test. The seasonal Mann-Kendall's test has the same computation procedure as the typical Mann-Kendall test, the only difference being that based on the user definition of seasons the Kendall's S-statistic is computed for every different season and combined to get the overall test statistic corresponding to which the p values are obtained to test the significance. The overall test statistic can be expressed as:

$$S = \sum_{k=1}^m S_k \quad \text{Eq. (4.6)}$$

Where:

S_k : S-statistic for each season

m = Number of seasons

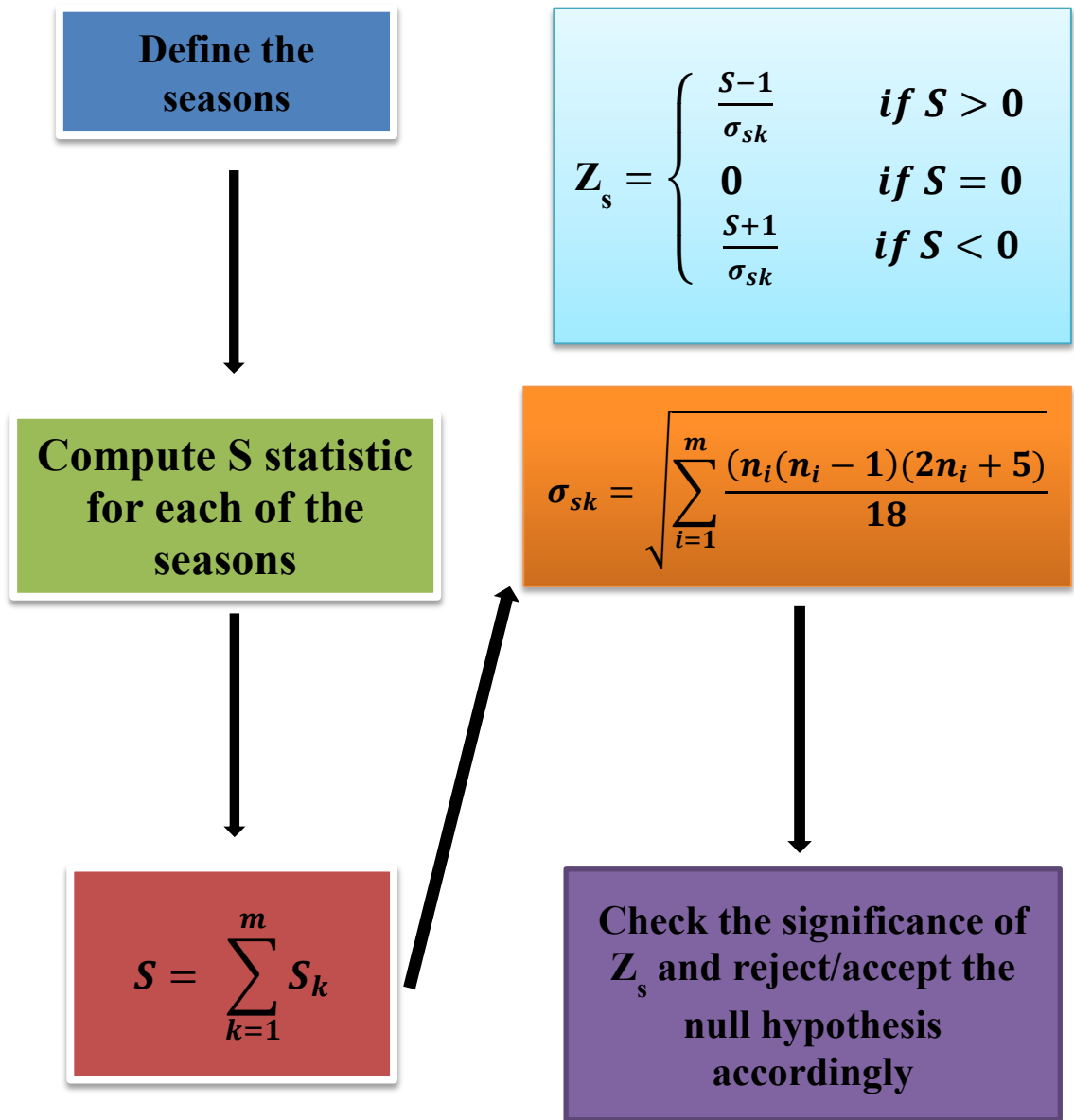


Figure 4.4: Flowchart of the Seasonal Mann-Kendall test

When the product of the number of seasons and the number of years exceeds 25, we can approximate the distribution of S_k as normal and use the approximate Mann-Kendall test [Helsel and Hirsch, 2002].

The Z-statistic can be calculated as earlier:

$$Z_s = \begin{cases} \frac{S - 1}{\sigma_{sk}} & \text{if } S > 0 \\ 0 & \text{if } S = 0 \\ \frac{S + 1}{\sigma_{sk}} & \text{if } S < 0 \end{cases} \quad \text{Eq. (4.7)}$$

Where:

$$\sigma_{sk} = \sqrt{\sum_{i=1}^m \frac{(n_i(n_i - 1)(2n_i + 5))}{18}}$$

n_i = Number of data points in the i^{th} season

If there are repeated values then the formula for σ_{sk} has to be modified as mentioned earlier. The computed Z-statistic is used to get the p-value from the normal distribution table which if less than $\alpha/2$ (two sided test) or α (one sided test) would result in rejection of the null hypothesis.

In addition to the daily average observations from Pico, the Mann-Kendall test was also applied to data derived from these observations. Table 4.1 lists the derived datasets. In order to eliminate any seasonal effects on the results of the test, the seasonal Mann-Kendall test was also used. Since data was not available for all the months of a year, the seasons were defined on a monthly basis. There were five monthly seasons defined (May, June, July, August and September) as datasets were most complete for these months. The Mann-Kendall test statistic was computed for each of these months

Table 4.1: Derived data sets used for performing the Mann-Kendall test

Derived Data	Description
Monthly Means	There was sufficient data available in the months of May, June, July, August and September. So the means were computed for these months only. The data points did not exceed 10 so the exact test was performed in each case.
Monthly Medians	The same months were considered with the medians for each month. The data points did not exceed 10 so the exact test was performed in each case
Daily averages for the summer months (June-August)	Daily averages for each of the summer months (June-August) were used since these months had the most data points available
Averages over the summer season (June-August)	Averages for the period June-August were used resulting in one data point for every year. The exact test was performed
Medians over the summer season (June-August)	Medians for the period June-August were determined resulting in one data point for every year. The exact test was performed

using the monthly means and monthly medians for each of them. Subsequently, an overall test statistic was computed by summing up the individual statistics obtained. Since the product of the number of seasons (5) and the number of years (there were variable number of data points available for each of the months, so an average of the number of years was computed as 7) was 35 which is greater than 25, the statistic could be approximated as behaving normally and the approximate Mann-Kendall test was used [Helsel and Hirsch, 2002].

4.4.2. Time Series Analysis

A Time Series is a sequence of observations of a specific quantity (e.g. concentration, flow rate, rainfall etc.) which span a definite time period. It is an important tool used in many fields including environmental engineering to monitor several parameters of interest. A time series can be described as a combination of three terms:

1.) Trend (T_t): It has been described earlier and can be stated as the long-term change in the mean of the variable of interest. The most commonly observed trend is a simple trend which can be represented by a straight line [*Wu et al.*, 2007a] and hence can be modeled as a linear term.

2.) Seasonality (S_t): It refers to the change in the variable which depends on the month/season in the calendar year. Such behavior results in the appearance of clearly defined cycles which indicate repetitive behavior after a fixed time period.

3.) Cycles (C_t): This component represents the cyclical changes that do not have a fixed frequency and hence is difficult to model.

4.) Fluctuations (F_t): These represent the erratic and irregular patterns in the data which are commonly referred to as noise. Generally, a suitable smoothing technique is applied to the data in order to minimize this component.

Decomposition of the time-series into its components can be done using an additive or multiplicative model. These models can be expressed mathematically as:

$$T = T_t + S_t + C_t + F_t \quad (\text{Additive model}) \quad \text{Eq. (4.8)}$$

$$T = T_t * S_t * C_t * F_t \quad (\text{Multiplicative model}) \quad \text{Eq. (4.9)}$$

Analysis of the time-series at Pico and the output from GEOS-Chem builds on these decomposition methods and uses an additive model consisting of the trend and seasonal terms which are believed to be the most dominant. The cyclical and fluctuation terms are combined together to form the residual term. In order to reduce the random component of the time-series so that the existing trends are more clearly visible, the data was subjected to the process of smoothing before fitting the regression model.

4.4.3. Smoothing schemes applied

As stated earlier, Smoothing refers to applying an approximate formula to the data at hand which results in reduction of unwanted short-term variations (noise) and helps in bringing out the important, underlying patterns in the data. Multiple smoothing schemes were applied to the data with subsequent checks of the performance of each in order to pick the most suitable. The schemes applied were:

1.) **Simple Moving Average (SMA) scheme:** The Simple Moving Average (SMA) scheme employs computation of the averages of values for a particular interval of time which is assigned to the last value of the interval. Hence, in order to proceed with the computation the number of data points to be used in computing the averages (period of the moving average) must be specified. For instance, in the case of a three day moving average, the method starts with the first three values of the series and assigns their average as the first term of the new series (which will correspond to the third term of the initial series). In the next computation the first value is dropped and the next three values are taken, assigning their average to the second value of the new series which

corresponds to the fourth value of the initial series and so on. The scheme can be represented by the following formula:

$$A_n = \frac{Y_n + Y_{n-1} \cdots + Y_1}{n} \quad \text{Eq. (4.10)}$$

Where:

A_n = Average of the n terms in the original data series and is the last term in the n terms considered for computing the moving average

Y_n 's = Terms in the original data series

n = Period of the moving average

Three smoothing periods: 5 day, 10 day and 15 day were used in this study.

2.) Centered Simple Moving Average (CSMA) Scheme: The computations of this scheme are exactly similar to the SMA scheme. The only difference lies in assigning the obtained average value. In the SMA scheme presented earlier, the average was assigned to the last data point in the interval. The current scheme assigns the average to the middle value of the interval. However, the computation procedure varies with whether the averaging period is odd or even. For an odd period, the middle term can be easily determined but this is not the case with an even period. The computation steps for both along with the respective formulas have been provided below:

a.) Odd period:

$$T_{\frac{n+1}{2}+j} = \frac{\sum_{k=0}^{n-1} T_{n+j-k}}{n} \quad \text{Eq. (4.11)}$$

Where:

n = Period of the moving average

$k = 0, 1, 2, \dots, (n-1)$

$j = 0, 1, \dots, (N-n)$ (1 value for every computation)

$N =$ Number of data points

The steps to compute the averages are listed below:

1.) Step 1: Compute the moving average for the first set of values (e.g. 1 to 5 for a 5 day moving average) and assign the average to the middle term (term 3 in this case)

2.) Step 2: Repeat Step 1 for other data points as well leaving out the earliest value (1st value in this case). The second step will span the 2nd and 6th values. Similar procedure is followed for the subsequent steps.

b.) Even period:

$$T_{\frac{n+1}{2}+j} = \frac{\sum_{k=0}^{n-1} T_{n+j-k}}{n} \quad \text{Eq. (4.12)}$$

$$T_{\frac{n+1}{2}+j+1} = \frac{\sum_{k=0}^{n-1} T_{n+j+1-k}}{n} \quad \text{Eq. (4.13)}$$

$$T_{\frac{n+1+2j+1}{2}} = \frac{T_{\frac{n+1}{2}+j} + T_{\frac{n+1}{2}+j+1}}{2} \quad \text{Eq. (4.14)}$$

Where:

$n \rightarrow$ Period of the moving average

$k = 0, 1, 2, \dots, n-1$

$j = 0, 1, \dots, N-n-1$ (1 value for each computation)

$N \rightarrow$ Number of data points

The steps to compute the averages are listed below:

- 1.) Step 1: Compute the moving average for the first set of values (e.g. 1 to 10 for a 10 day moving average) and assign the average to the middle term (hypothetical term 5.5 in this case)
- 2.) Step 2: Compute the moving average for the second set of values (e.g. 2 to 11 for a 10 day moving average) and assign the average to the middle term (hypothetical term 6.5 in this case)
- 3.) Step 3: Compute the average of the values obtained in Steps 1 & 2 assigning the value to the middle term (term 6 in this case)
- 4.) Step 4: Repeat Steps 1-3 for other data points as well with one value being common in computing the subsequent averages (e.g. for the second smoothed value the moving average would result from the average of the 10 day average for points 2 to 11 and 3 to 12. Similar for subsequent steps)

3 smoothing periods: 5 day, 10 day and 15 day were used in this study.

3.) **Centered Median (CM) Scheme:** The computation procedure is same for this scheme as compared to the CSMA scheme described above. The only difference lies in that instead of computing the average, the resulting values in the new series are the medians. This scheme also follows different procedures for odd and even periods.

a.) Odd period:

$$T_{\frac{n+1}{2}+j} = \mathbf{Median}(T_{n+j-k}) \quad \text{Eq. (4.15)}$$

Where:

n = Period of the moving average

k = 0, 1, 2, ..., (n-1)

$j = 0, 1, \dots, (N-n)$ (1 value for every computation)

N = Number of data points

The steps of computation are listed below:

1.) Step 1: Determine the median for the first set of values (e.g. 1 to 5 for a 5 day moving average) and assign it to the middle term (3 in this case)

2.) Step 2: Repeat Step 1 for other data points as well leaving out the earliest value (1st value in this case. The second step will span the 2nd and 6th values). Similar procedure is followed for the subsequent steps.

3 smoothing periods: 5 day, 10 day and 15 day were used in this study.

b.) Even Period:

$$T_{\frac{n+1}{2}+j} = \text{Median}(T_{n+j-k}) \quad \text{Eq. (4.16)}$$

$$T_{\frac{n+1}{2}+j+1} = \text{Median}(T_{n+j+1-k}) \quad \text{Eq. (4.17)}$$

$$T_{\frac{n+1+2j+1}{2}} = \text{Median}\left(T_{\frac{n+1}{2}+j}, T_{\frac{n+1}{2}+j+1}\right) \quad \text{Eq. (4.18)}$$

Where:

$n \rightarrow$ Period of the moving average

$k = 0, 1, 2, \dots, (n-1)$

$j = 0, 1, \dots, (N-n-1)$ (1 value for each computation)

$N \rightarrow$ Number of data points

The steps of computation are listed below:

- 1.) Step 1: Determine the median for the first set of values (e.g. 1 to 10 for a 10 day period) and assign it to the middle term (hypothetical term 5.5 in this case)
 - 2.) Step 2: Determine the median for the second set of values (e.g. 2 to 11 for a 10 day moving average) and it to the middle term (hypothetical term 6.5 in this case)
 - 3.) Step 3: Determine the median of the values obtained in Steps 1 & 2 assigning the value to the middle term (6 in this case)
 - 4.) Step 4: Repeat Steps 1-3 for other data points as well with one value being common in determining the subsequent medians (e.g. the second smoothed value would result from the median of the median of points 2 to 11 and 3 to 12. Similar for subsequent steps)
- 3 smoothing periods: 5 day, 10 day and 15 day were used in this study.

All of the above listed schemes were applied to the Pico observations for CO and O₃ and the Mean Square Error (MSE) was calculated for each of the schemes which would aid in identifying the most suitable scheme to be applied. The MSE can be defined as the sum of the squares of the difference between the observations and the series generated after applying the smoothing scheme, divided by the number of terms in the smoothed series. Mathematically, it can be written as:

$$\epsilon_T = \frac{\sum_{i=1}^N (X_i - \hat{X}_i)^2}{N} \quad \text{Eq. (4.19)}$$

$N \rightarrow$ Number of data points in the smoothed series

$X_i \rightarrow$ Observed value

$\hat{X}_i \rightarrow$ Corresponding value in the smoothed series

$\epsilon_T \rightarrow$ Mean Squared Error

The MSEs for the different schemes are listed in Table 4.2. The lowest MSE was obtained for the 5-day CM scheme (highlighted in green in Table 4.2) which was also very close to that obtained for the 5-day CSMA scheme (highlighted in orange in Table 4.2). However, owing to the past popularity of the moving average technique and considering the predominant application of the median scheme in image processing (where it is referred to as median filter and used to remove the outlying pixels utilizing the robustness of the statistic to outliers) [Jain *et al.*, 1995], the 5-day CSMA was selected to smooth the data. Although, the output from GEOS-Chem would not contain the magnitude of variations observed in the PICO observations, the data was smoothed in order to follow a consistent methodology throughout the analysis.

Table 4.2: MSE values obtained for different smoothing schemes

Smoothing Scheme	MSE value	
	CO	O ₃
5 day SMA	120.63	58.25
10 day SMA	157.69	68.17
15 day SMA	182.64	72.69
5 day CSMA	74.33	41.37
10 day CSMA	119.62	60.42
15 day CSMA	139.02	66.27
5 day CM	70.35	40.92
10 day CM	119.66	64.13
15 day CM	143.86	70.76

4.4.4. Regression Analysis

The seasonal behavior associated with both O₃ and CO is well documented [Bonasoni *et al.*, 2000; Derwent *et al.*, 1998; Logan, 1985; Logan and Kirchhoff, 1986; Narita *et al.*, 1999; Suthawaree *et al.*, 2008; Tiao *et al.*, 1975]. Most studies report a spring-time maximum and a summer-time minimum for O₃ and CO also exhibits a similar cycle with minor variations. Such cycles have also been reported for remote sites such as Mace Head [Derwent *et al.*, 1998] and mountaintop stations such as Mt Cimone [Bonasoni *et al.*, 2000]. Therefore, in order to fit a regression model to the observations and GEOS-Chem model output for PICO respectively it was deemed appropriate to use one with sinusoidal functions and a linear trend term. Sinusoidal functions are commonly used to model systems exhibiting periodicity and a similar methodology was adopted in this study as well. Mathematically, the model can be expressed as:

$$C_t = a_0 + a_1 t + \sum_{i=1}^n a_i \sin\left(\frac{2\pi t}{365}\right) + \sum_{i=1}^n a_i \cos\left(\frac{2\pi t}{365}\right) + e_t \quad \text{Eq. (4.20)}$$

Where:

C_t: Concentration of the species at a time t (in days) (time being measured from a reference year (01/01/1900 in this case))

a₀, a₁, a_i's: Regression coefficients

e_t: Residual from the model

The number of sinusoidal terms used would depend on the behavior of the variable being examined which if exhibiting multiple cycles of different periods per year

needs to be modeled using more than a pair of sinusoidal functions [Helsel and Hirsch, 2002]. However, since O₃ and CO are not known to exhibit such complex cycles the simplest case of the model (with a pair of sinusoidal functions) was used. This model is considered sufficient for most purposes in environmental engineering [Helsel and Hirsch, 2002]. The model has the following mathematical form:

$$C_t = a_0 + a_1 t + a_2 \sin\left(\frac{2\pi t}{365}\right) + a_3 \cos\left(\frac{2\pi t}{365}\right) + e_t \quad \text{Eq. (4.21)}$$

Where:

C_t : Concentration of the species at a time t (in days) (time being measured from a reference year (01/01/1900 in this case))

a_0, a_1, a_2, a_3 : Regression coefficients

e_t : Residual from the model

The coefficients in Eq. (4.21) are determined by the least squares method as discussed earlier and the significance of the t-statistic is checked by comparing the obtained p-value with the assumed α . Since, determining the trend in the concentrations is the objective of this study, the significance of only the linear term in time is checked. In this case, the null hypothesis states: “ a_0 is equal to zero”, whereas the alternate hypothesis would say: “ a_0 is significantly less/greater than zero” (depending on whether the test is one or two-sided).

This regression model was fit to the daily average observations from Pico and the time-series output from GEOS-Chem for Pico respectively. The five-day centered smoothing algorithm as described earlier was applied to both the datasets before fitting the regression model. Subsequently, a similar procedure to that described above was followed to test the statistical significance of the trend.

For the monthly mean data (e.g. biogenic emissions etc.) archived from the full chemistry simulation with fixed anthropogenic emissions, the following modified regression model was used:

$$C_t = a_0 + a_1 t + a_2 \sin\left(\frac{2\pi t}{12}\right) + a_3 \cos\left(\frac{2\pi t}{12}\right) + e_t \quad \text{Eq. (4.22)}$$

Where:

C_t : Concentration of the species at a time t (in months) (time being measured from a reference year (01/01/2000 in this case))

a_0, a_1, a_2, a_3 : Regression coefficients

e_t : Residual from the model

Chapter 5 : Results & Discussion

5.1. Mann-Kendall's test

The Mann-Kendall and the Seasonal Mann-Kendall test were applied to the datasets (daily averages and derived) described in Chapter 4. This section provides the results of these tests and the associated interpretations.

5.1.1. Application to the Daily Average Observations for PICO-NARE

Null Hypothesis: "No significant trends exist at Pico for both CO & O₃ over 2001-2010"

Alternate Hypothesis (one-sided): "Decreasing trends exist at Pico for both CO & O₃ over 2001-2010"

Results from the test are tabulated in Table 5.1 below. The application of the test to the daily average observations for Pico from 2001-2010 for CO and O₃ yielded decreasing trends which were statistically significant for CO (at $\alpha = 0.05$) but not for O₃. Since the number of data points was greater than 10, the approximate test was performed. The results indicate that there has been a decrease in the concentrations of CO at Pico over the period 2001-2010. Although several data points are missing in the dataset, the Mann-Kendall test is designed such that if there has been a consistent decrease in either of the species during these years, it will show in the final test statistic. However, there are several additional factors that need to be considered. The normal test does not account for seasonal variations associated with CO and O₃ and carries out comparisons across seasons which might influence the end result. Also, the possible long term decreases in

Table 5.1: Mann-Kendall test results for PICO-NARE daily average data

Species (→) Test details (↓)	CO	O₃
Number of data points	901	1046
Kendall's S-statistic	-33988	-17639
Kendall's Z-statistic	-3.77	-1.55
P-value (one sided test)	0.00008	0.059

the CO transported to Pico might be offset by increases due to biomass burning events which also result in CO getting transported all the way to Pico as described earlier, but considering the results for daily averages at face value it seems that there has been a decrease in CO concentrations at Pico which is statistically significant. The same cannot be said for O₃ though since the test statistic is not significant at the pre-specified significance level ($\alpha=0.05$).

5.1.2. Application of the Exact and Approximate Mann-Kendall Tests to the Derived Datasets

Null Hypothesis: "No significant trends exist at Pico for both CO & O₃ over 2001-2010"

Alternate Hypothesis (one-sided): "Decreasing trends exist at Pico for both CO & O₃ over 2001-2010"

The derived datasets have already been listed in Table 4.1. Depending on the number of data points in the derived datasets the exact or approximate Mann-Kendall test was used. Table 5.2 lists the comparisons that were made in each test in order to compute the test-statistic and the results obtained. Since a major part of the data was available for the months of May, June, July, August and September, these months were mostly used in

Table 5.2: Exact & approximate Mann-Kendall test results for derived datasets

Derived Data	Comparisons	Results
Monthly means for May, June, July, August and September (Exact test)	E.g. Monthly mean of May 2001 compared to monthly means for May in subsequent years. May 2001 compared to May 2002-May 2010, May 2002 compared to May 2003-2010 etc.	No significant trends for both CO & O ₃ at $\alpha = 0.05$
Monthly medians for May, June, July, August and September (Exact test)	Same comparisons as above with the representative statistic being the monthly medians	No significant trends for CO in any of the months. Significant trend at $\alpha = 0.05$ for O ₃ in June
Daily averages for the summer months (June-August) (Approximate test)	Daily averages of only summer months considered. So, daily averages from June to August 2001 compared with the daily averages for June-August in the following years.	No significant trends at $\alpha = 0.05$ for CO and O ₃
Summer averages (June-August) (Exact test)	Summer means from June-August for each year compared with those for the following years. E.g. Summer mean for 2001 compared with summer means of 2002 onwards	No significant trends at $\alpha = 0.05$ for CO and O ₃
Summer medians (June-August) (Exact test)	Same comparisons as above with the representative statistic being the monthly medians	No significant trends at $\alpha = 0.05$ for CO and O ₃

the analysis. In order to ascertain whether the data from individual months showed any trends, the monthly means of each month were compared with those for the same month in the following years. Similar methodology was adopted to compare the monthly

medians for each of the months as well. However, with the exception of the month of June which showed a significant trend at $\alpha = 0.05$ for O_3 , none of the months showed any trends. These results contradict the results obtained from the daily average data. This can be attributed to the influence of seasonal variation of CO and O_3 on the test with daily averages and a relatively short time series being analyzed if monthly averages are considered. Although the analysis covers 11 years of time, due to missing data for multiple years the monthly data sets have 6-8 data points. The test results will depend on the number of data points being considered since this determines the number of comparisons and the computed S-statistic. This might be a cause for the test not being able to discern significant trends. With this few data points a statistically significant trend can be discerned if there exists a monotonous decrease/increase in the concentrations of the species. However, as mentioned earlier, it can be possible that a decrease in the concentrations is offset by pollution from biomass burning episodes being transported to Pico which would result in an increase in the monthly means and would contribute to nullifying the existing trend. In the case of monthly medians, the impact of high concentrations due to episodic transport of biomass burning pollution would be reduced as medians are less susceptible to extreme values, but the shortcoming of too few data points still remains and could be the possible reason behind no significant trend being obtained.

The test was also carried out with the daily averages, means and medians for the summer months of June-August in order to ascertain whether significant trends existed for the summer season. However, there were no significant trends for any of the datasets. This could be due to the fact that the test makes comparisons across months and all the

months may not have the same trend direction, resulting in the nullification of a decreasing trend in one month (say June) by increasing ones in other months (say July, August). Also, it can be possible that the test statistic is not statistically significant for every season in the year. The unavailability of sufficient observations precludes an investigation of the behavior in other seasons. Thus, the only conclusion that can be drawn from this analysis is that the summer season does not show significant trends for both CO and O₃ over 2001-2010.

5.1.3. Application of the Seasonal Mann-Kendall Test

The seasonal variation associated with both CO and O₃ necessitates the usage of tests that take into account this variation. This is why the application of the approximate Mann-Kendall test to the daily averages in section 5.1.1 was not considered appropriate. Thus, the Seasonal Mann-Kendall test which does not make comparisons across seasons was applied to the datasets for both CO and O₃. However, there was limited data available for seasons other than summer. Thus, the months of May, June, July, August and September were considered as separate seasons. This has been shown in Table 5.3 below. The approximate test was performed for the daily averages whereas the exact test was carried out for the monthly means and medians. Each data point for a month was compared to the subsequent data points for that month only, thus in a way resembling the basic idea of not carrying out comparisons across seasons (months in this case). The overall S-statistic was computed as the sum of the S-statistics obtained for each of the considered months. Table 5.4 contains a summary of the datasets used, the involved comparisons and the results. No significant trends were obtained for any of the datasets.

This could again be due to the trend nullification by the existing opposite trends in different months. When the S-statistic is summed up from May-August the overall seasonal S-statistic will be reduced if there exist S-statistics with opposite signs for the months considered and will be increased if the S-statistic for the individual months have the same sign. In the case of both CO and O₃ it was found that the S-statistics were of different signs for some months which could have resulted in nullification of the overall seasonal S-statistic. This is expected in the Seasonal Kendall test since there could be different trends in different months but since datasets are not available for the whole year (which would have facilitated more robust results from this test and would have provided a clearer picture of the existing trends for both CO and O₃), the results can be classified as inconclusive. A more comprehensive dataset could have resulted in a statistically significant trend (increasing/decreasing) or the net cancellation of the trends in the individual seasons resulting in no trend at all.

Table 5.3: Seasons defined for the Seasonal Mann-Kendall test

Season	Month
Season 1	May
Season 2	June
Season 3	July
Season 4	August
Season 5	September

Table 5.4: Seasonal Mann-Kendall test results

Data	Comparisons	Results
Daily Averages	Daily Averages of each season compared to the daily averages of the same season in the following years.	No significant trends for CO and O ₃ at $\alpha = 0.05$
Monthly Means	Similar comparisons as above. The only difference is the use of monthly means	No significant trends for CO and O ₃ at $\alpha = 0.05$
Monthly Medians	Similar comparisons as above. The only difference is the use of monthly medians	No significant trends for CO and O ₃ at $\alpha = 0.05$

5.2. Evaluation of the 5 Day CSMA Scheme

As mentioned earlier, several smoothing schemes were applied to the daily average observations of CO and O₃ from PICO-NARE to decide on a suitable scheme for the entire analysis. The MSE analysis has already been discussed and how it was used to select the 5 day centered moving average scheme. In order to evaluate this scheme the regression model was fit to the Pico observations after the application of all the smoothing schemes discussed. This section contains the plots of the regression fits to the CO and O₃ data sets from 2001-2010 for different smoothing schemes which will explain the necessity of using the smoothing scheme.

Figures 5.1-5.10 show the plots of the regression model & observations v/s time for CO. Figure 5.1 shows the plot with no smoothing applied to the data whereas Figures 5.2 to 5.4 present the same plots with the Simple Moving Average (SMA) scheme applied. The Centered Simple Moving Average (CSMA) & Centered Median (CM) schemes were applied in Figure sets 5.5-5.7 & 5.8-5.10 respectively. Three periods of smoothing were considered for each scheme (5 days, 10 days and 15 days) and it can be

observed from each set of figures (5.2-5.4, 5.5-5.7 and 5.8-5.10) that applying a greater period of smoothing results in better fits which is due to a reduction in noise due to averaging as well as modification of the data. Similar behavior can be observed in the plots for O₃ for which Figure 5.11 represents the plot with no smoothing scheme applied and Figures 5.12 to 5.20 show the results with different schemes and periods (Figures 5.12-5.14: SMA, Figures 5.15-5.17: CSMA, Figures 5.18-5.20: CM). Tables 5.5 & 5.6 list the regression fit statistics along with the goodness of fit measure R² for CO and O₃ respectively. An increase in the R² with the period of smoothing can be seen for any particular smoothing scheme. However, selection of a large period of smoothing would involve significant modification of the observed data. Also, considering the fact that the observations for Pico do not cover the full period 2001-2011, using a larger period may have magnified effects as compared to a data set spanning the whole period. Of all the smoothing schemes applied, the CSMA scheme gives R² values which are the highest for a given period of smoothing (Highlighted in Tables 5.5 & 5.6 for CO & O₃ respectively). Based on these results, it could be concluded that the 5 day CSMA scheme serves the dual purpose of not significantly modifying the dataset (as 5 days is a short smoothing period and the MSE is minimum) and also being the most effective in reducing random fluctuations of the other 5 day smoothing schemes discussed.

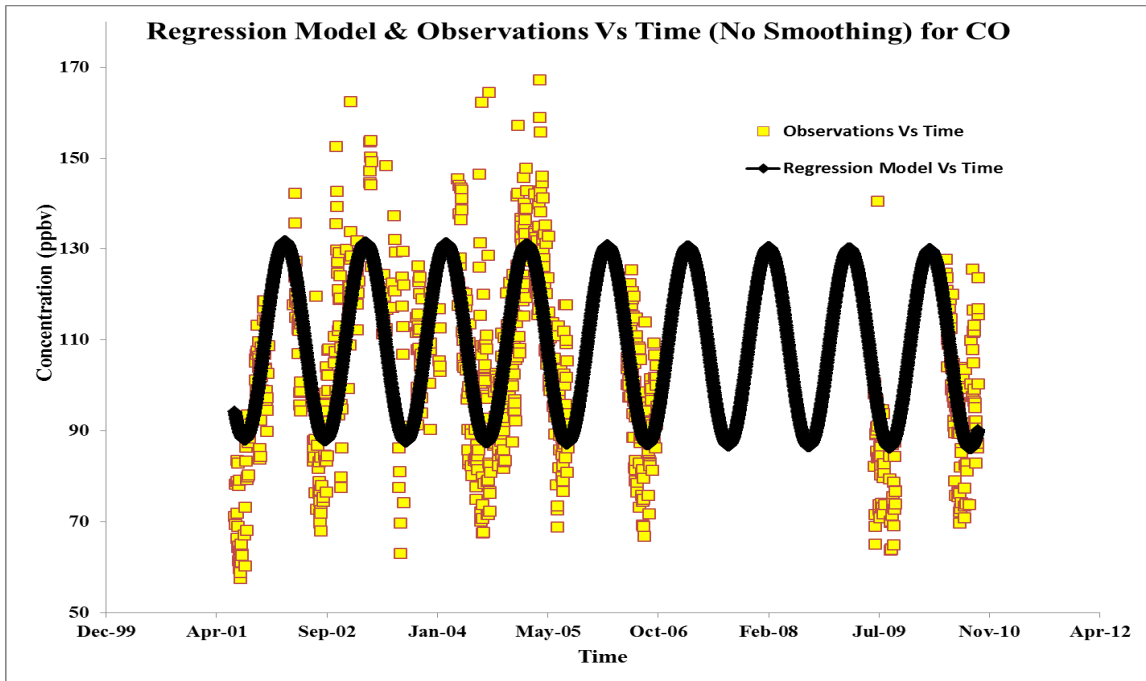


Figure 5.1: Regression model & observations V/s time for CO with no smoothing

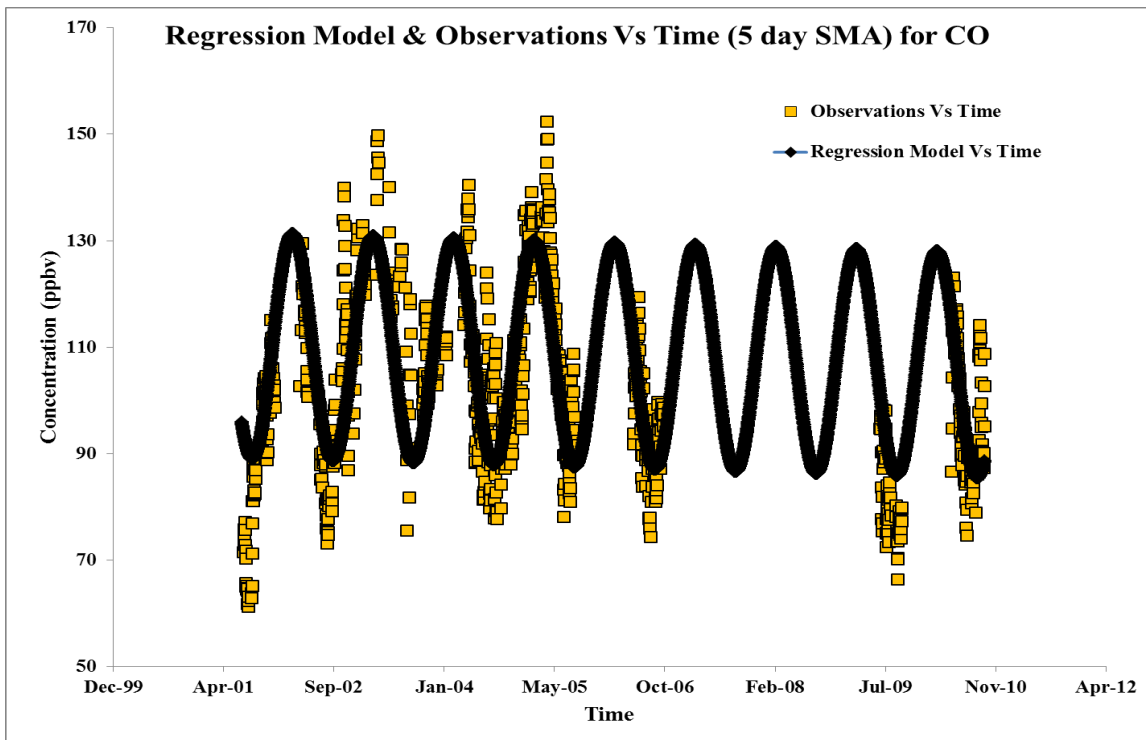


Figure 5.2: Regression model & observations V/s time for CO with 5 day SMA scheme

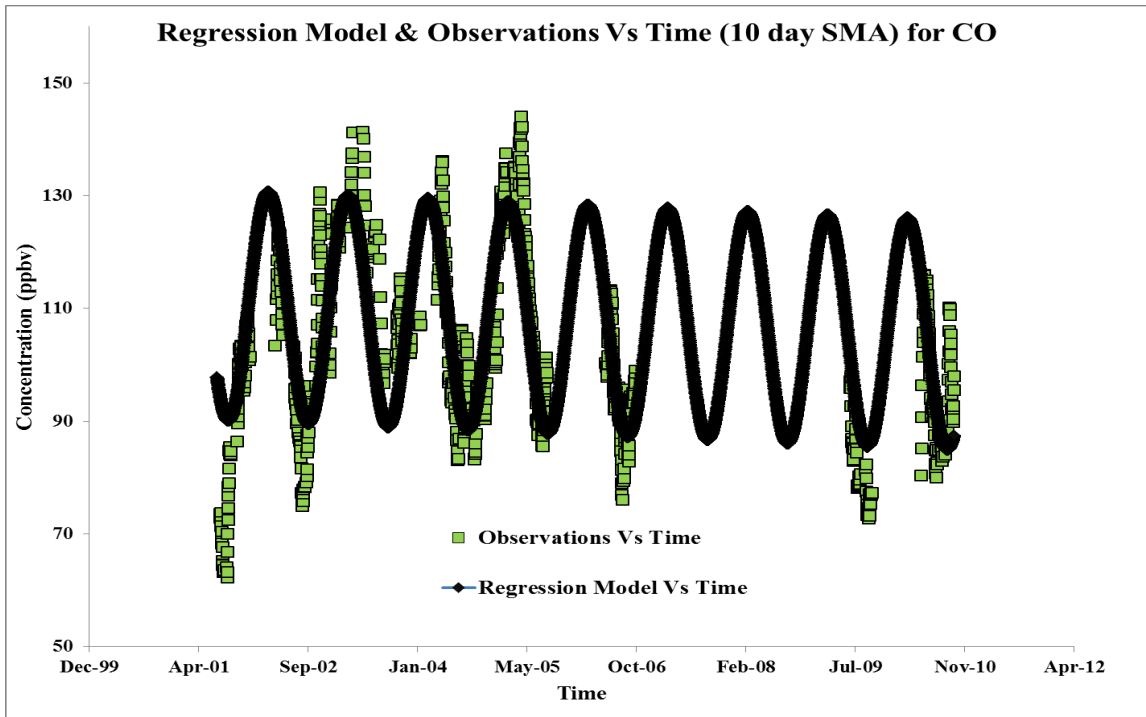


Figure 5.3: Regression model & observations V/s time for CO with 10 day SMA scheme

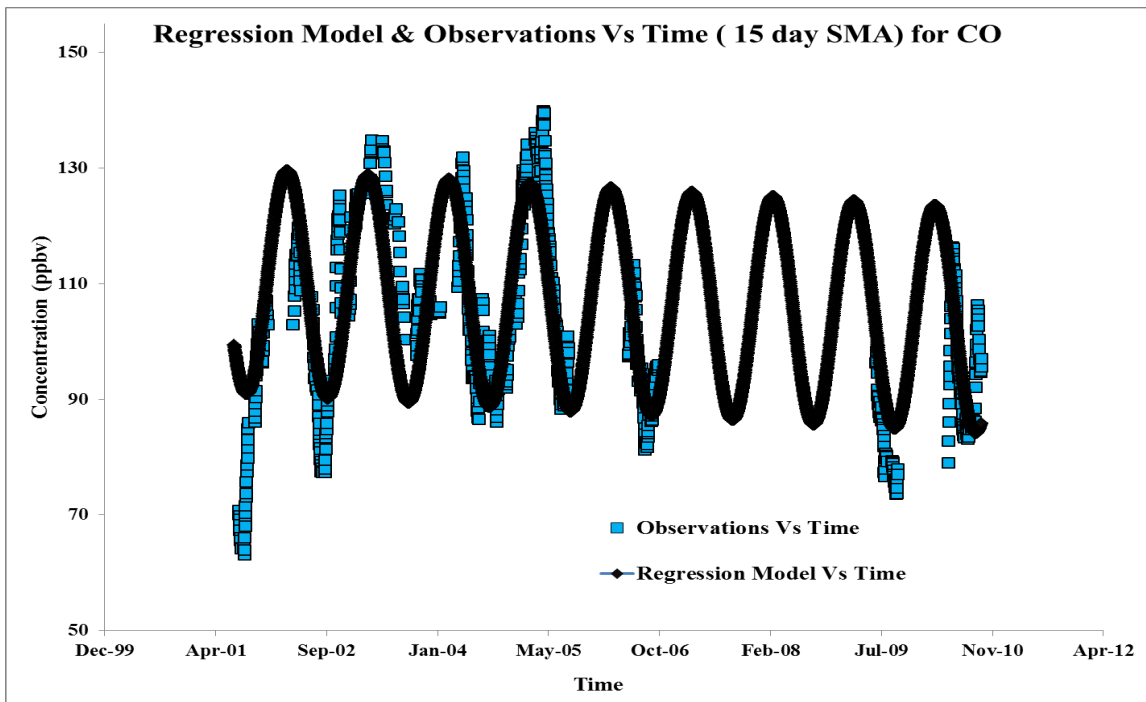


Figure 5.4: Regression model & observations V/s time for CO with 15 day SMA scheme

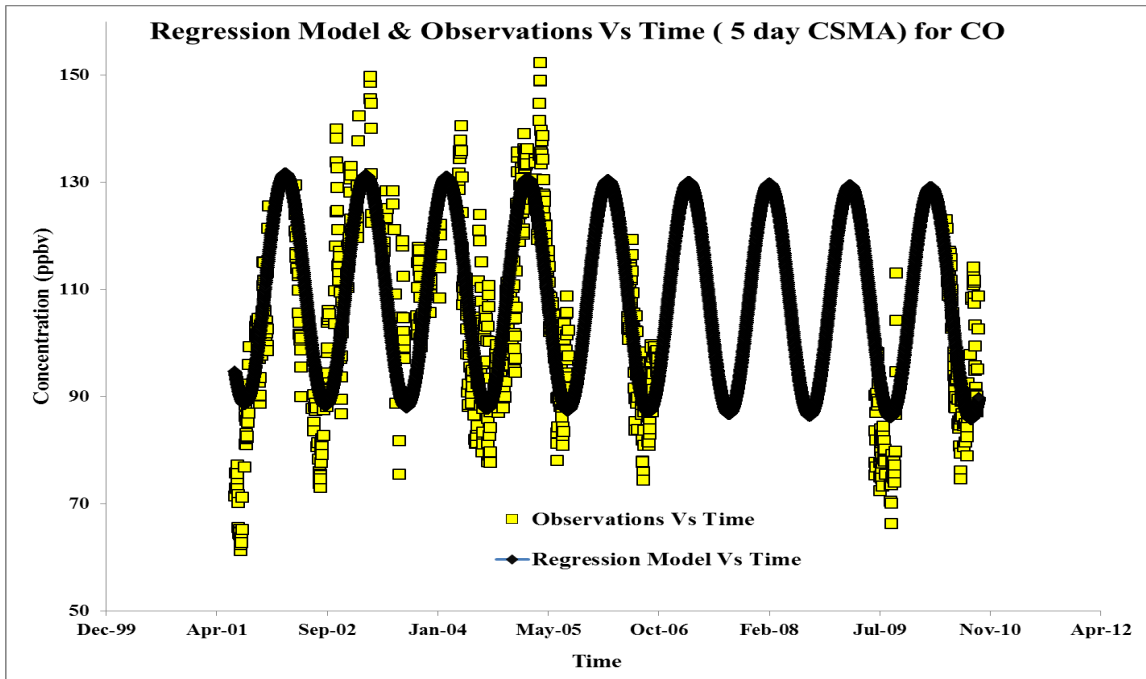


Figure 5.5: Regression model & observations V/s time for CO with 5 day CSMA scheme

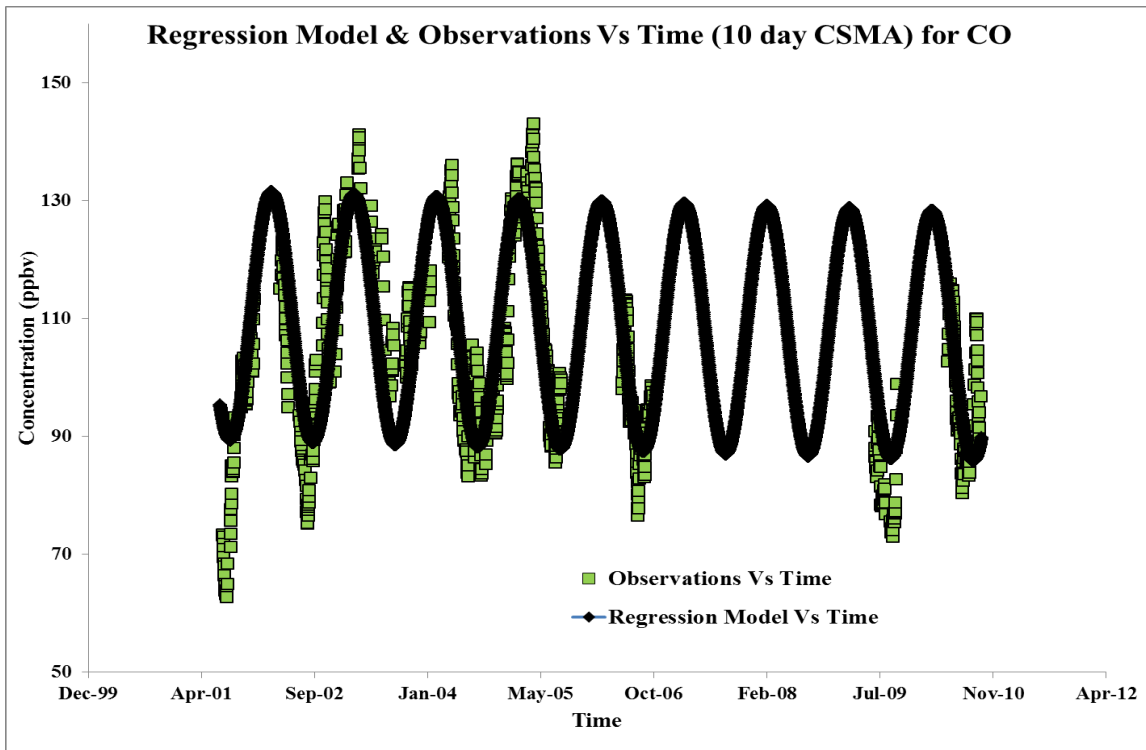


Figure 5.6: Regression model & observations V/s time for CO with 10 day CSMA scheme

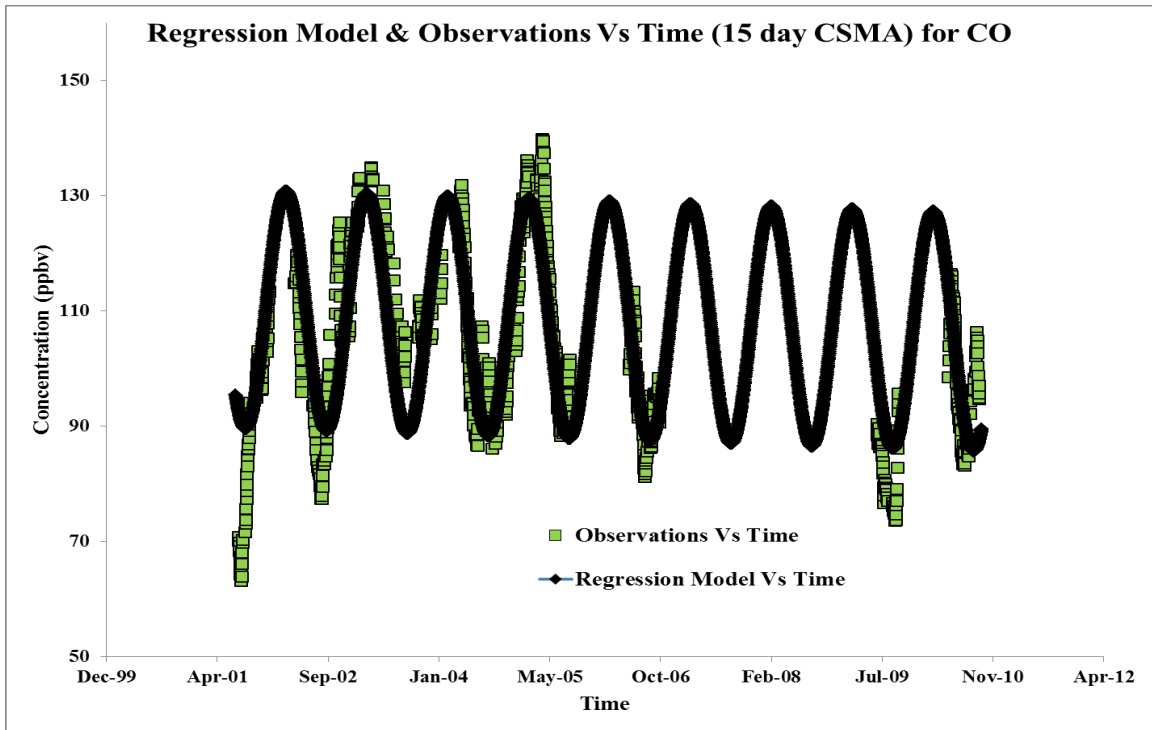


Figure 5.7: Regression model & observations V/s time for CO with 15 day CSMA scheme

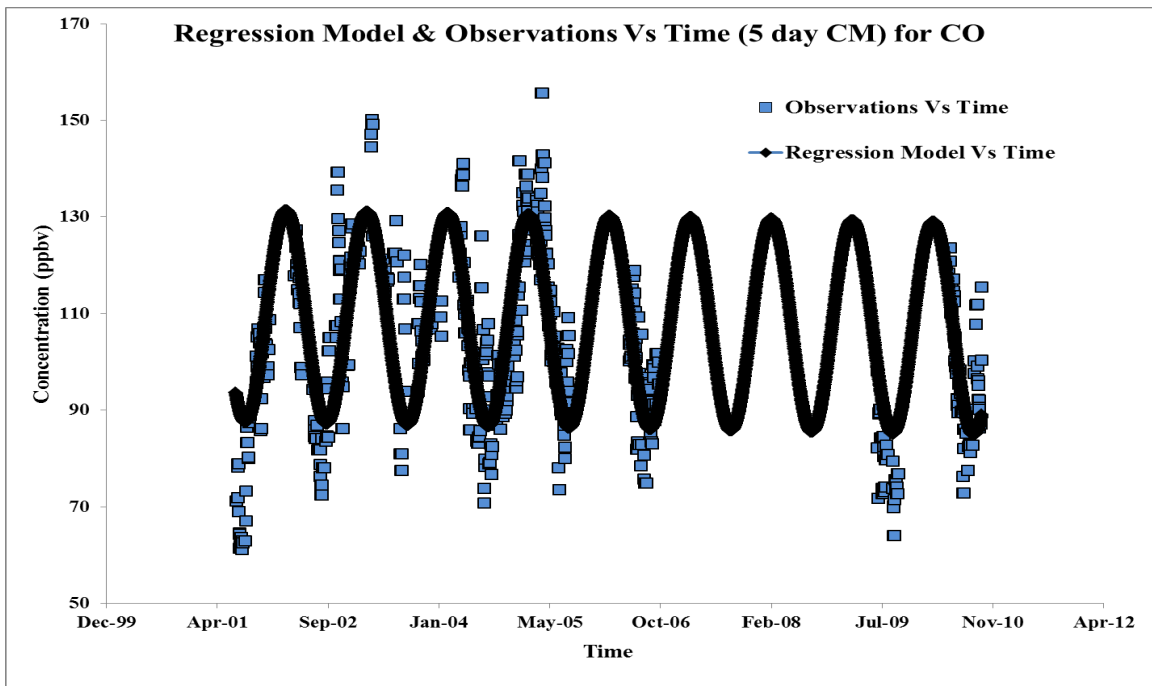


Figure 5.8: Regression model & observations V/s time for CO with 5 day CM scheme

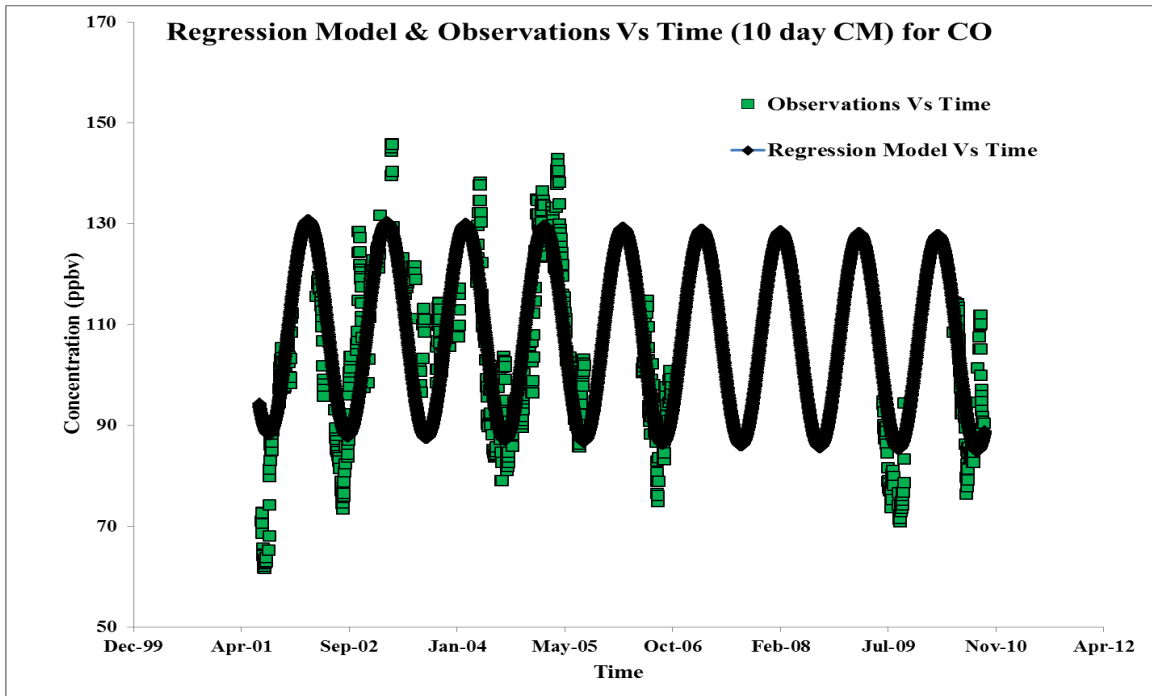


Figure 5.9: Regression model & observations V/s time for CO with 10 day CM scheme

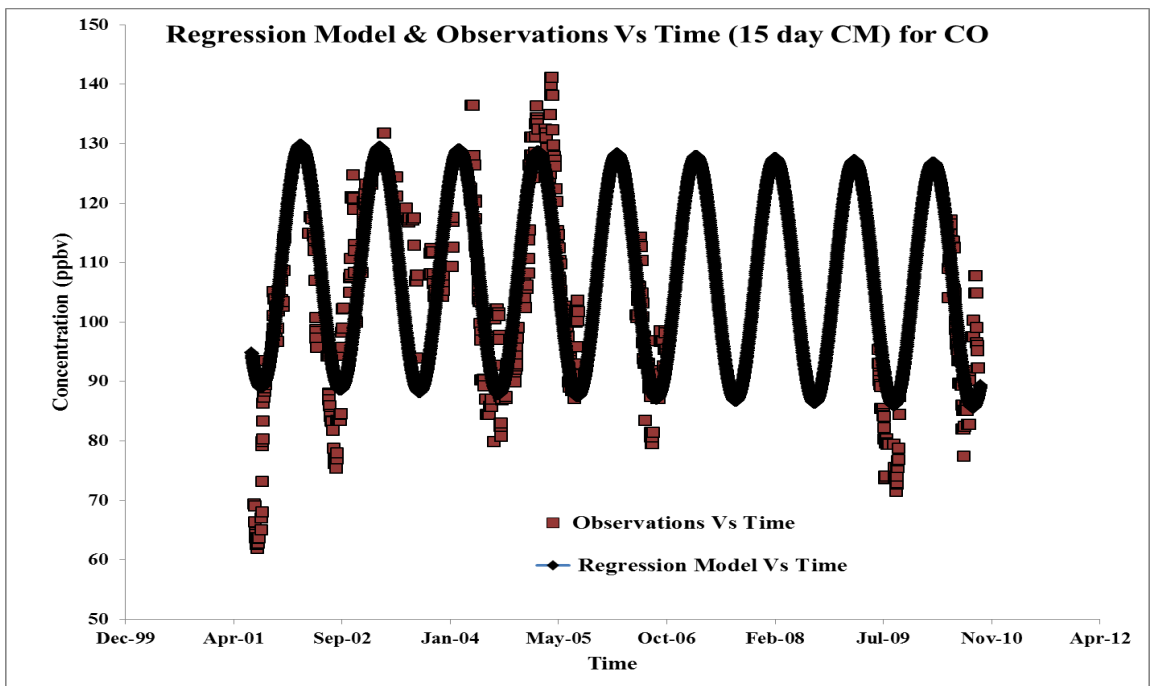


Figure 5.10: Regression model & observations V/s time for CO with 15 day CM scheme

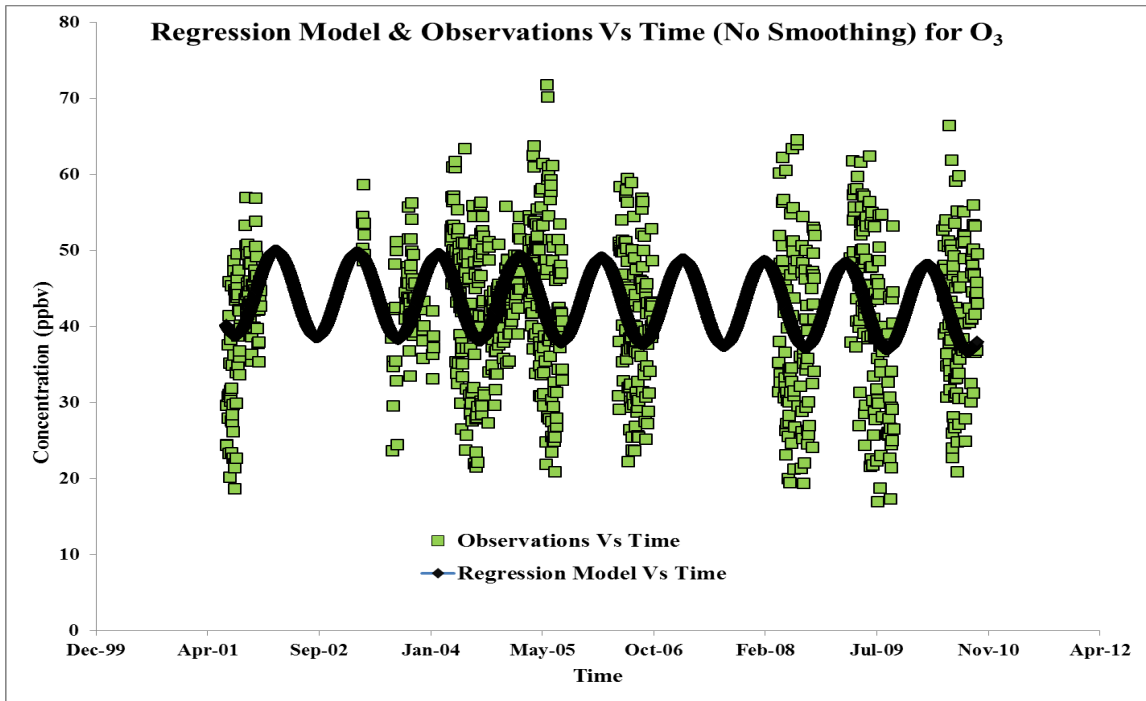


Figure 5.11: Regression model & observations V/s time for O₃ with no smoothing

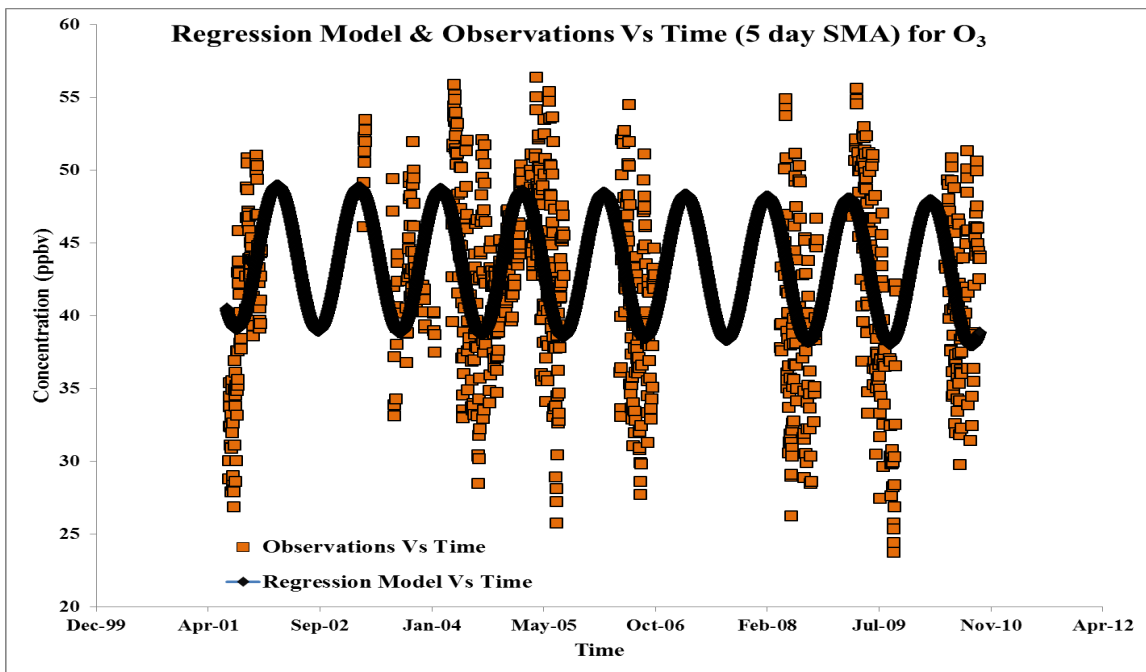


Figure 5.12: Regression model & observations V/s time for O₃ with 5 day SMA scheme

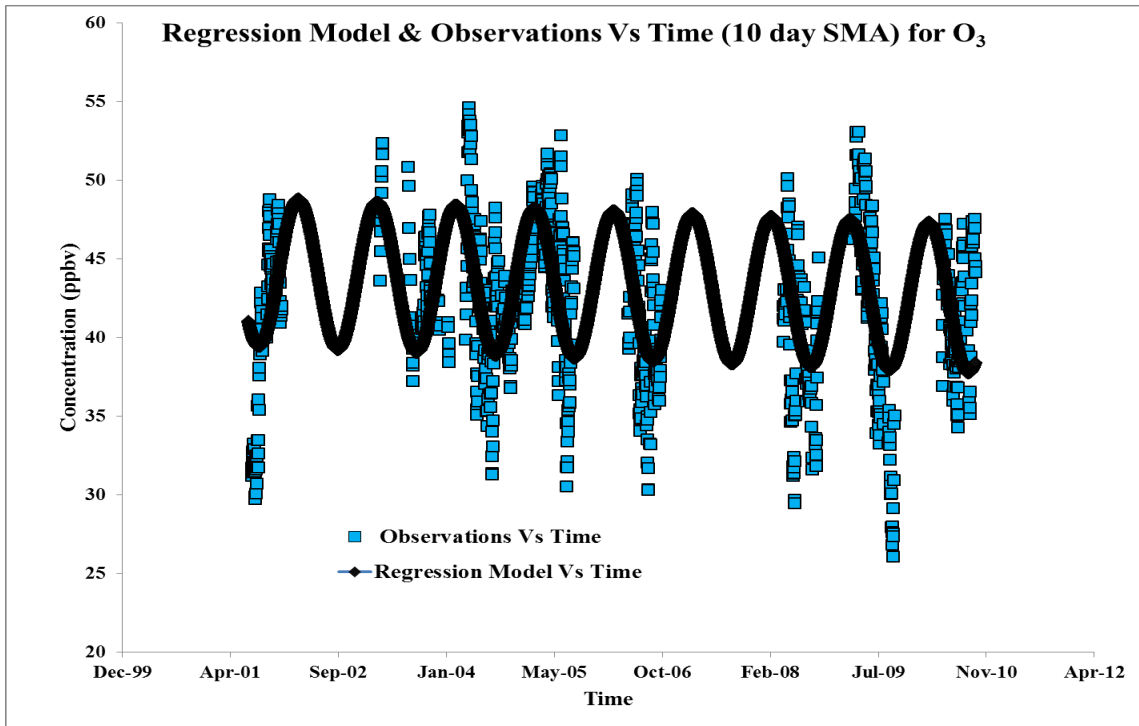


Figure 5.13: Regression model & observations V/st for O₃ with 10 day SMA scheme

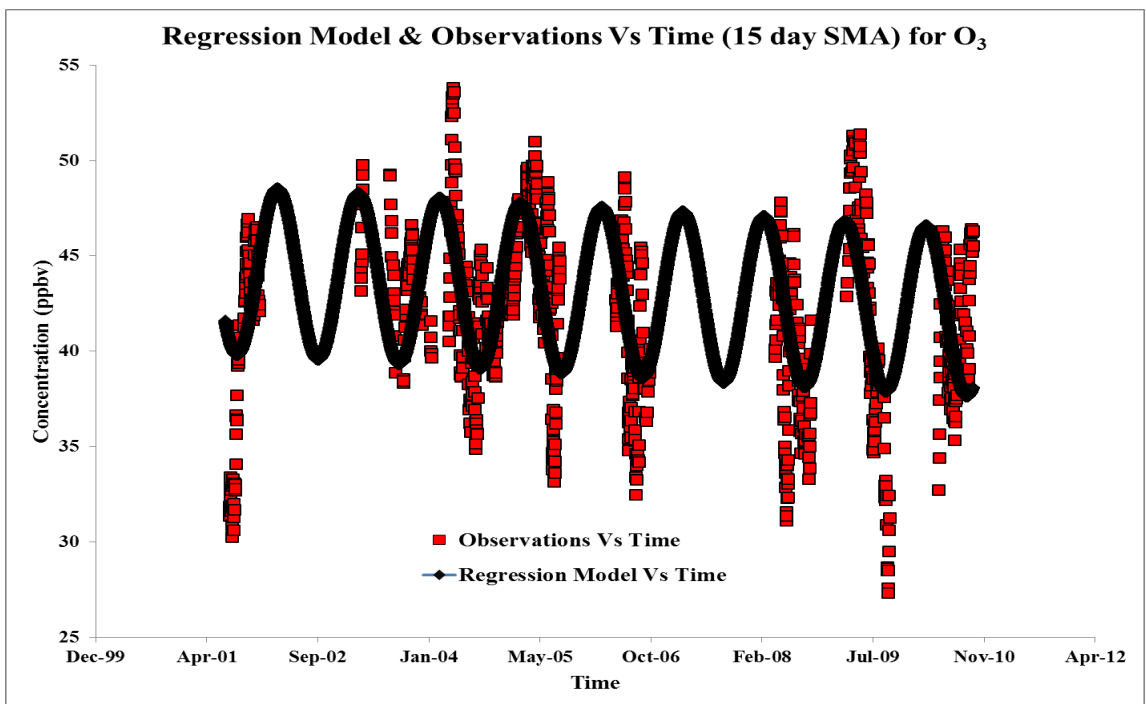


Figure 5.14: Regression model & observations V/s time for O₃ with 15 day SMA scheme

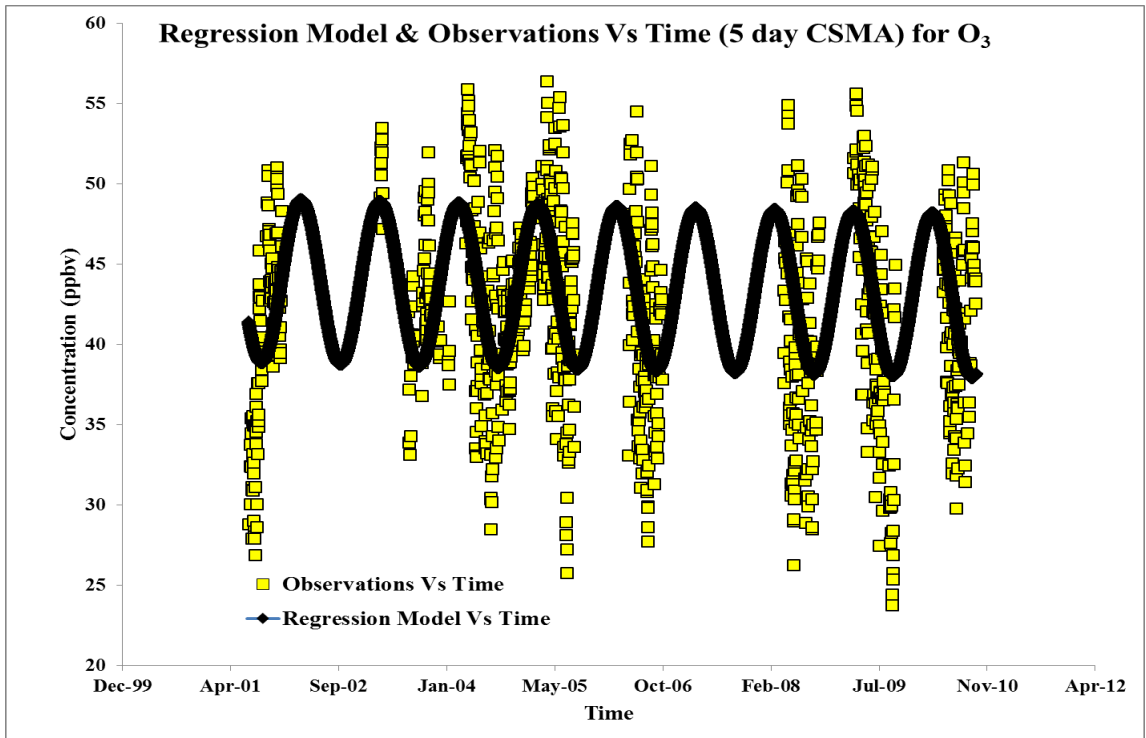


Figure 5.15: Regression model & observations V/s time for O₃ with 5 day CSMA scheme

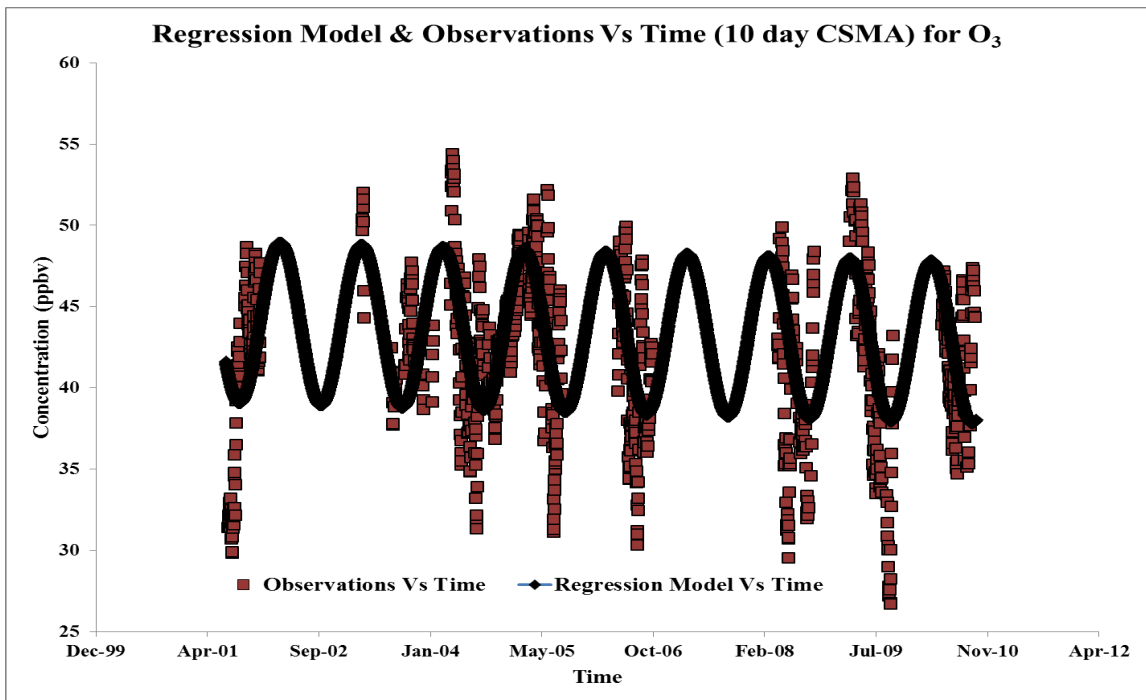


Figure 5.16: Regression model & observations V/s time for O₃ with 10 day CSMA scheme

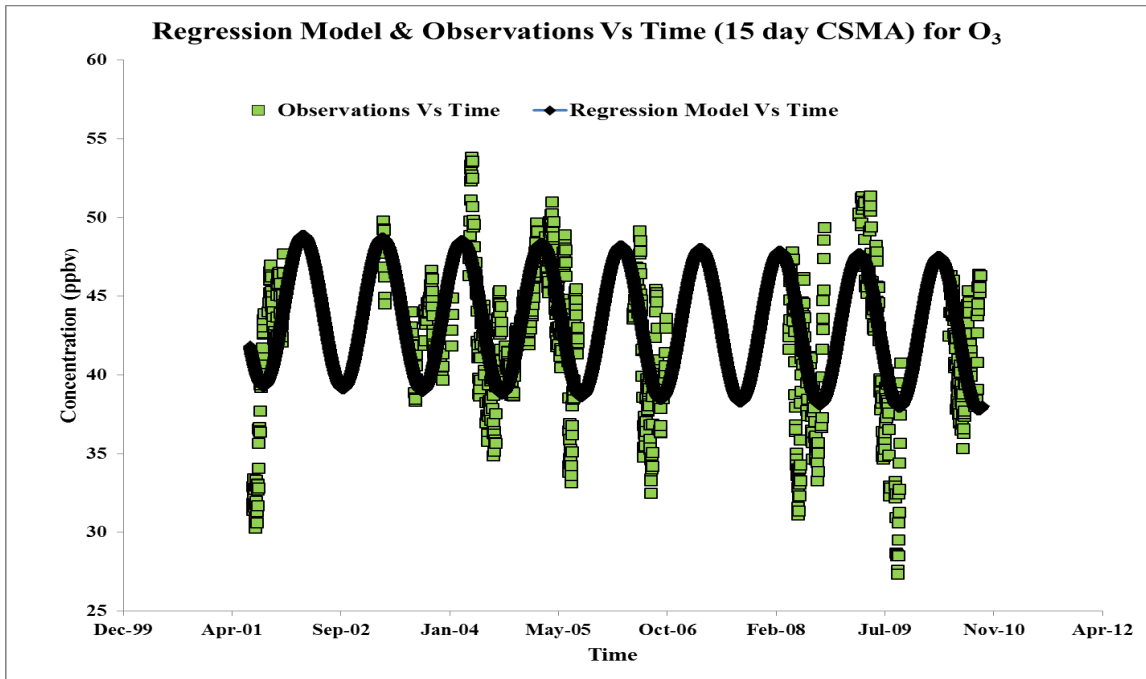


Figure 5.17: Regression model & observations V/s time for O₃ with 15 day CSMA scheme

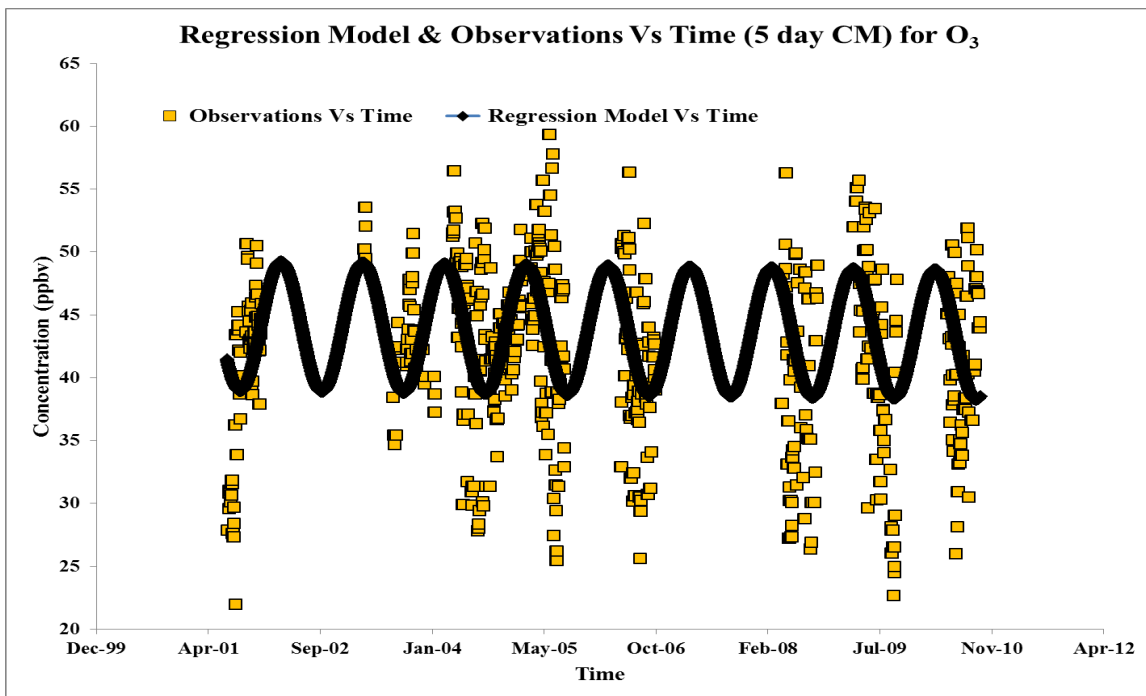


Figure 5.18: Regression model & observations V/s time for O₃ with 5 day CM scheme

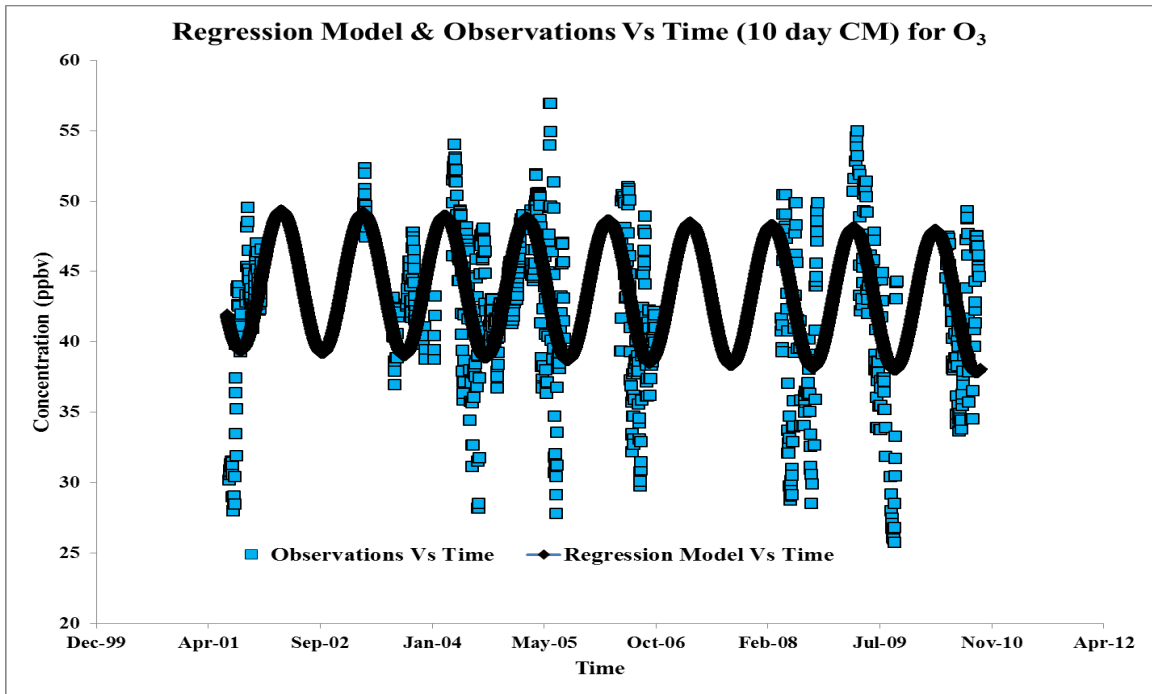


Figure 5.19: Regression model & observations V/s time for O₃ with 10 day CM scheme

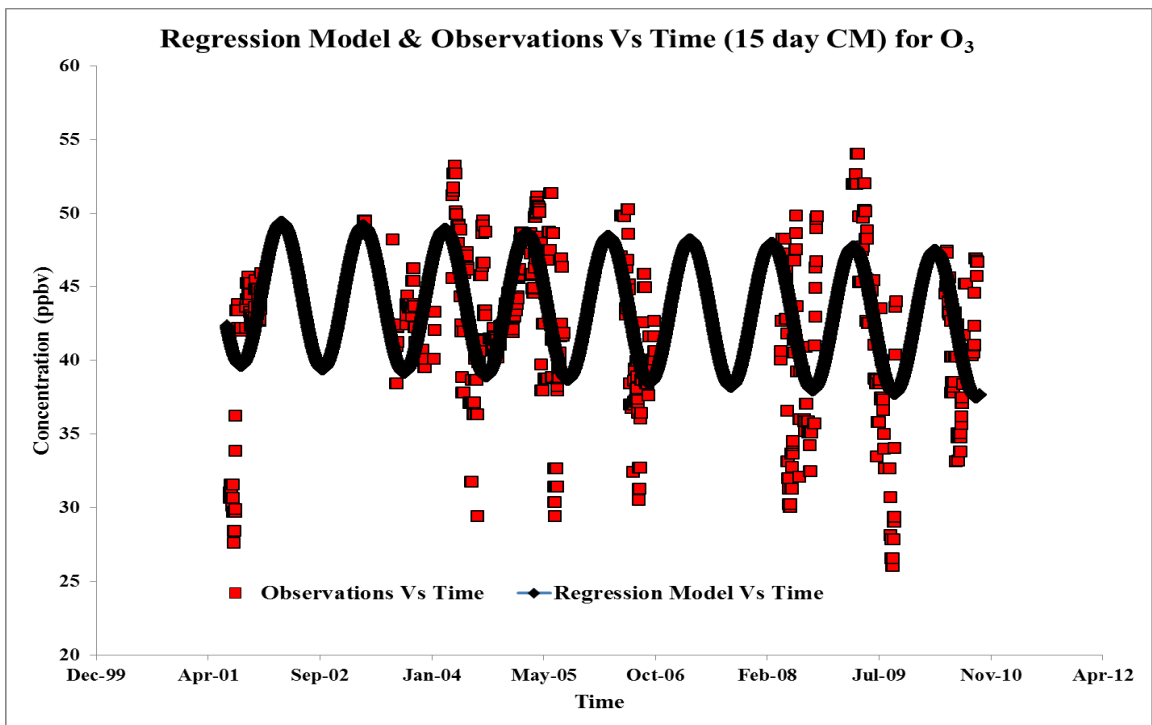


Figure 5.20: Regression model & observations V/s time for O₃ with 15 day CM scheme

Table 5.5: Statistics for the regression model fit to observations for CO at PICO-NARE (2001-2010)

Data	Intercept	Slope	Sine Coefficient	Cosine Coefficient	R²
No smoothing	131.78	-0.000589	21.53	3.82	0.434
5 day SMA	151.05	-0.001100	21.09	2.48	0.554
10 day SMA	168.77	-0.001573	20.40	0.97	0.597
15 day SMA	186.52	-0.002046	19.53	-0.48	0.605
5 day CSMA	142.10	-0.00086	21.28	3.68	0.568
10 day CSMA	150.19	-0.00107	20.84	3.63	0.630
15 day CSMA	154.83	-0.00120	20.42	3.57	0.653
5 day CM	139.19	-0.00080	21.68	3.85	0.534
10 day CM	146.60	-0.00100	21.01	3.57	0.598
15 day CM	147.32	-0.00102	20.23	3.44	0.605

Table 5.6: Statistics for the regression model fit to observations for O₃ at PICO-NARE (2001-2010)

Data	Intercept	Slope	Sine Coefficient	Cosine Coefficient	R²
No smoothing	50.61	-0.000180	5.02	1.25	0.102
5 day SMA	56.96	-0.000348	4.89	0.85	0.22
10 day SMA	62.86	-0.000505	4.72	0.42	0.311
15 day SMA	68.78	-0.000662	4.42	0.07	0.346
5 day CSMA	54.33	-0.00028	4.98	1.14	0.228
10 day CSMA	58.13	-0.00038	4.86	1.03	0.333
15 day CSMA	61.18	-0.00046	4.71	0.96	0.382
5 day CM	51.88	-0.00021	5.01	1.19	0.171
10 day CM	61.83	-0.00047	4.89	1.06	0.256
15 day CM	68.70	-0.00065	4.85	0.83	0.300

5.3. Analysis of PICO-NARE Observations & GEOS-Chem Full Chemistry (with Normal Emissions) Simulation Output using the Regression Model

This section presents the results of the regression model fit applied to the in-situ observations at PICO-NARE and GEOS-Chem full chemistry simulation (with normal emissions) output for Pico.

5.3.1. Regression fit to the PICO-NARE observations

Null Hypothesis: “No significant trends exist at PICO-NARE for both CO (2001-2010) & O₃ (2001-2011) or the slope term in the regression equation is equal to zero”

Alternate Hypothesis (one-sided): “Decreasing trends exist at PICO-NARE for both CO (2001-2010) & O₃ (2001-2011) or the slope term in the regression equation is significantly less than zero”

Figures 5.21 & 5.22 show the regression model fit to the Pico observations for CO (2001-2010) and O₃ (2001-2011) respectively with the regression statistics listed in Table 5.7. Table 5.8 lists the overall annual trends observed for both CO and O₃ along with their statistical significance. Decreasing trends are obtained for both the species at Pico over the period of study with CO showing a stronger trend (-0.314 ppbv/year) than O₃ (-0.208 ppbv/year). Since transport of pollution from upwind regions is the only source of CO to Pico, a decreasing trend in CO could point towards a decrease in the transport of CO from both anthropogenic sources as well as biomass burning from upwind regions. This decreasing trend also corresponds to the decrease in the anthropogenic emissions in the US. A decreasing trend in O₃ indicates a decrease in the O₃ being transported to or

being formed at Pico. In the absence of anthropogenic influence, O_3 destruction would be expected over the oceans considering the high amount of water vapor present. However, in the case of increasing anthropogenic precursors, this destruction could be offset by a corresponding increase in the production of O_3 and could result in a net production of O_3 over the oceans. This balance could also be affected by changes in meteorological factors due to long term climate change such as increase in humidity which would further enhance the destruction of O_3 . If it can be assumed that there has been no significant influence due to climate change over this period, it can be stated that the decrease in O_3 could be due to a decrease in the transport of O_3 and its precursors from source regions.

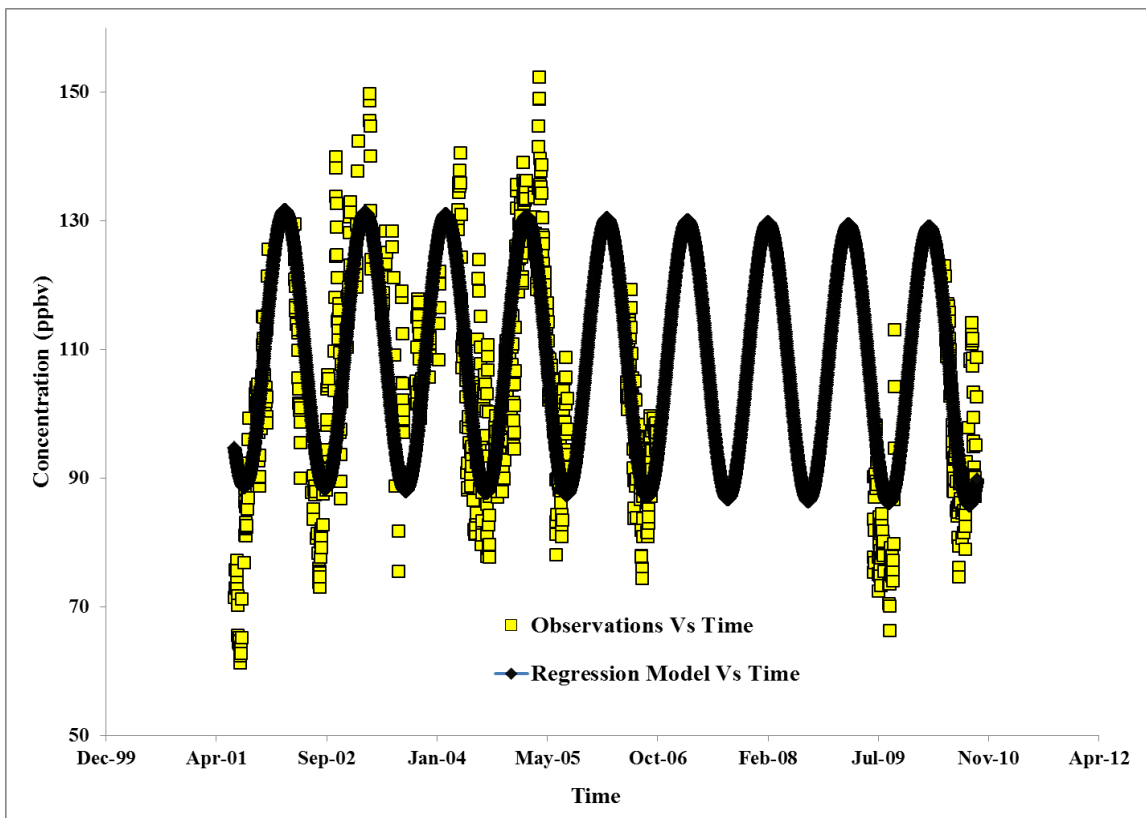


Figure 5.21: Regression model fit to the Pico observations for CO (2001-2010)

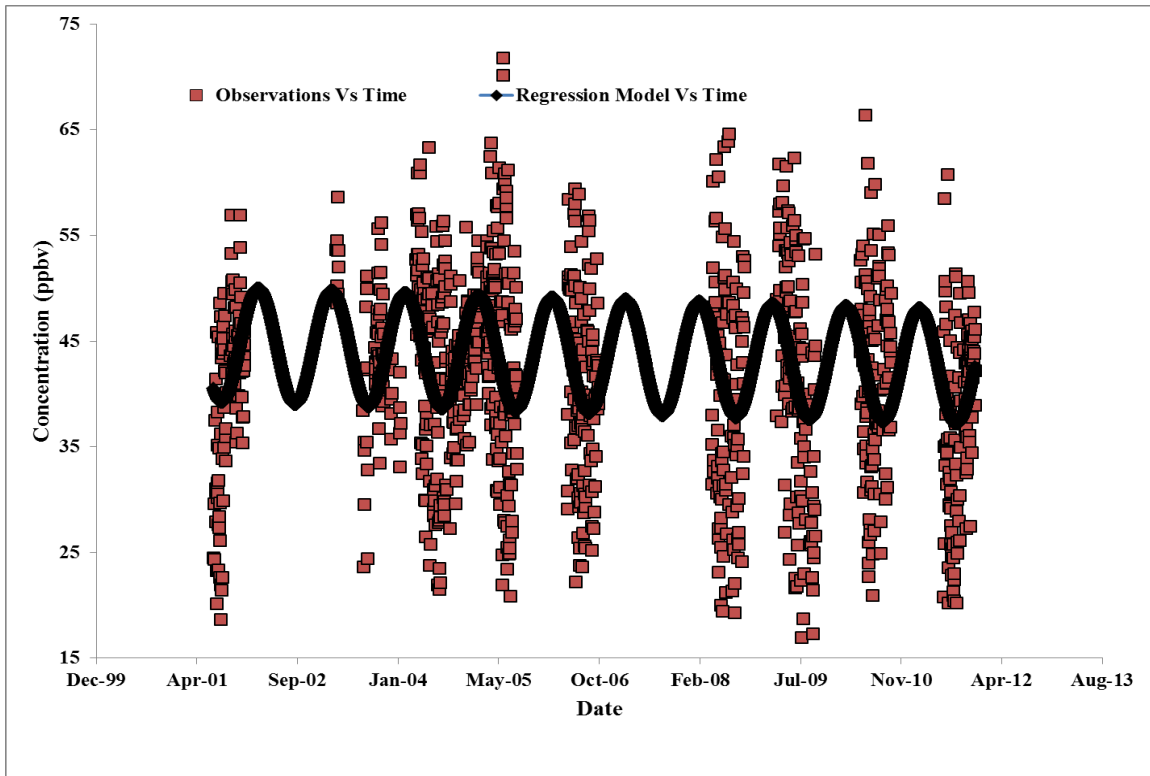


Figure 5.22: Regression model fit to the Pico observations for O₃ (2001-2011)

Table 5.7: Statistics for the regression fit to the Pico observations for CO (2001-2010) and O₃ (2001-2011)

Species	Intercept	Slope	Sine coefficient	Cosine coefficient	R ²
CO	142.10	-0.00086	21.28	3.68	0.57
O ₃	65.80	-0.00057	4.57	2.94	0.26

Table 5.8: Trends obtained for CO (2001-2010) and O₃ (2001-2011) from observations at Pico

Species	Trend (ppbv/year)	P-value (one-sided test)	Significance @ $\alpha=0.05$
CO	-0.314	0.022	Significant
O ₃	-0.208	0.0001	Significant

5.3.2. Regression Fit to GEOS-Chem Output from the Full Chemistry Simulation with Normal Emissions

Null Hypothesis: “No significant trends exist at PICO-NARE for both CO (2001-2010) & O₃ (2001-2011) or the slope term in the regression equation is equal to zero”

Alternate Hypothesis (one-sided): “Decreasing trends exist at PICO-NARE for both CO (2001-2010) & O₃ (2001-2011) or the slope term in the regression equation is significantly less than zero”

Figures 5.23 & 5.24 show the regression model fit to the GEOS-Chem output for CO (2001-2010) and O₃ (2001-2011) respectively with the regression statistics listed in Table 5.9. Table 5.10 lists the overall annual trends for both CO and O₃ along with their statistical significance. Similar to the observations, decreasing trends were observed for GEOS-Chem output as well which further strengthens the findings with the observations. CO shows a similar annual trend of -0.343 ppbv/year, which is very close to the decrease observed with the observations. This could be due to the decrease in the anthropogenic emissions over the period of study being represented well by the emission inventories being used by the model. O₃, on the other hand shows a larger decrease of -0.526 ppbv/year. This greater decrease in O₃ as compared to CO could point to the fact that in addition to the decrease in anthropogenic emissions, there could be influence of the long term change of meteorology on the concentrations of O₃ in the model. Studying this aspect requires a different approach which would involve eliminating the effects of the anthropogenic emissions and ascertaining the long term change in concentrations of O₃ over Pico. Any changes in concentrations observed in this case would be solely due to long term changes in the background meteorological parameters such as specific

humidity. The fixed emissions simulation used in this study as described earlier has been utilized for this purpose. Results obtained from it would be discussed in later sections.

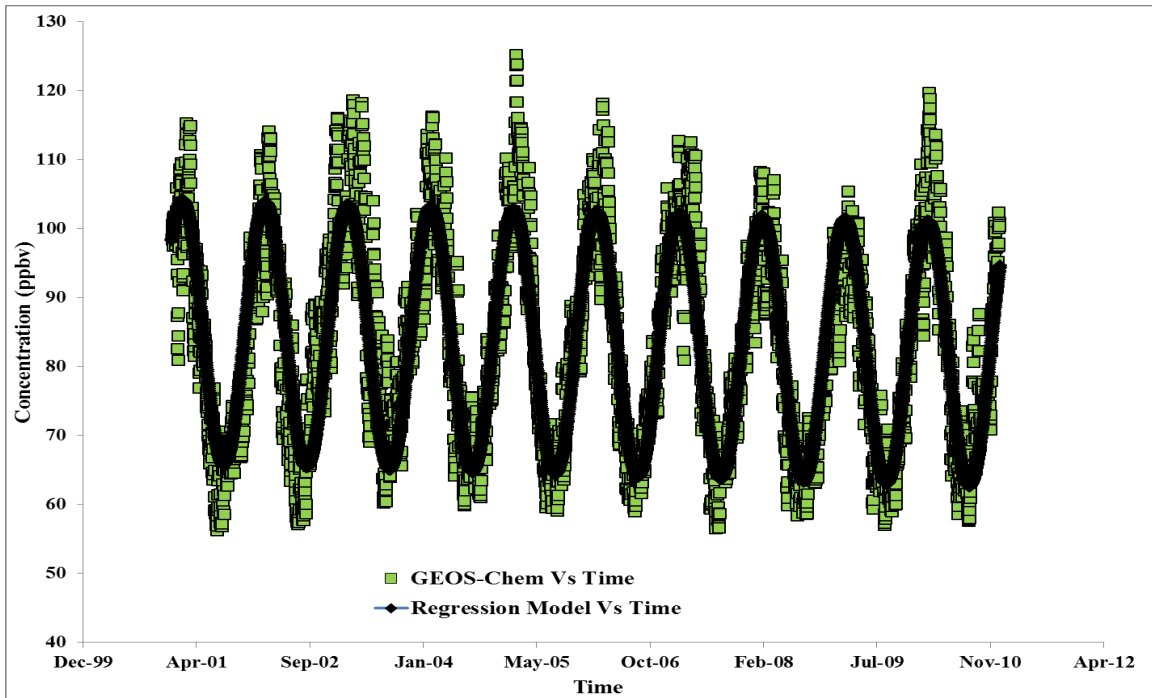


Figure 5.23: Regression model fit to the GEOS-Chem output (from full chemistry simulation with normal emissions) for CO (2001-2010)

Table 5.9: Statistics for the regression fit to the GEOS-Chem output (full chemistry with normal emissions) for CO (2001-2010) and O₃ (2001-2011)

Species	Intercept	Slope	Sine coefficient	Cosine coefficient	R ²
CO	119.74	-0.00094	15.60	11.09	0.79
O ₃	104.00	-0.00144	3.52	-1.49	0.35

Table 5.10: Trends obtained for CO (2001-2010) and O₃ (2001-2011) from the GEOS-Chem output (full chemistry with normal emissions)

Species	Trend (ppbv/year)	P-value (one-sided test)	Significance at $\alpha=0.05$
CO	-0.3431	1.75E-17	Significant
O ₃	-0.5256	4.63E-113	Significant

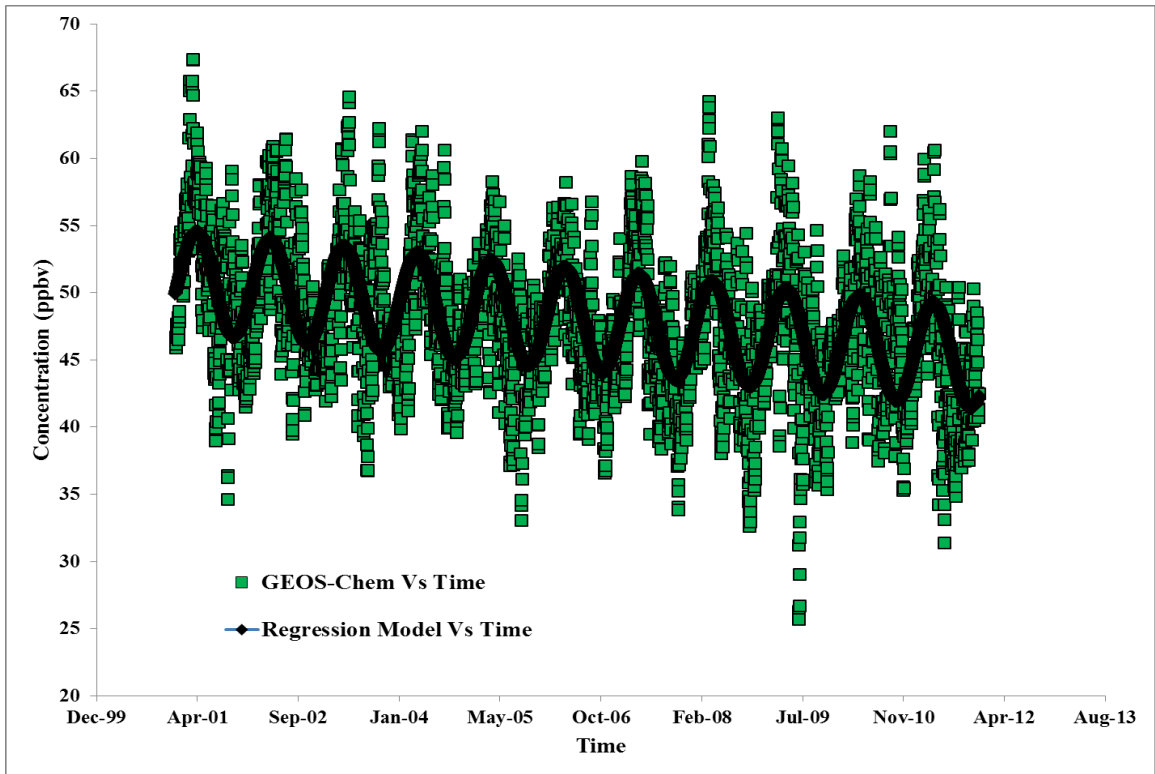


Figure 5.24: Regression model fit to the GEOS-Chem output (from full chemistry simulation with normal emissions) for O₃ (2001-2011)

5.4. Results from Regression Analysis of the Output from GEOS-Chem Full Chemistry Simulation (with Fixed Anthropogenic Emissions)

5.4.1. Trends for CO and O₃ at PICO-NARE

Null Hypothesis: “No significant trends exist at PICO-NARE for both CO (2001-2010) & O₃ (2001-2011) or the slope term in the regression equation is equal to zero”

Alternate Hypothesis (two-sided): “Significant (Increasing/Decreasing) trends exist at PICO-NARE for both CO (2001-2010) & O₃ (2001-2011) or the slope term in the regression equation is significantly different (greater/less) than zero”

Similar to the full chemistry simulation with normal emissions, the instantaneous CO (2001-2010) and O₃ (2001-2011) concentrations at Pico were archived at a time-step of 4 hours. Table 5.11 shows the statistics of the regression fit to CO and O₃ and Table 5.12 lists the statistical significance of the trends for both species. The regression fit plots are shown in Figures 5.25 & 5.26. As compared to the full chemistry simulation with normal emissions, the decrease in O₃ is larger whereas CO shows an increase of a greater magnitude than the decrease observed earlier. Since the anthropogenic emissions are held constant, a larger decrease in O₃ indicates a greater influence of climate change on its concentrations at Pico. This implies that this large decrease due to change in climate was offset by an increase in O₃ production, resulting in a lower net decrease which was observed earlier (sections 5.3.1 & 5.3.2). As the North American anthropogenic emissions have shown a decrease, the increase in O₃ production could be due to the

influence of Asian precursor emissions as well as increase in NO_x contribution from other (e.g. lightning) sources. The NO_x from these sources affects the O₃ concentrations in the fixed emissions simulation as well. In both simulations, the destruction of O₃ due to change in water vapor appears to be the dominant factor resulting in a decreasing trend in O₃ for both. Hence ascertaining the trends in NO_x from sources other than anthropogenic fossil fuel combustion and humidity change in the region extending from NA to Pico becomes imperative to clearly understand the factors other than anthropogenic emission changes that contribute to the observed trends in O₃. The increasing trend in CO could be due to corresponding increases in biogenic emissions of VOCs or change in the OH/CH₄ concentrations which significantly influence CO budgets. Hence, trends in these would have to be determined to account for the increase in CO.

Table 5.11: Regression statistics for CO and O₃ at Pico for full chemistry simulation with fixed anthropogenic emissions

Data	Intercept	Slope	Sine coefficient	Cosine coefficient	R²
CO	31.65	0.0015	19.16	12.57	0.80
O ₃	112.35	-0.0017	2.72	-1.29	0.28

Table 5.12: Trends for CO and O₃ at Pico for full chemistry simulation with fixed anthropogenic emissions

Data	Trend (ppbv/year)	P-value (two-sided test)	Significance at $\alpha=0.05$
CO	0.564	6.66E-33	Significant
O ₃	-0.613	1.31E-135	Significant

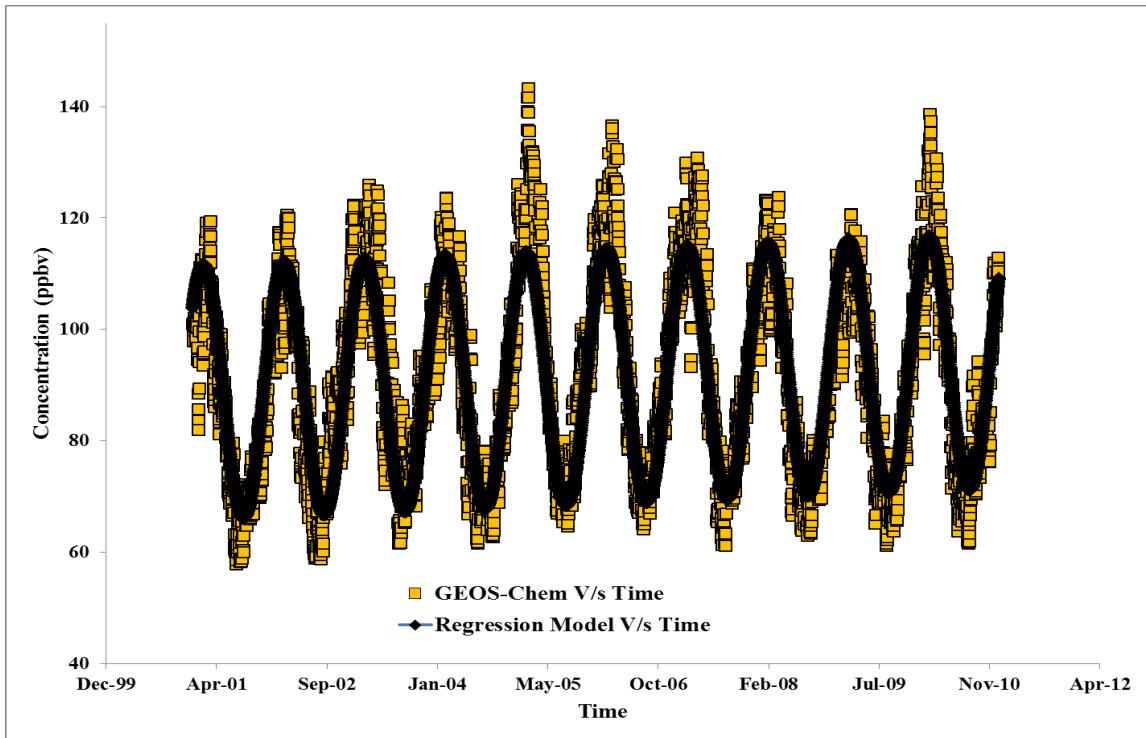


Figure 5.25: Regression model fit to CO (2001-2010) at Pico for full chemistry simulation with fixed anthropogenic emissions

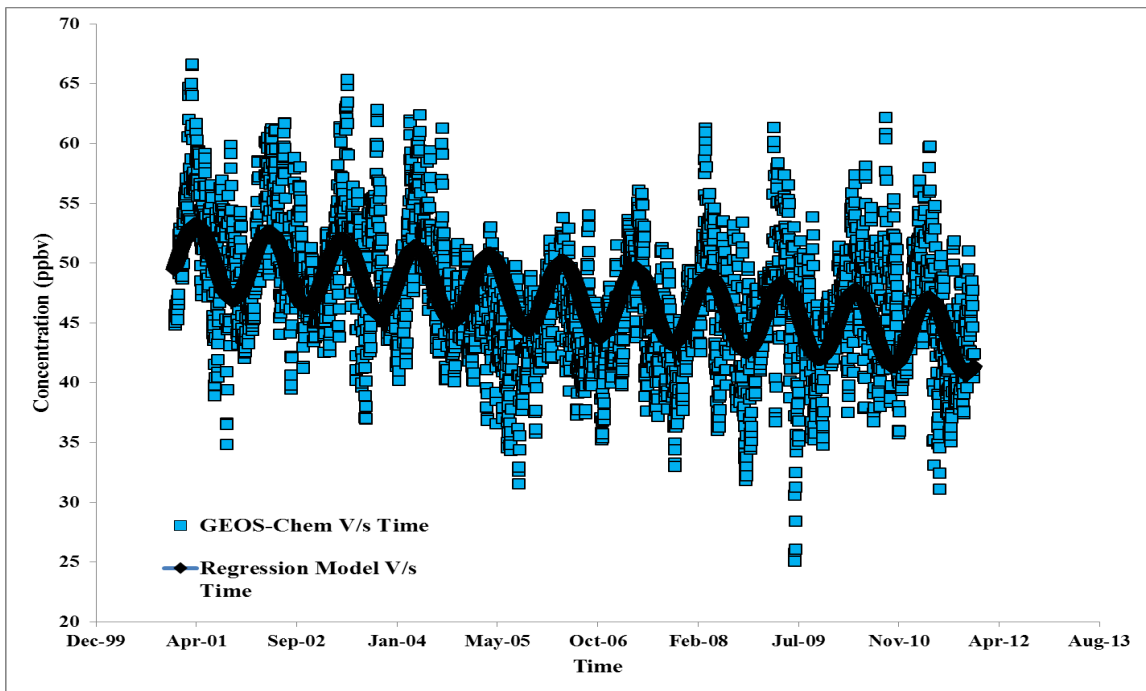


Figure 5.26: Regression model fit to O₃ (2001-2011) at Pico for full chemistry simulation with fixed anthropogenic emissions

5.5. Regression Analysis of output from the GEOS-Chem Tagged CO Simulation

The regression model in Eq. 4.21 was fit to the time-series output for PICO-NARE from the tagged CO simulation in GEOS-Chem. The null & alternate hypotheses are stated below. Since the anthropogenic emission trends for CO from USA and Asia were well known [Ohara *et al.*, 2007]; (<http://www.epa.gov/airtrends/2010/>), a one-sided alternate hypothesis was used for CO from fossil fuel combustion in these regions whereas for all the other sources/regions, a two-sided hypothesis was used.

Null Hypothesis: “There exists no trend in the CO (from source X & region X) at PICO-NARE over the period 2001-2010 or the slope term in the regression equation is not significantly different from zero”

Alternate Hypothesis (one-sided): “There exists a decreasing trend in the CO (from USA) at PICO-NARE over the period 2001-2010 or the slope term in the regression equation is significantly less than zero”

Alternate Hypothesis (one-sided): “There exists an increasing trend in the CO (from Asia) at PICO-NARE over the period 2001-2010 or the slope term in the regression equation is significantly greater than zero”

Alternate Hypothesis (two-sided): “There exists a significant trend (increasing/decreasing) in the CO (from source X & region X) over the period 2001-2010 or the slope term in the regression equation is significantly different (greater/less) from zero”

Table 5.13 lists the regression statistics for the different tracers whereas Table 5.14 contains the trends and their significance. The anthropogenic (fossil fuel combustion) CO at Pico from USA has shown a significant decrease whereas that from Asia has increased over the period of study which is consistent with the emission trends in the two regions. CO from biomass burning in Europe (which includes parts of Russia, according to the definition of the region in the simulation) and USA has decreased and that from Asia has increased. Thus, the Asian contribution has increased the CO concentrations at Pico but it seems that the simultaneous decrease in CO emissions from the US and Europe has had a greater impact resulting in an overall decreasing CO trend obtained from the observations and the full chemistry simulation with normal emissions. Also, the decrease in CO from global biofuel emissions and biomass burning in NA and Europe further support the decreasing CO trends. The CO production from CH₄ has also shown a significant increase. Since the tagged CO simulation uses fixed OH concentrations, but does incorporate the yearly variations in CH₄ concentrations, this result points to an increase in CO due to increasing CH₄ concentrations. Figures 5.27 to 5.30 show the regression fits for CO at Pico due to anthropogenic (fossil fuel) emissions from USA, anthropogenic (fossil fuel) emissions from Asia, global CH₄ oxidation and global biofuel emissions respectively. Figure 5.30 shows very high CO concentrations at Pico before April 2001 as compared to subsequent years. Since transport from continents would be the only source of CO due to biofuel in the North Atlantic, greater transport of CO produced over continents (due to biofuel emissions) to Pico during those months could be the cause behind the high concentrations. Figures 5.31 & 5.32 show the CO

emissions due to biofuels for the months of January and April 2001 while CO concentrations due to biofuels for the months of January – April 2001 are shown in Figures 5.33 and 5.34. It can be seen that Europe has greater biofuel emissions as compared to North America and also the highest CO concentrations. Hence transport from it could be the dominant source of biofuel CO at Pico. Figures 5.33 and 5.34 also show a decrease in the concentrations observed over the North Atlantic region in April 2001 as compared to the previous months in the year suggesting that pollution was transported more effectively from Europe during those months as compared to the subsequent months. Moreover, concentrations quite close to January-March 2001 were observed at a similar time in 2005 (Figure 5.30) as well. Thus, variability in transport could be the reason behind this observed anomaly.

Table 5.13: Regression statistics for the fit to CO concentrations (from various sources) at Pico (2001-2010)

Species	Intercept	Slope	Sine coefficient	Cosine coefficient	R ²
CO(USA)	45.34	-0.00073	5.15	2.65	0.46
CO(Asia)	-19.68	0.00096	8.34	4.67	0.84
CO(bb Asia)	-4.54	0.00014	0.98	-0.49	0.52
CO(bb Europe)	34.25	-0.00082	-1.74	-0.16	0.25
CO(bb North America)	5.46	-8.9E-05	-1.75	-0.85	0.33
CO(Methane)	17.18	0.00035	-1.39	-0.76	0.81
CO (Biofuels)	10.71	-0.00018	1.76	1.35	0.74

Table 5.14: Trends obtained for CO (from different sources) at Pico (2001-2010)

Species	Trend (ppbv/year)	P-value (Two-sided test)	Significance @ $\alpha = 0.05$
CO(USA)	-0.2670	9.2E-24	Significant
CO(Asia)	0.3510	6.29E-89	Significant
CO(bb Asia)	0.0510	5.02E-32	Significant
CO(bb Europe)	-0.2981	7.92E-88	Significant
CO(bb North America)	-0.0325	0.0037	Significant
CO(Methane)	0.1278	6.66E-261	Significant
CO (Biofuels)	-0.0657	5.71E-32	Significant

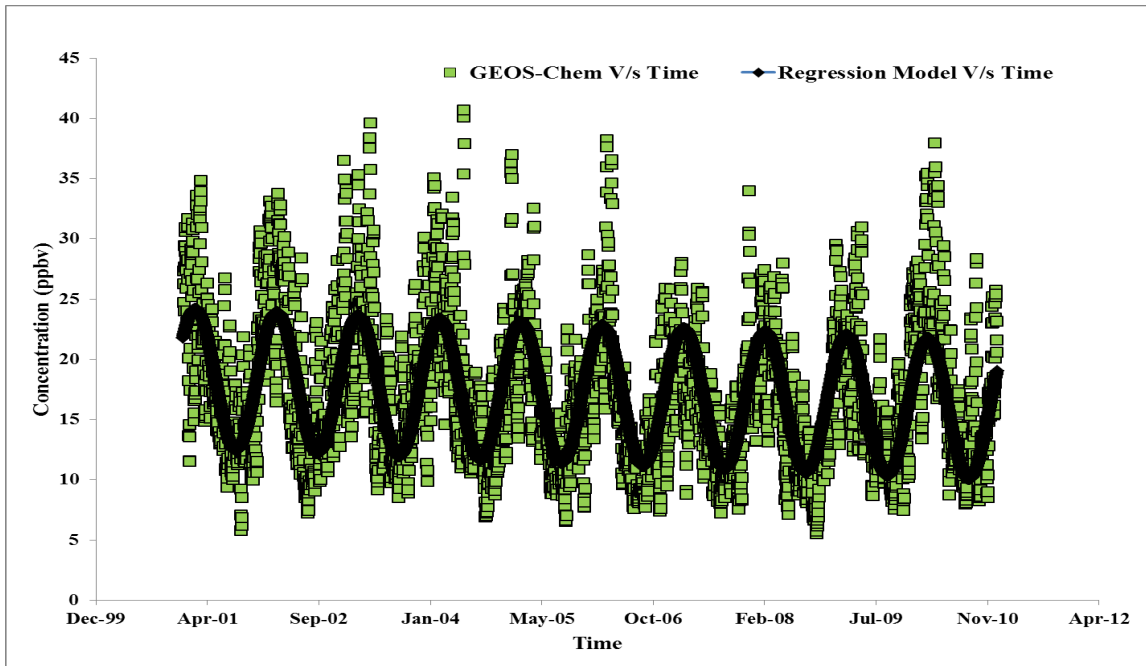


Figure 5.27: Regression fit for CO at Pico from anthropogenic (fossil fuel) emissions in USA

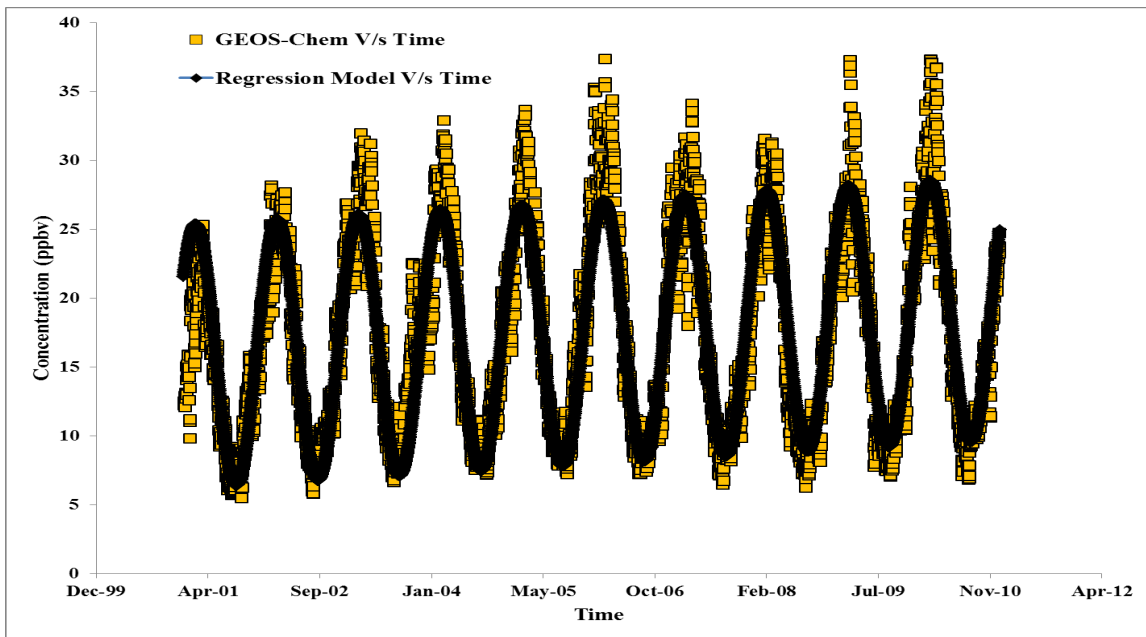


Figure 5.28: Regression fit for CO at Pico from anthropogenic (fossil fuel) emissions in Asia

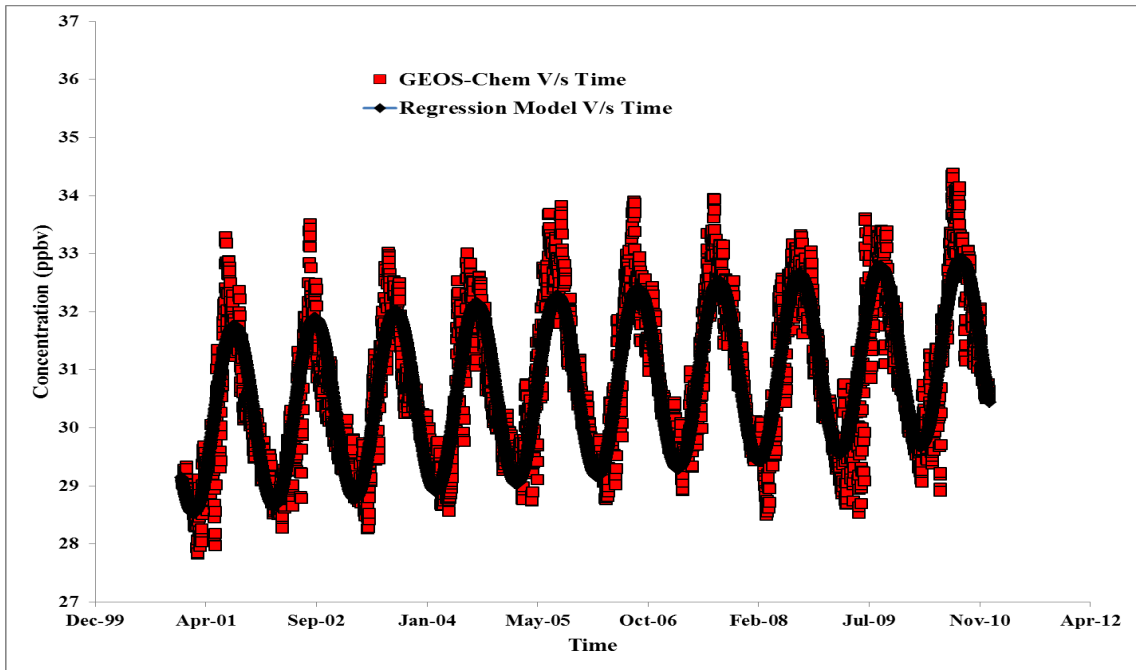


Figure 5.29: Regression fit for CO at Pico due to global Methane oxidation

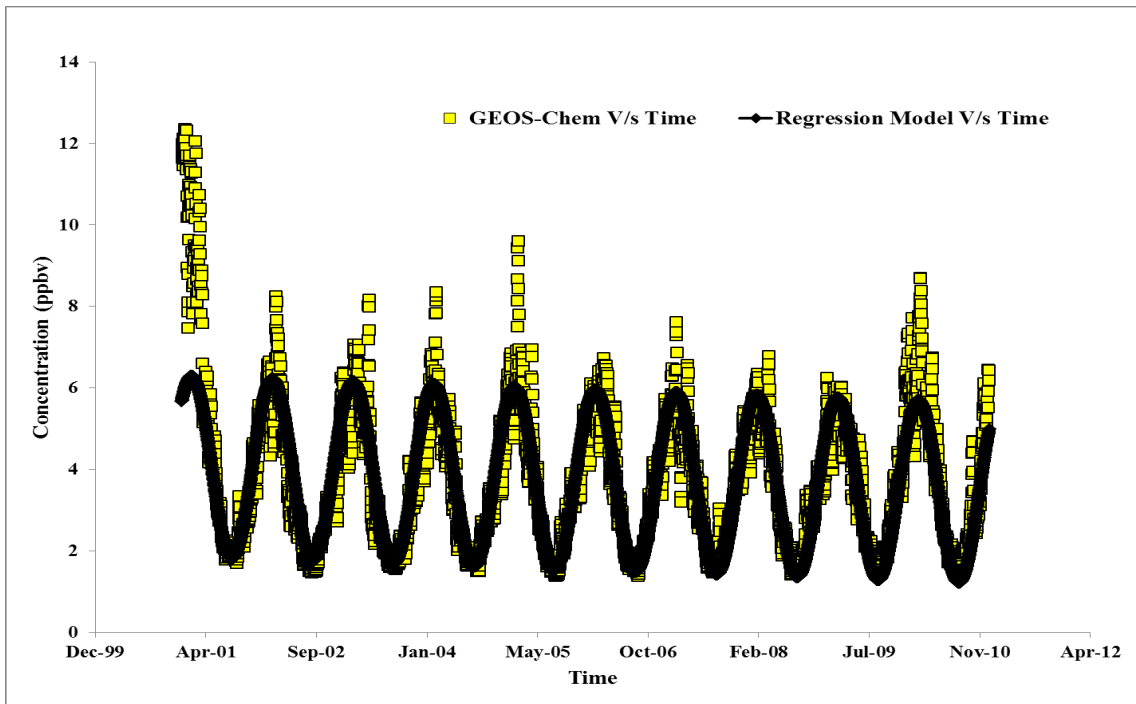


Figure 5.30: Regression fit for CO at Pico due to global biofuel emissions

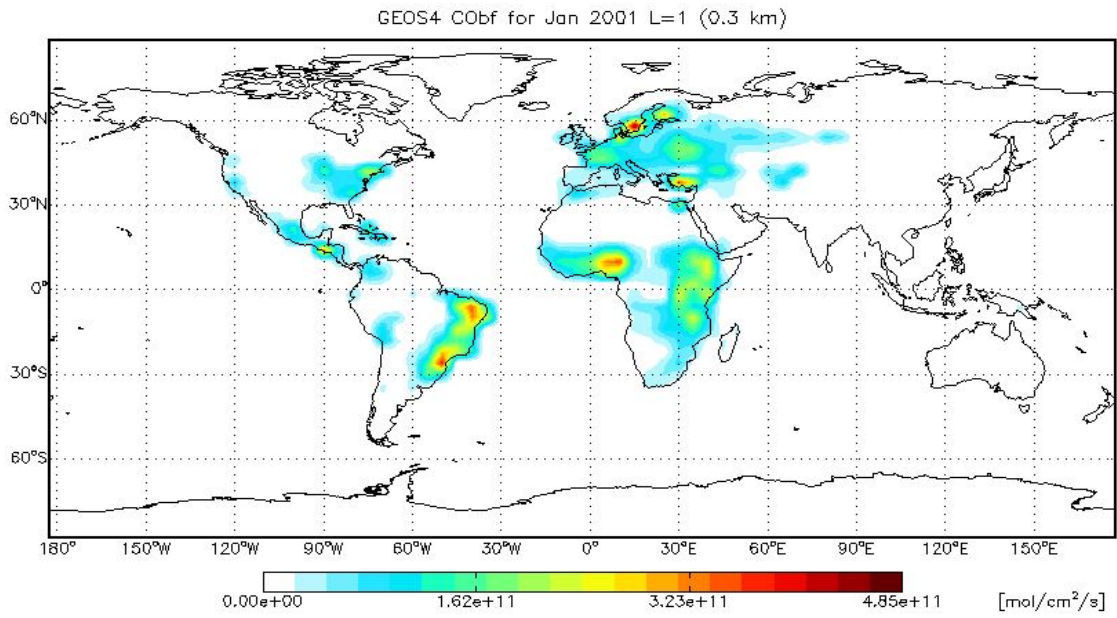


Figure 5.31: CO emissions from biofuels in January 2001

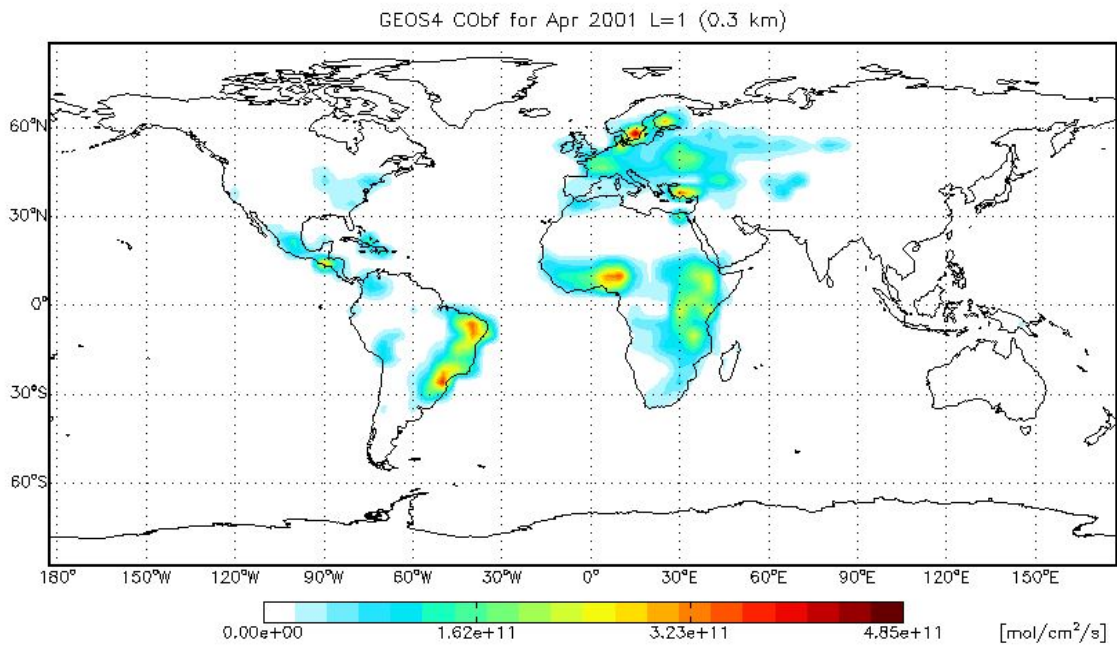


Figure 5.32: CO emissions from biofuels in April 2001

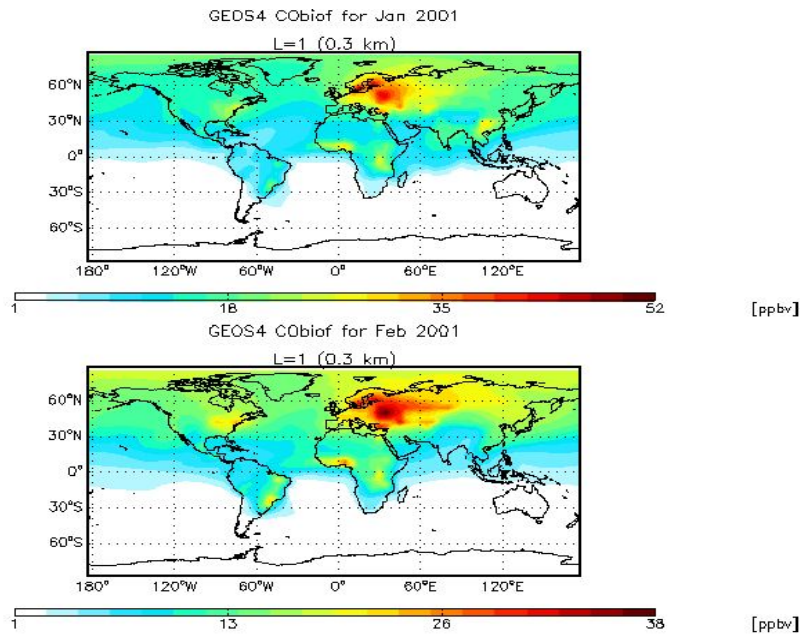


Figure 5.33: CO concentrations due to global biofuel emissions for January and February 2001

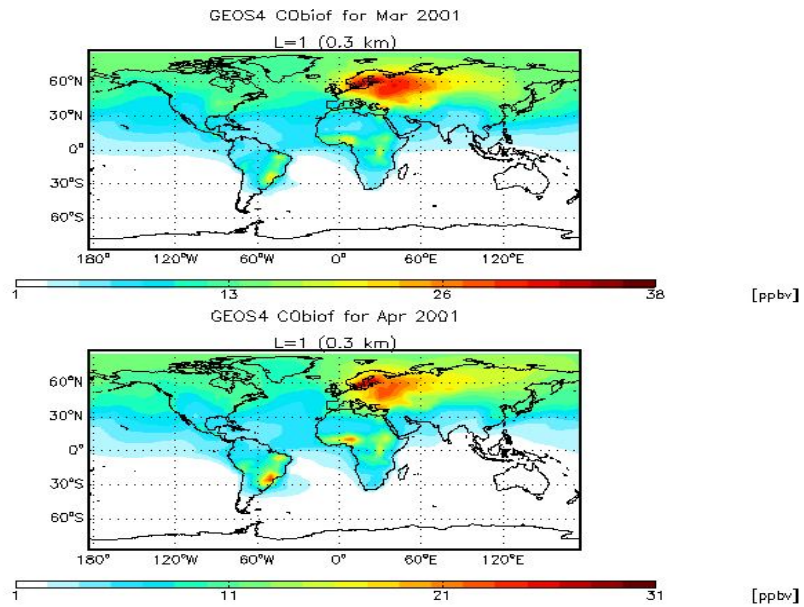


Figure 5.34: CO concentrations due to global biofuel emissions for March and April 2001

5.6. Interpretation of the Trends in CO

In order to interpret the obtained trends for CO, it would be necessary to consider the changes in emissions from sources other than anthropogenic as well. The changes in anthropogenic emissions from different regions such as USA and Asia are known as mentioned earlier. However, changes in biogenic emissions and CH₄ concentrations could also affect the CO concentrations at Pico as the CO from distant source regions or formed due to chemical transformations could be transported to the station. An analysis in this direction and interpretation of the trends observed at Pico is presented in the following sections.

5.6.1. Trends in Global Biogenic Emissions of VOCs

Biogenic sources contribute significantly to CO emissions. VOCs emitted by various plant species when subjected to environmental factors such as sunlight and temperature can be oxidized in the atmosphere to produce CO. These VOCs are highly diversified and numerous compounds have been shown to be emitted by biogenic sources [Owen *et al.*, 2001]. However, Isoprene and Monoterpenes are regarded as the most important [Klinger *et al.*, 1998]. The CO produced could be transported over long distances and affect the concentrations downwind. GEOS-Chem uses the MEGAN inventory which contains emissions for several species that can be oxidized to produce CO. Since the biogenic emissions depend on factors such as sunlight and temperature, they would exhibit seasonal variation with maximum emissions during summer when temperatures are high and sunlight exists in abundance. Hence the regression model shown in Eq. 4.22 could be used to model them. Global monthly mean biogenic

emissions were archived from the full chemistry simulation with fixed anthropogenic emissions for 2001-2011. Table 5.15 lists the species archived. The total biogenic emissions were computed as the sum of emissions of all these species. Following are the null and alternate hypotheses used:

Null Hypothesis: "There exists no trend in the global biogenic emissions (sum of emissions of all species) over the period 2001-2011 or the slope term in the regression equation is not significantly different from zero"

Alternate Hypothesis(two-sided): "There exists a trend (increasing/decreasing) in the global biogenic emissions (sum of emissions of all species) over the period 2001-2011 or the slope term in the regression equation is significantly different (greater/less) from zero"

Table 5.16 contains the global annual total of biogenic emissions for the period 2001-2011. The total biogenic emissions for each month were computed as the sum of the monthly mean emissions of all the compounds listed in Table 5.15. Tables 5.17 & 5.18 list the regression statistics and the trends respectively. The monthly mean total biogenic emissions do not show a significant trend over 2001-2011. This leads to the conclusion that globally, biogenic emissions (total) over the period 2001-2011 do not show significant variations. However, since we are interested in the contribution of biogenic emissions to CO at Pico, it would be more relevant to investigate the emission trends in the US or in the region extending from North America to Pico which is more likely to influence the CO concentrations at the station. This analysis is presented in the next section.

Table 5.15: Biogenic VOCs incorporated in GEOS-Chem

Compound	Compound
Isoprene	Acetone
Propane & Alkenes with > 3 carbons	Monoterpenes
Methly Butenol	α -Pinene
β -Pinene	Limonene
Sabinene	Myrcene
3-Carene	Ocimene

Table 5.16 : Global annual total biogenic emissions

Year	Biogenic VOC Emissions (Tg C/year)
2001	669.48
2002	688.69
2003	673.06
2004	695.25
2005	732.43
2006	699.28
2007	694.25
2008	655.93
2009	669.26
2010	689.22

Note: 2011 was not included as the simulation was run only till November 2011 due to meteorology for December not being available

Table 5.17: Regression statistics for the monthly mean biogenic emissions (total) of VOCs (2001-2011)

Species	Intercept	Slope	Sine Coefficient	Cosine Coefficient	R²
Total Biogenic emissions	57.79	-0.0087	-6.74	-5.35	0.78

Table 5.18: Trends obtained for monthly mean biogenic emissions (total) (2001-2011)

Species	Trend (Tg C/yr)	P-value (Two-sided test)	Significance @ $\alpha = 0.05$
Total Biogenic emissions	-0.104	0.25	Not Significant

5.6.2. Trends in Biogenic Emissions from North America

Although the analysis of global biogenic emissions (total) did provide some insight into their long-term variation, it was not sufficient to interpret the trends of CO at Pico. A better methodology would be to analyze emissions in the regions from which transport of pollutants frequently occurs to Pico. Continental North America is such a region as described in Chapter 1 and hence total biogenic emissions in this region were analyzed for trend using the same regression model as for the global biogenic emissions. The selected domain for this analysis extended from 162.5° W – 57.5° W (longitude) and 12° N – 72° N (latitude) and is shown in Figure 5.35. Monthly mean emissions for this domain were extracted from the global output (Section 5.6.1) for 2001-2011. The same compounds were considered and their emissions were summed up to get the total biogenic emissions. The null & alternate hypotheses are stated below.

Null Hypothesis: “There exists no trend in the biogenic emissions (sum of emissions from all species) from North America over the period 2001-2011 or the slope term in the regression equation is not significantly different from zero”

Alternate Hypothesis (two-sided): “There exists a trend (increasing/decreasing) in the biogenic emissions (sum of emissions from all species) over the period 2001-2011 or the slope term in the regression equation is significantly different (greater/less) from zero”

Table 5.19 shows the annual totals of biogenic emissions in North America for 2001-2010 while Tables 5.20 and 5.21 show the regression statistics and trends respectively. The total biogenic emissions did not show statistically significant trends over the period 2001-2011. Thus, the null hypothesis cannot be rejected at $\alpha = 0.05$ and it

can be concluded that the biogenic emissions over North America have not showed any significant variation from 2001-2011.



Figure 5.35: Domain including North America

Table 5.19: Annual totals of biogenic emissions in North America (2001-2010)

Year	Biogenic Emissions (Tg C/year)
2001	53.50
2002	53.25
2003	55.35
2004	53.34
2005	59.18
2006	59.83
2007	59.57
2008	55.29
2009	52.75
2010	54.62

Note: 2011 was not included as the simulation was run only till November 2011 due to meteorology for December not being available

Table 5.20: Regression statistics for the monthly mean biogenic emissions (total) of VOCs in North America (2001-2011)

Species	Intercept	Slope	Sine Coefficient	Cosine Coefficient	R ²
Total Biogenic emissions	4.60	0.0005	-2.41	-4.01	0.88

Table 5.21: Trends obtained for monthly mean biogenic emissions (total) of VOCs in North America (2001-2011)

Species	Trend (Tg C/year)	P-value (Two-sided test)	Significance @ $\alpha = 0.05$
Total Biogenic emissions	0.0060	0.86	Not Significant

5.6.3. Possible Reasons for the Trends in CO at PICO-NARE

The results obtained from previous analysis of in-situ observations (Section 5.3.1) and GEOS-Chem output (Section 5.3.2) showed decreasing trends for CO from 2001-2010. However, the full chemistry simulation with fixed anthropogenic emissions showed increasing trends over the same period. Since there were no trends obtained for the biogenic emissions over NA their contribution to the observed CO trends can be ruled out. But since an increase in the CO produced from CH₄ oxidation was observed in the tagged CO simulation results, a possible reason for the positive trends obtained with the fixed anthropogenic emissions simulation could be the increase in CH₄ concentrations over 2001-2010. The overall decrease in CO concentrations at Pico seen with the observations and full chemistry simulation with normal emissions is due to the reduction in anthropogenic emissions of CO in NA and decreases in CO from biomass burning in NA and Europe. There have been simultaneous increases in CO emissions from both anthropogenic sources and biomass burning in Asia (according to tagged CO simulation results) but they do not seem to have effects strong enough to result in an increase in CO concentrations at PICO-NARE over 2001-2010.

5.7. Interpretation of the Trends in O₃

O₃ can be produced chemically in the atmosphere in the presence of precursors (e.g. NO_x, VOCs) which have natural as well as anthropogenic sources. Thus, in order to better understand the causes behind the observed trends it is essential to ascertain the trends in the precursor emissions from both natural and anthropogenic sources. Trends in anthropogenic emissions of these precursors for different regions (e.g. Asia) are well known as mentioned earlier. Biogenic VOCs which have been discussed in section 5.6 do not show any significant variation over the period of study. In this section, changes in precursor emissions from other important sources and meteorological parameters which influence the O₃ budget in the troposphere are discussed.

5.7.1. Trends in Global Lightning Flashes

Lightning is considered to be an important source of NO_x and contributes around 10-15 % of the total NO_x emissions [Pickering *et al.*, 2009]. GEOS-Chem incorporates two kinds of lightning flashes: The In-Cloud (IC) and the Cloud to Ground (CG) flashes. The total lightning flashes (TL) in the model are equal to the sum of the two. Monthly means of the total and the two types of lightning flashes were archived from the full chemistry simulation with fixed anthropogenic emissions for the period 2001-2011. The regression model in Eq. (4.22) was fit to the data. The null and alternate hypotheses were as follows:

Null Hypothesis: "There exists no trend in the lightning flashes (of each type as well as total) over the period 2001-2011 or the slope term in the regression equation is not significantly different from zero"

Alternate Hypothesis (two-sided): “There exists a trend (increasing/decreasing) in the lightning flashes (of each type as well as total) over the period 2001-2011 or the slope term in the regression equation is significantly different (greater/less) from zero”

Table 5.22 contains the global annual totals of lightning flashes from 2001-2010. Tables 5.23 and 5.24 contain the regression statistics and trends respectively whereas Figures 5.36 & 5.37 show the regression fits for the TL and CG flashes respectively. The TL flashes show a significant increase over 2001-2011 and so do the CG flashes. However, there was no significant trend for the IC flashes indicating that the overall increase in TL flashes is due to the increase in CG flashes. Since there has been an overall increase in the TL flashes, it could result in an increase in the lightning NO_x as well. This has been discussed in the next section.

Table 5.22: Global annual totals of lightning flashes (2001-2010)

Year	TL flashes (No of flashes)	IC lightning flashes (No of flashes)	CG lightning flashes (No of flashes)
2001	1.49E+09	1.23E+09	2.57E+08
2002	1.44E+09	1.19E+09	2.52E+08
2003	1.41E+09	1.17E+09	2.42E+08
2004	1.35E+09	1.12E+09	2.34E+08
2005	1.37E+09	0.92E+09	4.56E+08
2006	1.48E+09	1.01E+09	4.63E+08
2007	1.51E+09	1.03E+09	4.74E+08
2008	1.54E+09	1.06E+09	4.85E+08
2009	1.75E+09	1.19E+09	5.61E+08
2010	1.78E+09	1.16E+09	5.58E+08

Note: 2011 was not included as the simulation was run only till November 2011 due to meteorology for December not being available

Table 5.23: Regression statistics for the fit to the monthly means of global lightning flashes (2001-2011)

Species	Intercept	Slope	Sine Coefficient	Cosine Coefficient	R ²
TL flashes	1.09E+08	2.24E+05	-2.2E+07	-2.2E+07	0.76
IC flashes	0.96E+08	-0.51E+05	-1.5E+07	-1.1E+07	0.58
CG flashes	0.17E+08	2.61E+05	-0.56E+07	-0.89E+07	0.79

Table 5.24: Trends obtained for the monthly means of global lightning flashes (2001-2011)

Species	Trend (No of flashes/year)	P-value (Two-sided test)	Significance @ $\alpha = 0.05$
TL flashes	2.68E+06	6.9E-11	Significant
IC flashes	-0.61E+06	0.06	Not Significant
CG flashes	3.13E+07	9.31E-35	Significant

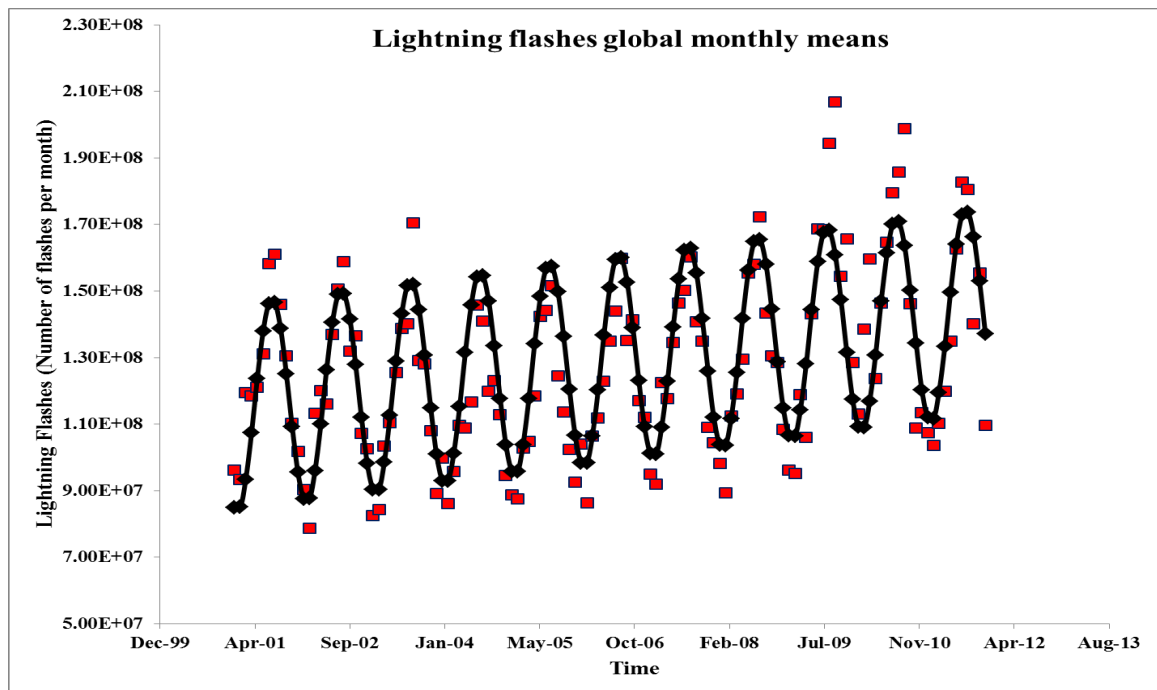


Figure 5.36: Regression fit for global monthly means of total lightning flashes (2001-2011)

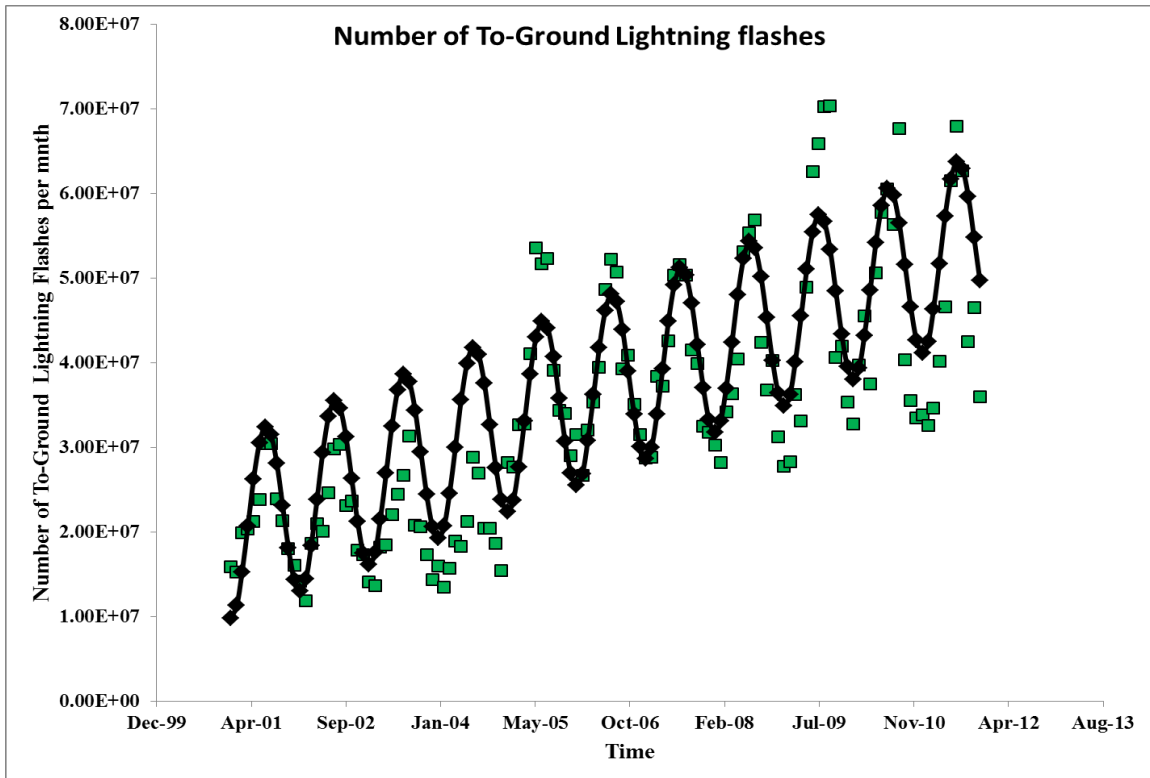


Figure 5.37: Regression fit for global monthly means of cloud to ground (CG) lightning flashes (2001-2011)

5.7.2. Trends in Global Lightning NO_x

Monthly means of global NO_x emissions from lightning flashes were archived from the full chemistry simulation with fixed anthropogenic emissions for 2001-2011 and the regression model in Eq. (4.22) was fit to the data. The null and alternate hypotheses were as follows:

Null Hypothesis: "There exists no trend in the NO_x from lightning flashes over the period 2001-2011 or the slope term in the regression equation is not significantly different from zero"

Alternate Hypothesis (two-sided): “There exists a trend (increasing/decreasing) in the NO_x from lightning flashes over the period 2001-2011 or the slope term in the regression equation is significantly different (greater/less) from zero”

Table 5.25 contains the global annual totals of lightning NO_x emissions from 2001-2010. Tables 5.26 and 5.27 contain the regression statistics and the trend respectively whereas Figure 5.38 shows the regression fit. There has been an increase in the global NO_x produced from lightning flashes over 2001-2011, which corresponds with the increase in TL and CG flashes. However, in order to determine the effect of lightning NO_x on O₃ at Pico, trends in lightning flashes and NO_x in the region extending from NA to Pico would be more relevant since NO_x from lightning could promote formation of O₃ in the exported pollution plumes. Hence a domain including NA and Pico was selected and the analysis was carried out again.

Table 5.25: Global annual totals of NO_x emissions from lightning from 2001-2010

Year	NO_x emissions (Tg N/year)
2001	6.25
2002	6.10
2003	5.94
2004	5.70
2005	5.85
2006	6.20
2007	6.35
2008	6.42
2009	7.26
2010	7.43

Note: 2011 was not included as the simulation was run only till November 2011 due to meteorology for December not being available

Table 5.26: Regression statistics for the fit to the monthly means of global NO_x from lightning for 2001-2011

Species	Intercept	Slope	Sine Coefficient	Cosine Coefficient	R ²
Lightning NO _x	0.46	0.00088	-0.12	-0.15	0.83

Table 5.27: Trends obtained for the monthly means of global NO_x from lightning for 2001-2011

Species	Trend (Tg N/yr)	P-value (Two-sided test)	Significance at $\alpha = 0.05$
Lightning NO _x	0.0105	6.57E-08	Significant

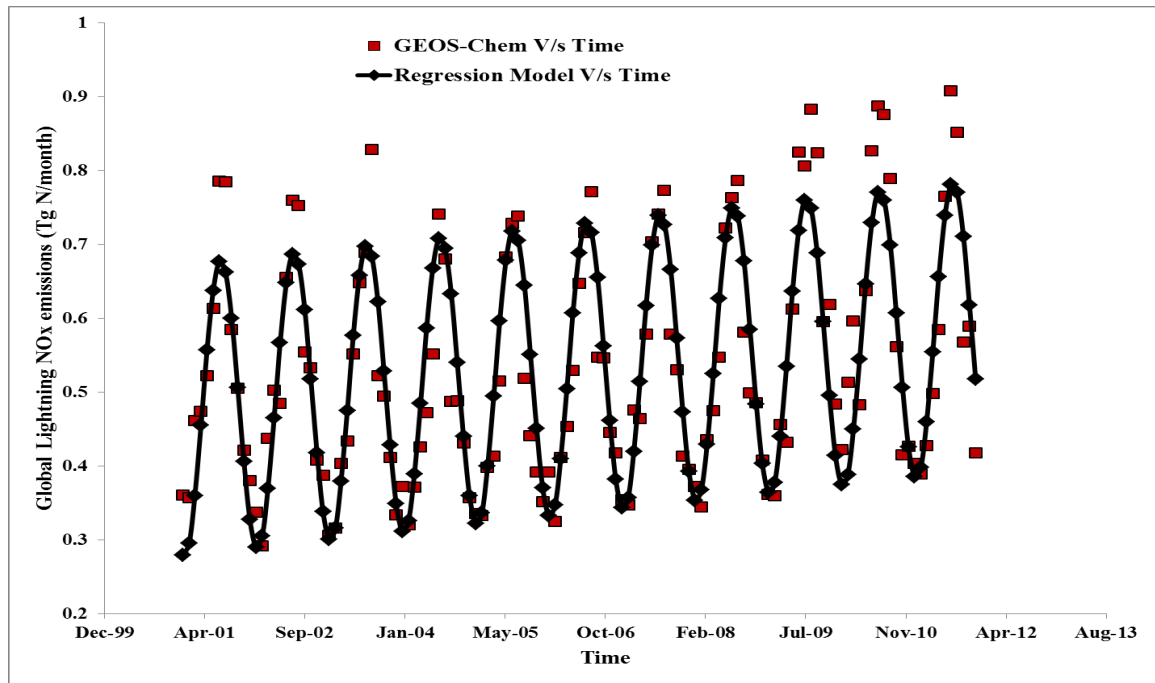


Figure 5.38: Regression fit to the monthly means of global NO_x from lightning for 2001-2011

5.7.3. Trends in Lightning Flashes in the Region from North America to PICO-NARE

Figure 5.39 shows the domain extending from NA to Pico. The region extends from 122.5° W to 17.50° W (longitude) and 28° N to 52° N (latitude) and includes the PICO-NARE observatory. The monthly means of lightning flashes for this domain were extracted from the global output (Section 5.7.1) for 2001-2011 and the regression model from Eq. (4.22) was fit to the data. Table 5.28 lists the annual totals of lightning flashes over this region and Tables 5.29 and 5.30 show the regression statistics and the trends respectively. No significant trends were observed for TL and IC flashes, but the CG flashes showed an increase over 2001-2011. However, this increase appears to be compensated by variations in the IC flashes resulting in no significant change in the TL flashes. Thus, the null hypothesis cannot be rejected for the TL flashes over the considered domain and it can be concluded that there is no trend in the TL flashes for the period 2001-2011 over the domain covering NA and PICO-NARE.



Figure 5.39: Domain extending from North America to PICO-NARE

Table 5.28: Annual totals of lightning flashes (2001-2010) over the domain extending from North America to PICO-NARE

Year	TL flashes (No of flashes)	IC flashes (No of flashes)	CG flashes (No of flashes)
2001	1.30E+08	1.02E+08	2.82E+07
2002	1.37E+08	1.08E+08	2.87E+07
2003	1.14E+08	8.94E+07	2.48E+07
2004	1.15E+08	8.98E+07	2.55E+07
2005	1.17E+08	6.38E+07	5.29E+07
2006	1.18E+08	6.56E+07	5.21E+07
2007	1.36E+08	8.00E+07	5.65E+07
2008	1.18E+08	6.50E+07	5.34E+07
2009	1.32E+08	7.55E+07	5.65E+07
2010	1.47E+08	8.98E+07	5.68E+07

Note: 2011 was not included as the simulation was run only till November 2011 due to meteorology for December 2011 not being available

Table 5.29: Regression statistics for the fit to the monthly means of lightning flashes (2001-2011) over the region from North America to PICO-NARE

Species	Intercept	Slope	Sine Coefficient	Cosine Coefficient	R ²
TL flashes	9.80E+06	1.09E+04	-4.96E+06	-1.18E+07	0.77
IC flashes	8.11E+06	-1.52E+04	-3.82E+06	-8.28E+06	0.73
CG flashes	1.69E+06	2.61E+04	-1.13E+06	-3.49E+06	0.77

Table 5.30: Trends obtained for the monthly means of lightning flashes (2001-2011) over the region from North America to PICO-NARE

Species	Trend (No of flashes/year)	P-value (Two-sided test)	Significance @ $\alpha = 0.05$
TL flashes	0.13E+06	0.35	Not Significant
IC flashes	-0.18E+06	0.10	Not Significant
CG flashes	0.31E+06	2.32E-11	Significant

5.7.4. Trends in Lightning NO_x in the Region from North America to PICO-NARE

The TL flashes over the domain from NA to PICO-NARE did not show significant changes over 2001-2011. To determine whether NO_x from these flashes shows a significant trend the monthly mean NO_x emissions from lightning were extracted for the same domain as before (Section 5.7.3) and analyzed using the regression model in Eq. (4.22). Table 5.31 shows the lightning NO_x emissions over the domain and Tables 5.32 and 5.33 contain the regression statistics and trend respectively. No significant trend was obtained for lightning NO_x over the domain from NA to PICO-NARE, leading to the acceptance of the null hypothesis and indicating that lightning NO_x contribution to the O₃ formation over the North Atlantic has not varied significantly over the period of study. It can thus be stated that the NO_x due to lightning has had no significant influence on the O₃ trends observed at Pico.

Table 5.31: Annual totals of NO_x from lightning (2001-2010) for the domain extending from North America to PICO-NARE

Year	NO _x emissions (Tg N/year)
2001	0.91
2002	0.95
2003	0.80
2004	0.80
2005	0.81
2006	0.82
2007	0.95
2008	0.83
2009	0.92
2010	1.02

Note: 2011 was not included as the simulation was run only till November 2011 due to meteorology for December not being available

Table 5.32: Regression statistics for the fit to the monthly means of NO_x from lightning (2001-2011) for the domain extending from North America to PICO-NARE

Species	Intercept	Slope	Sine Coefficient	Cosine Coefficient	R ²
Lightning NO _x	0.068	7.54E-05	-0.035	-0.082	0.77

Table 5.33: Trend obtained for the monthly means of NO_x from lightning (2001-2011) for the domain extending from North America to PICO-NARE

Species	Trend (Tg N/year)	P-value (Two-sided test)	Significance at $\alpha = 0.05$
Lightning NO _x	9.05E-04	0.35	Not Significant

5.7.5. Trends in Global NO_x from Biomass Burning

Biomass burning also contributes significantly to the global NO_x emissions with estimates of 8 Tg N/yr reported by *Price et al.* [1997]. It has both anthropogenic and natural origins and exhibits seasonal and inter-annual variability. Since Pico is frequently influenced by biomass burning emissions and NO_x thus produced could have effects on the O₃ concentrations at Pico, it is necessary to study the trends in NO_x emissions from this source. The monthly mean global NO_x emissions were archived from the full chemistry simulation with fixed anthropogenic emissions for 2001-2011 and the regression model in Eq. (4.22) was used to analyze them. The null and alternate hypotheses were:

Null Hypothesis: "There exists no trend in the global NO_x from biomass burning over the period 2001-2011 or the slope term in the regression equation is not significantly different from zero"

Alternate Hypothesis (two-sided): "There exists a trend (increasing/decreasing) in the global NO_x from biomass burning over the period 2001-2011 or the slope term in the regression equation is significantly different (greater/less) from zero"

Table 5.34 shows the global annual totals of NO_x emissions from biomass burning and Tables 5.35 and 5.36 contain the regression statistics and the trend respectively. The regression fit is shown in Figure 5.40. Decreasing trends significant @ $\alpha = 0.05$ were obtained which led to the rejection of the null hypothesis. Thus, global NO_x from biomass burning has decreased from 2001-2011. However, since Pico is frequently impacted by biomass burning pollution outflow from NA, it would be more useful to determine the trends in NO_x from biomass burning in NA. This has been discussed in the next section.

Table 5.34: Global annual totals of NO_x from biomass burning from 2001-2010

Year	NO _x emissions (Tg N/year)
2001	5.25
2002	5.68
2003	5.49
2004	5.32
2005	5.31
2006	5.07
2007	5.43
2008	4.56
2009	4.55
2010	4.55

Note: 2011 was not included as the simulation was run only till November 2011 due to meteorology for December not being available

Table 5.35: Regression statistics for the fit to the monthly means of global NO_x from biomass burning for 2001-2011

Species	Intercept	Slope	Sine Coefficient	Cosine Coefficient	R ²
Biomass Burning NO _x	0.49	-0.00088	-0.13	-0.005	0.31

Table 5.36: Trend obtained for the monthly means of global NO_x from biomass burning for 2001-2011

Species	Trend (Tg N/yr)	P-value (Two-sided)	Significance at $\alpha = 0.05$
Biomass Burning NO _x	-0.011	0.01	Significant

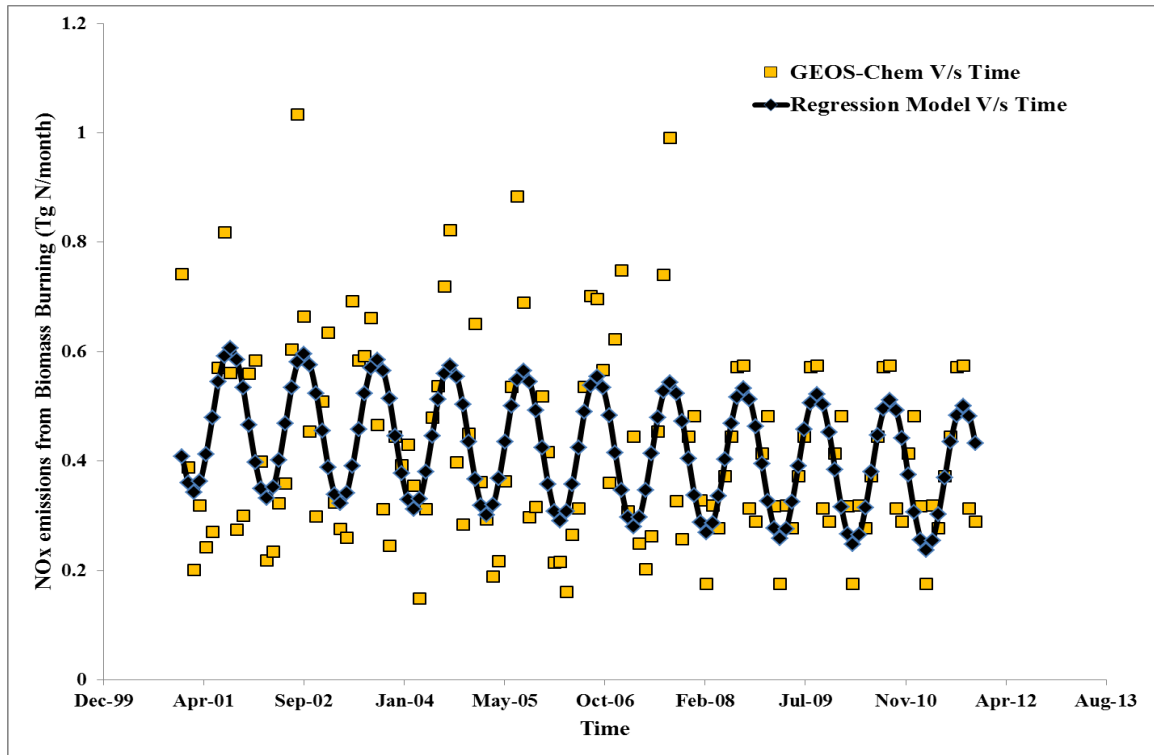


Figure 5.40: Regression fit for global NO_x from biomass burning for 2001-2011

5.7.6. Trends in NO_x from Biomass Burning in North America

Monthly mean NO_x emissions from biomass burning for the North American domain (used earlier in section 5.6.2) were extracted from the global output (in section 5.7.5) and the regression model in Eq. (4.22) was fit to the data. Table 5.37 shows the annual total of NO_x emissions from NA and Tables 5.38 and 5.39 show the regression statistics and trend respectively. The null and alternate hypotheses were as follows:

Null Hypothesis: "There exists no trend in the NO_x from biomass burning in North America over the period 2001-2011 or the slope term in the regression equation is not significantly different from zero"

Alternate Hypothesis (two-sided): “There exists a trend (increasing/decreasing) in the global NO_x from biomass burning in North America over the period 2001-2011 or the slope term in the regression equation is significantly different (greater/less) from zero”

There was no significant trend obtained for NO_x from biomass burning in NA. Hence it can be said that the monthly mean NO_x from biomass burning in NA has showed no significant variation over 2001-2011.

Table 5.37: Annual totals of NO_x from biomass burning in North America from 2001-2010

Year	NO _x emissions (Tg N/yr)
2001	0.104
2002	0.260
2003	0.360
2004	0.315
2005	0.259
2006	0.183
2007	0.183
2008	0.160
2009	0.163
2010	0.163

Note: 2011 was not included as the simulation was run only till November 2011 due to meteorology for December not being available

Table 5.38: Regression statistics for the fit to the monthly means of NO_x from biomass burning in North America from 2001-2011

Species	Intercept	Slope	Sine Coefficient	Cosine Coefficient	R ²
NO _x from Biomass burning	0.02	-6.8E-05	-0.004	-0.016	0.39

Table 5.39: Trend obtained for monthly mean NO_x from biomass burning in North America from 2001-2011

Species	Trend (Tg N/yr)	P-value (Two-sided test)	Significance at $\alpha = 0.05$
NO _x from Biomass burning	-8.16E-04	0.054	Not Significant

5.7.7. Trends in NO_x from Soils

Soil is also considered to be an important source of NO_x with emission estimates that are comparable to other sources such as biomass burning. These estimates vary across different studies (5-21 Tg N/yr [Jaeglé *et al.*, 2004], 12 Tg N/yr [Price *et al.*, 1997]) due to complex dependence on soil texture, fertilizer application, climatic factors such as temperature and precipitation. Since soils could contribute significantly to the NO_x budget, their contribution to the observed trends in O₃ at Pico cannot be neglected. Owing to the dependence of soil NO_x emissions on factors such as temperature and precipitation, seasonal variation can be associated with them. In GEOS-Chem, soil emissions are based on factors such as vegetation type, temperature, fertilizer usage, precipitation and the fraction of soil NO_x exported to the atmosphere after loss within canopies. Thus, soil NO_x emissions would include the NO_x from fertilizers as well. Monthly means of NO_x emissions from soils were archived from the full chemistry simulation with fixed anthropogenic emissions for 2001-2011. The regression model of Eq. 4.22 was fit to the data. The null and alternate hypotheses were stated as follows:

Null Hypothesis: "There exists no trend in the global NO_x from soils over the period 2001-2011 or the slope term in the regression equation is not significantly different from zero"

Alternate Hypothesis: "There exists a trend (increasing/decreasing) in the global NO_x from soils over the period 2001-2011 or the slope term in the regression equation is significantly different (greater/less) from zero"

Table 5.40 lists the annual totals of global emissions of NO_x from soils from 2001-2010. Tables 5.41 & 5.42 show the regression statistics and trend for NO_x from

soils respectively whereas Figure 5.41 shows the regression fit. A statistically significant increasing trend was obtained for the global soil NO_x which could be attributed to increases in fertilizer usage in some regions (e.g. Asia) or long term change in parameters such as temperature, precipitation etc. However, again the global emissions cannot be used to interpret the trends at Pico. Hence, the same domain as used for biomass burning and biogenic emissions was used to obtain the soil NO_x emissions from NA. The analysis is presented in the next section.

Table 5.40: Global annual totals of NO_x emissions from soils for 2001-2010

Year	Soil NO _x (Tg N/yr)
2001	5.82
2002	5.85
2003	5.82
2004	5.85
2005	6.08
2006	6.08
2007	6.03
2008	5.96
2009	6.04
2010	6.11

Note: 2011 was not included as the simulation was run only till November 2011 due to meteorology for December not being available

Table 5.41: Regression statistics for the fit to the monthly means of global NO_x emissions from soils for 2001-2011

Species	Intercept	Slope	Sine coefficient	Cosine coefficient	R ²
Soil NO _x	0.48	0.00017	-0.06	-0.09	0.96

Table 5.42: Trend obtained for the monthly means of global NO_x emissions from soils for 2001-2011

Species	Trend (Tg N/yr)	P-value (Two-sided test)	Significance @ $\alpha = 0.05$
Soil NO _x	0.0021	2.49E-06	Significant

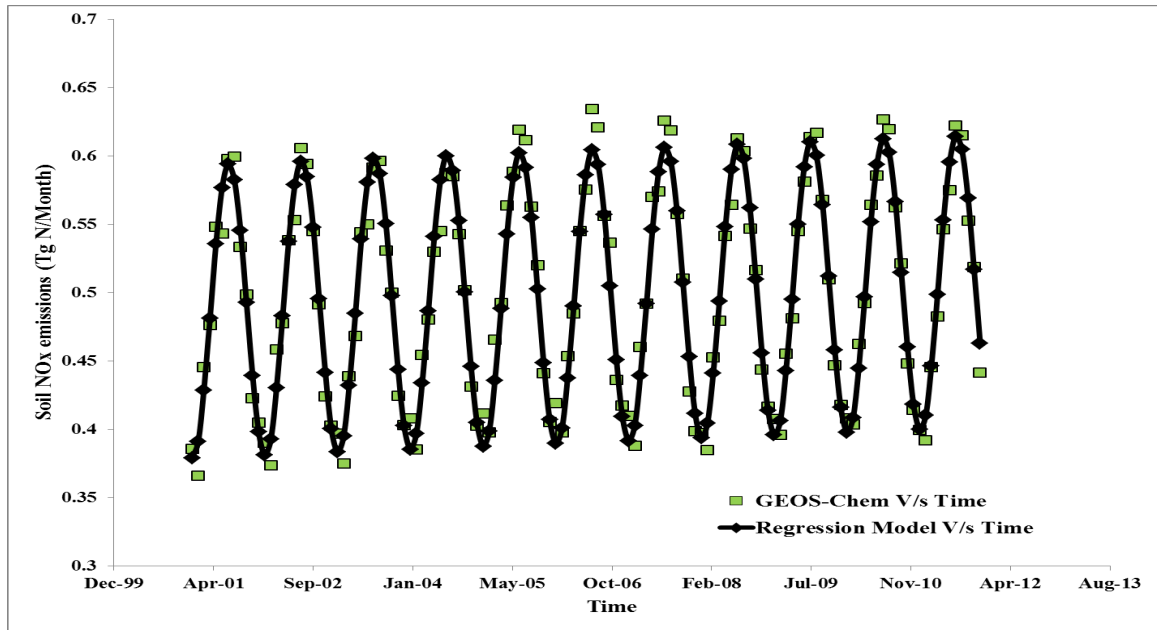


Figure 5.41: Regression fit to the monthly means of global NO_x emissions from soils for 2001-2011

5.7.8. Trends in Soil NO_x from North America

This analysis was carried out for the domain described in section 5.6.2. Monthly mean emissions of NO_x from soils were extracted for this domain from the global output (section 5.7.7) for 2001-2011 and the regression model of Eq. (4.22) was fit to the data.

The null and alternate hypotheses were stated as:

Null Hypothesis: "There exists no trend in the NO_x from soils in North America over the period 2001-2011 or the slope term in the regression equation is not significantly different from zero"

Alternate Hypothesis (two-sided): "There exists a trend (increasing/decreasing) in the NO_x from soils in North America over the period 2001-2011 or the slope term in the regression equation is significantly different (greater/less) from zero"

Table 5.43 contains the annual total soil NO_x emissions from NA for 2001-2010. Tables 5.44 and 5.45 contain the regression statistics and the trend respectively. No significant trend was obtained for soil NO_x from NA which indicates that the increase in global soil NO_x could be due to increases in other regions. This also weakens the possibility of significant changes in contributions of NO_x sources other than anthropogenic fossil fuel combustion to O₃ production at Pico or in the pollution plumes being exported from NA. Hence changes in NO_x emissions from sources other than anthropogenic fossil fuel combustion could not be the reason for the decreasing trend obtained for O₃ in the full chemistry simulation (both with fixed and normal anthropogenic emissions).

Table 5.43: Annual totals of NO_x emissions from soils for North America from 2001-2010

Year	Soil NO_x (Tg N/yr)
2001	0.580
2002	0.550
2003	0.575
2004	0.570
2005	0.616
2006	0.623
2007	0.618
2008	0.584
2009	0.585
2010	0.588

Note: 2011 was not included as the simulation was run only till November 2011 due to meteorology for December not being available

Table 5.44: Regression statistics for the fit to the monthly means of NO_x emissions from soils in North America for 2001-2011

Species	Intercept	Slope	Sine coefficient	Cosine coefficient	R ²
Soil NO _x	0.05	1.52E-05	-0.02	-0.03	0.96

Table 5.45: Trend obtained for the monthly means of NO_x emissions from soils in North America for 2001-2011

Species	Trend (Tg N/yr)	P-value (Two-sided test)	Significance at $\alpha = 0.05$
Soil NO _x	1.83E-04	0.18	Not Significant

5.7.9. Trends in Humidity for the Domain Extending from North America to PICO-NARE

In the previous sections, trends in NO_x from sources other than anthropogenic fossil fuel combustion have been investigated. Although significant trends were obtained for global NO_x emissions, no such behavior was observed for the domains that would influence Pico the most (e.g. North America). The final factor that could aid in interpreting the trends of O₃ at Pico would be humidity. As water vapor can cause O₃ destruction and the transport of O₃ occurs over the North Atlantic where the water vapor content would be high, it can play an important role in the O₃ budget over the region. Changes in water vapor content in the domain considered in this study could affect the O₃ concentrations at both Pico and in the plumes being transported. In this direction, the specific humidity values in a domain extending from North America to PICO-NARE were extracted from the GEOS meteorology fields used by GEOS-Chem for the period

2001-2010. The average values of specific humidity for 2001-2005 and 2006-2010 were computed for this domain and the differences between the two were determined. GEOS-4 meteorology was used for 2001-2005 and GEOS-5 from 2006-2010. Figures 5.42-5.45 show the plots. Figure 5.42 shows the average specific humidity from 2001-2005 (Upper left plot) and 2006-2010 (Upper right plot) for the domain extending from 120°W to 15°W (longitude) at the latitude of 40°N (i.e. specific humidity averaged over 38°N – 42°N latitude). The plots in the lower panel show the difference (Lower left plot) and percentage difference (Lower right plot) respectively between average specific humidity from 2006-2010 & 2001-2005. Figure 5.43 shows similar plots but covers a wider latitudinal extent (specific humidity averaged over 30° N to 50° N). Since transport of pollution from NA to Pico can occur by low-level direct advection and simultaneous lifting and transport by WCBs in mid latitude cyclones, the change in specific humidity along the resulting pathways would have significant influences on the O₃ formation in the transported plume. Also, the change in humidity near Pico would help determine the fate of O₃ that is transported to or is formed (due to transportation of O₃ precursors) at/near the site. Transport due to WCBs would be expected to occur at higher altitudes (6-8 km (490-380 hPa) [Owen *et al.*, 2006]). In both Figures 5.42 and 5.43, an increase in humidity (ranging from 3-27%) is observed in the region extending from 600-400 hPa with minor patches which show decreases (ranging from 3-11%). Figure 5.44 shows the average specific humidity in the region extending from 120°W to 15°W (averaged over 38°N – 42°N latitude) for the summer (June-August) for 2001-2005 (Upper left panel) and 2006-2010 (Upper right panel). The lower panels show the difference (lower left

panel) and percentage difference (lower right panel) respectively between the averages of 2006-2010 & 2001-2005. Figure 5.45 shows the same plots but with specific humidity values averaged from 30°N to 50°N (latitude). Since low-level transport (< 3 km (< 720 hPa)) is the major transport pathway in the summer [Owen *et al.*, 2006], these plots can provide the humidity change in the lower altitudes during this time. As can be seen in the lower panel plots in Figure 5.44, there is an increase in the specific humidity (3-19%) in the lower levels (< 3 km (< 720 hPa)) with small areas showing a decrease (-3 to -11 %). Similar patterns are observed in the lower panel plots of Figure 5.45 as well. Such increases can also be observed around Pico (longitude (28⁰ W) and altitude (2.25 km, 780 hPa)) where all the plots show an increase in the specific humidity over the past decade. The increase in specific humidity in the region at altitudes relevant to the transport pathways could contribute to enhanced destruction of O₃ that is formed at the source and is transported by either of the two mechanisms (WCBs and low altitude advection) or that is formed in the pollution plumes en route to Pico. Lifetime calculations for O₃ at altitudes of 7 km (relevant to WCB transport) and 2 km (during summer (June-August), relevant to low level advection) with average humidity changes of 5% (from Figure 5.43) and 6.5% (from Figure 5.45) respectively yielded corresponding decreases of 1 day (5.13%) and 2.6 hours (5.73%). These decreases in the lifetime of O₃ imply an increase in its destruction during transport to Pico. Also, specific humidity increase around the station would increase the destruction of O₃ formed locally in the presence of NO_x transported as PAN.

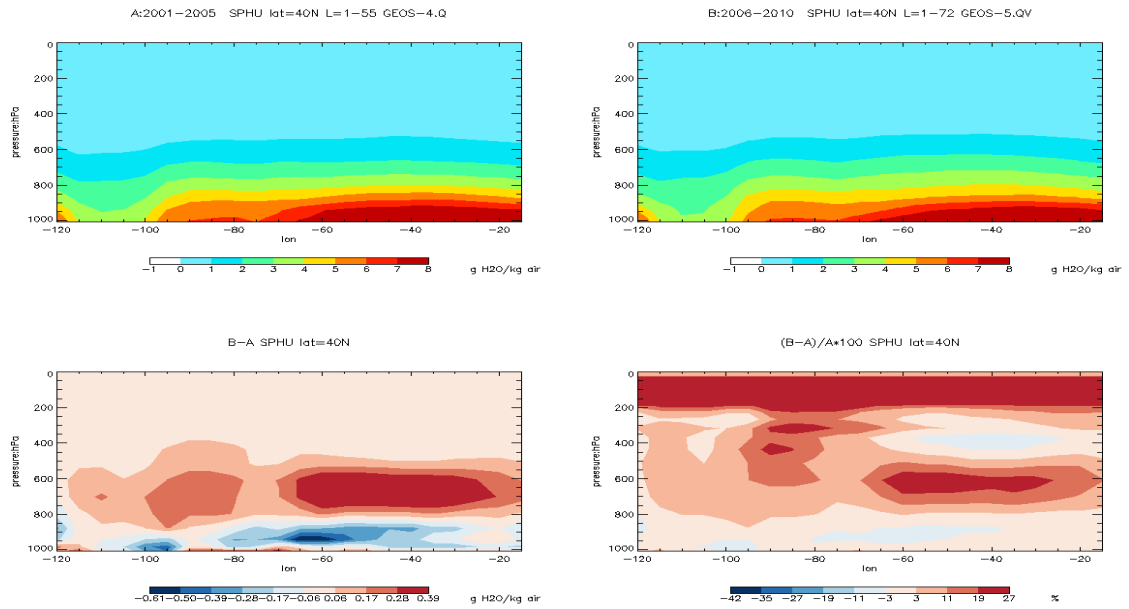


Figure 5.42: Specific Humidity over the region extending from North America to PICO-NARE (averaged over 38°N-42°N latitude)

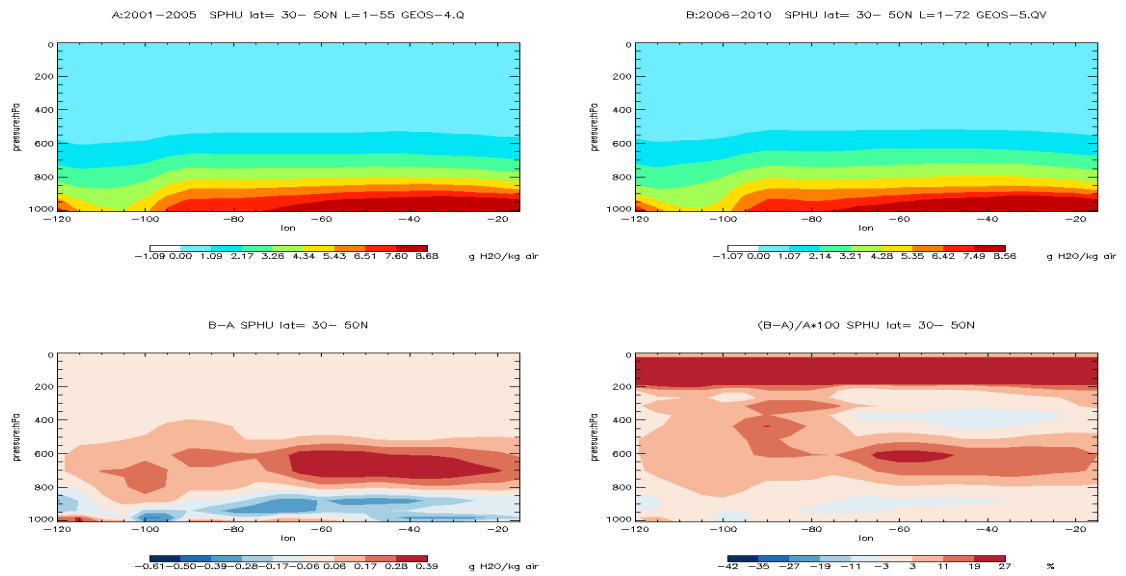


Figure 5.43: Specific Humidity over the region extending from North America to PICO-NARE (averaged over 30°N-50°N)

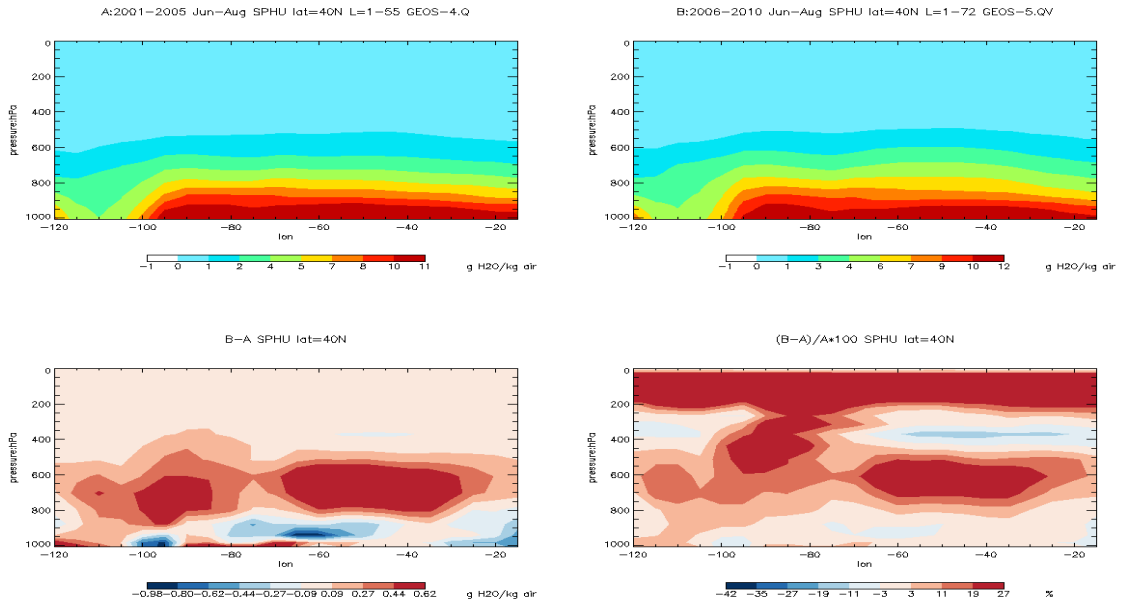


Figure 5.44: Specific Humidity over the region extending from North America to PICO-NARE for the summer (June-August) (averaged over 38°N-42°N)

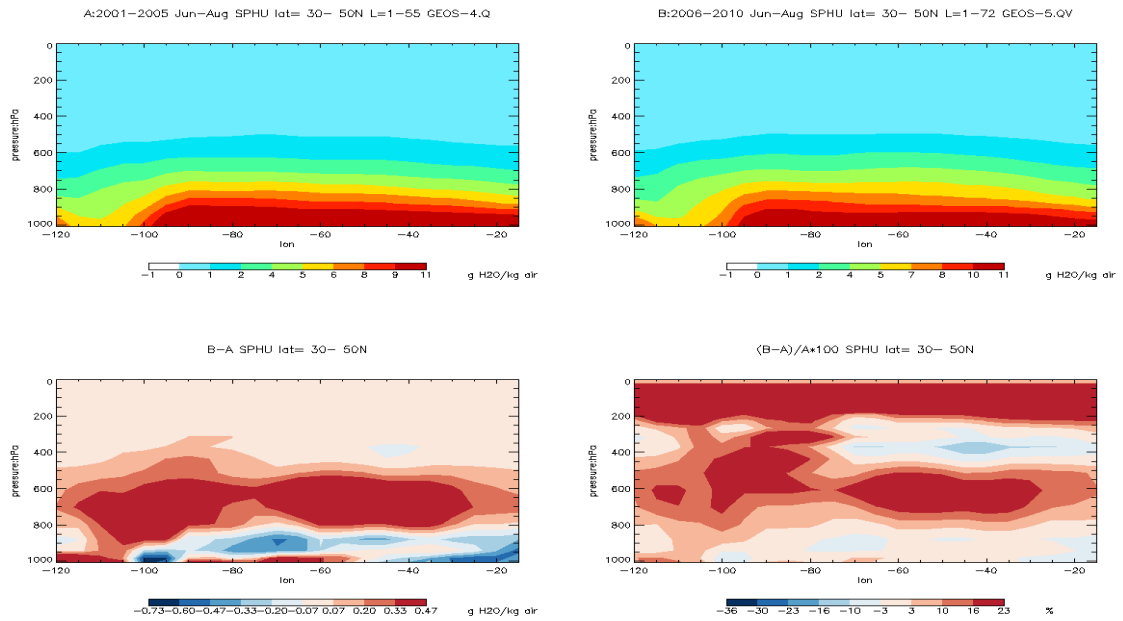


Figure 5.45: Specific Humidity over the region extending from North America to PICO-NARE for the summer (June-August) (averaged over 30°N-50°N)

5.7.10. Possible reasons for the trends of O₃ at PICO-NARE

Based on the results from the analyses in the previous sections, it can be concluded that the decreasing trends for O₃ at Pico could be caused by an increase in the water vapor over the period 2001-2010. This decrease appears to be countered by an increase in O₃ due to transport of anthropogenic pollution to the station which is evident in the smaller magnitude of decrease observed with the full chemistry simulation with normal emissions as compared to the simulation with fixed anthropogenic emissions. In the fixed emissions simulation the anthropogenic emissions were constant, and it showed a greater decrease in O₃ over 2001-2011, which in the absence of significant variations in NO_x from the sources considered in sections 5.7.1-5.7.8 was probably caused by increase in humidity, whereas in the normal emissions simulation the anthropogenic emissions varied which could change the anthropogenic pollution transport to the station according to the emission trends in different regions resulting in a lesser decrease. Since North American anthropogenic O₃ precursor emissions (e.g. NO_x) have decreased over the period of study, the increase in O₃ formation could be attributed to the transport of Asian precursor emissions which have increased over the same period. Thus, the overall decrease visible with the observations and the normal emissions simulation is due to long term change in climatic conditions in the North Atlantic region resulting in an increase in water vapor content and causing significant destruction of O₃.

Chapter 6: Conclusions

Following is a summary of the important results obtained and the conclusions that can be drawn from the analyses carried out during this study.

- 1.) The Mann-Kendall test did not yield results based on which concrete conclusions could be drawn about the trends of CO and O₃ at PICO-NARE. This was even after several derived datasets (e.g. monthly means etc.) in addition to the daily average dataset were analyzed using the test and the Seasonal Mann-Kendall test was employed as well. A major reason for this was the unavailability of sufficient data points which hindered a complete analysis using this test. Most of the data was available for the summer which meant that the analysis would have to be confined to the months in this season. Performing the approximate Mann-Kendall test with the complete dataset yielded significant decreasing trends for CO whereas those for O₃ were close to significant too but since this test did not take into account the seasonal variation associated with the two species these results could not be used to arrive at conclusions. There was no significant trend observed for the summer using the Mann-Kendall test (i.e. exact test for monthly means of summer months (June-August), approximate test for daily averages of summer months). The Seasonal Mann-Kendall test also did not yield any significant trends for CO and O₃ with each month from May-September used as a separate season. Availability of data for other seasons could have resulted in a more comprehensive analysis which could have aided in arriving at definite conclusions.
- 2.) The regression model with sinusoidal terms and a linear trend term was more appropriate for analysis as the sinusoidal terms accounted for the seasonal variation of

CO and O₃ and the linear term could be used to determine the trend. Application of this regression model to the daily average values of CO and O₃ at PICO-NARE yielded decreasing trends for both CO (2001-2010) and O₃ (2001-2011). Similar trends were obtained when the model was fit to the time-series output for CO and O₃ at PICO-NARE from the GEOS-Chem full chemistry simulation with normal emissions. With the GEOS-Chem full chemistry simulation with fixed anthropogenic emissions, an increasing trend was obtained for CO and a decreasing trend for O₃ which was greater in magnitude than earlier (normal emissions simulation).

3.) The decreasing trends in CO over 2001-2010 could be attributed to the decline in the anthropogenic and biomass burning emissions in different regions (e.g. USA). The regression model when fit to the time-series of CO concentrations (due to different sources and regions) at PICO-NARE archived using the GEOS-Chem tagged CO simulation yielded decreasing trends in CO from anthropogenic (fossil fuel) emissions in USA, biomass burning emissions from North America and Europe (which included parts of Russia) and global biofuel emissions. In contrast, increasing trends were obtained for anthropogenic (fossil fuel) and biomass burning emissions in Asia and global CH₄ oxidation. However, the increases in CO from Asia and CH₄ oxidation do not outweigh the corresponding decreases in CO from NA and Europe resulting in an overall decreasing trend over 2001-2010. The increase in CO from CH₄ could be a reason for the increasing trend in CO observed with the fixed emissions simulation since the natural sources of CO (biogenic emissions) did not show significant trends both globally as well as for North America.

4.) The decreasing trends in O₃ over 2001-2011 could be due to a change in the water vapor content over the region including North America and extending to PICO-NARE over the North Atlantic Ocean. Average specific humidity over this region from 2006-2010 has increased as compared to the average from 2001-2005. Also, the anthropogenic NO_x in the US has decreased over this period and there has been no significant variation in the NO_x emissions from other sources (e.g. lightning, soil) for domains relevant to PICO-NARE (Soil NO_x and biomass burning NO_x over North America, lightning NO_x over the region extending from North America to PICO-NARE). Moreover, the specific humidity increases have been at both high (around 6-8 km relevant to WCB transport) and low (< 3 km relevant to low-level transport) altitudes which would imply that there would be enhanced destruction of O₃ being transported from North America by any of the two possible pathways (WCB uplifting and transport as well as low level advection). The increase in humidity was also observed around PICO-NARE at altitudes close to the station which would increase the destruction of O₃ formed in the vicinity of the site due to NO_x being transported as PAN. This increase in specific humidity due to climate change could be the major reason behind the greater decrease in O₃ observed with the fixed emissions simulation. This decrease is countered by an increase in O₃ concentrations at PICO-NARE, predominantly due to increasing anthropogenic influence from Asia which is the reason for the lesser decrease in O₃ in the full chemistry simulation with normal emissions. However, this increase in O₃ concentrations is not sufficient to overcome the increase in destruction due to long-term climate change and hence an overall decreasing trend is observed.

5.) In the end, it can be stated that the observed trends in CO and O₃ at PICO-NARE have been caused by a combination of changes in anthropogenic emissions in regions around the globe (e.g. Asia, USA) and long term change in climate. No impact of climate change on CO could be discerned which appears to be affected by the anthropogenic & biomass burning emission shifts in USA, Asia and Europe as well as by the chemistry of species such as CH₄. However, climate change does affect the O₃ trend significantly with the increase in water vapor over the past decade promoting its destruction in the region extending from North America to PICO-NARE causing a decrease over the period of study which could not be outweighed by an increase in O₃ transport/formation at the station possibly due to increasing O₃ precursor emissions in Asia.

References

- Alvo, M., and P. Cabilio (1995), Rank correlation methods for missing data, *Canadian Journal of Statistics*, 23(4), 345-358.
- Bey, D. J. Jacob, J. A. Logan, and R. M. Yantosca (2001a), Asian chemical outflow to the Pacific in spring: Origins, pathways, and budgets, *Journal of geophysical research*, 106(D19), 23,097-023,113.
- Bey, D. J. Jacob, R. M. Yantosca, J. A. Logan, B. D. Field, A. M. Fiore, Q. Li, and H. Y. Liu (2001b), Model description and evaluation, *Journal of geophysical research*, 106(D19), 23,073-023,095.
- Bonasoni, P., A. Stohl, P. Cristofanelli, F. Calzolari, T. Colombo, and F. Evangelisti (2000), Background ozone variations at Mt. Cimone station, *Atmos Environ*, 34(29), 5183-5189.
- Calvert, J. G. (1983), *Acid deposition: atmospheric processes in eastern North America: a review of current scientific understanding*, National Academies.
- Chatfield, R., and D. Baumgardner (1997), Biomass burning and deep convection in southeastern Asia: Results from ASHOC/MAESA, *Journal of geophysical research*, 102(D11), 13,291-213,299.
- Cooper, and D. D. Parrish (2004), Air pollution export from and import to North America: Experimental evidence, *Air Pollution*, 41-67.
- Cooper, R. Doherty, P. Hess, and A. Stohl Conceptual Overview of Hemispheric or Intercontinental Transport Processes.
- Cooper, J. Moody, D. Parrish, M. Trainer, T. Ryerson, J. Holloway, G. Hübler, F. Fehsenfeld, S. Oltmans, and M. Evans (2001), Trace gas signatures of the airstreams within North Atlantic cyclones: Case studies from the North Atlantic Regional Experiment (NARE'97) aircraft intensive, *Journal of geophysical research*, 106(D6), 5437-5456.
- Cooper, D. Parrish, A. Stohl, M. Trainer, P. Nédélec, V. Thouret, J. Cammas, S. Oltmans, B. Johnson, and D. Tarasick (2010), Increasing springtime ozone mixing ratios in the free troposphere over western North America, *Nature*, 463(7279), 344-348.
- Corbett, J. J., P. S. Fischbeck, and S. N. Pandis (1999), Global nitrogen and sulfur inventories for oceangoing ships, *Journal of geophysical research*, 104(D3), 3457-3470.
- Cowles, M., and C. Davis (1982), On the origins of the .05 level of statistical significance, *American Psychologist*, 37(5), 553.
- Crutzen, P. J., and V. Ramanathan (2003), The parasol effect on climate, *Science*, 302(5651), 1679.
- Derwent, R., P. Simmonds, S. Seuring, and C. Dimmer (1998), Observation and interpretation of the seasonal cycles in the surface concentrations of ozone and carbon monoxide at Mace Head, Ireland from 1990 to 1994, *Atmos Environ*, 32(2), 145-157.
- Dismuke, C., and R. Lindrooth (2006), Ordinary least squares, *Methods and Designs for Outcomes Research*, 93.
- Duncan, B., J. Logan, I. Bey, I. Megretskaia, R. Yantosca, P. Novelli, N. Jones, and C. Rinsland (2007), Global budget of CO, 1988–1997: Source estimates and validation with a global model, *Journal of geophysical research*, 112(D22), D22301.

Eckhardt, S., A. Stohl, H. Wernli, P. James, C. Forster, and N. Spichtinger (2004), A 15-year climatology of warm conveyor belts, *Journal of climate*, 17(1), 218-237.

Eller, P., K. Singh, A. Sandu, K. Bowman, D. Henze, and M. Lee (2009), Implementation and evaluation of an array of chemical solvers in the Global Chemical Transport Model GEOS-Chem, *Geoscientific Model Development*, 2, 89-96.

Giglio, L., G. Van Der Werf, J. Randerson, G. Collatz, and P. Kasibhatla (2005), Global estimation of burned area using MODIS active fire observations, *Atmospheric Chemistry and Physics Discussions*, 5(6), 11091-11141.

Hack, J. J. (1994), Parameterization of moist convection in the National Center for Atmospheric Research community climate model (CCM2), *Journal of geophysical research*, 99(D3), 5551-5568.

Hamed, K. H., and A. Rao (1998), A modified Mann-Kendall trend test for autocorrelated data, *Journal of Hydrology*, 204(1), 182-196.

Hatakeyama, S., K. Izumi, T. Fukuyama, H. Akimoto, and N. Washida (1991), Reactions of OH with α -pinene and β -pinene in air: estimate of global CO production from the atmospheric oxidation of terpenes, *Journal of geophysical research*, 96(D1), 947-958.

Helsel, D. R., and R. M. Hirsch (2002), *Statistical methods in water resources*, US Geological survey Reston, Va.

Holtzlag, A., and B. Boville (1993), Local versus nonlocal boundary-layer diffusion in a global climate model, *Journal of climate*, 6, 1825-1825.

Honrath, R. Owen, M. V. Martin, J. Reid, K. Lapina, P. Fialho, M. Dziobak, J. Kleissl, and D. Westphal (2004), Regional and hemispheric impacts of anthropogenic and biomass burning emissions on summertime CO and O₃ in the North Atlantic lower free troposphere, *J. Geophys. Res.*, 109, D24310.

Huntrieser, H., J. Heland, H. Schlager, C. Forster, A. Stohl, H. Aufmhoff, F. Arnold, H. Scheel, M. Campana, and S. Gilge (2005), Intercontinental air pollution transport from North America to Europe: Experimental evidence from airborne measurements and surface observations, *J. Geophys. Res.*, 110, D01305.

Jacob, D. J., J. A. Logan, and P. P. Murti (1999), Effect of rising Asian emissions on surface ozone in the United States, *Geophys Res Lett*, 26(14), 2175-2178.

Jaeglé, L., R. Martin, K. Chance, L. Steinberger, T. Kurosu, D. Jacob, A. Modi, V. Yoboué, L. Sigha-Nkamdjou, and C. Galy-Lacaux (2004), Satellite mapping of rain-induced nitric oxide emissions from soils, *J. Geophys. Res.*, 109(D21), D21310.

Jaffe, D., T. Anderson, D. Covert, R. Kotchenruther, B. Trost, J. Danielson, W. Simpson, T. Berntsen, S. Karlsdottir, and D. Blake (1999), Transport of Asian air pollution to North America, *Geophys Res Lett*, 26(6), 711-714.

Jain, R., R. Kasturi, and B. G. Schunck (1995), *Machine vision*, McGraw-Hill New York.

Kallos, G., V. Kotroni, K. Lagouvardos, and A. Papadopoulos (1998), On the long-range transport of air pollutants from Europe, *Geophys Res Lett*, 25(5), 619-622.

Keeling, C. D., R. B. Bacastow, A. E. Bainbridge, C. A. Ekdahl Jr, P. R. Guenther, L. S. Waterman, and J. F. S. Chin (1976), Atmospheric carbon dioxide variations at Mauna Loa observatory, Hawaii, *Tellus*, 28(6), 538-551.

Kendall (1955), *Rank correlation methods*, 2d ed., 196 p. pp., C. Griffin, London,.

Kendall (1970), *Rank Correlation Methods* (4th edn.) Griffin, London, UK.

- Kleissl, J., R. Honrath, M. Dziobak, D. Tanner, M. V. Martin, R. Owen, and D. Helmig (2007), Occurrence of upslope flows at the Pico mountaintop observatory: A case study of orographic flows on a small, volcanic island, *JOURNAL OF GEOPHYSICAL RESEARCH-ALL SERIES-*, 112(D10), 10.
- Klinger, L., G. Guenther, G. Tyndall, P. Zimmerman, M. Bangui, J. M. Moutsamboté, and D. Kenfack (1998), Patterns in volatile organic compound emissions along a savanna-rainforest gradient in central Africa, *Journal of geophysical research*, 103(D1), 1443-1454.
- Law, K. (2010), More ozone over North America, *Nature*, 463, 21.
- Logan, J. A. (1985), Tropospheric ozone: Seasonal behavior, trends, and anthropogenic influence, *Journal of geophysical research*, 90(10), 463-410.
- Logan, J. A., and V. Kirchhoff (1986), Seasonal variations of tropospheric ozone at Natal, Brazil, *Journal of geophysical research*, 91, 7875-7881.
- Mann, H. B. (1945), Nonparametric tests against trend, *Econometrica: Journal of the Econometric Society*, 245-259.
- Moorthi, S., and M. Suarez (1992), Relaxed Arakawa-Schubert- A parameterization of moist convection for general circulation models, *Mon Weather Rev*, 120(6), 978-1002.
- Narita, D., P. Pochanart, J. Matsumoto, K. Someno, H. Tanimoto, J. Hirokawa, Y. Kajii, H. Akimoto, M. Nakao, and T. Katsuno (1999), Seasonal variation of carbon monoxide at remote sites in Japan, *Chemosphere-Global Change Science*, 1(1), 137-144.
- Ohara, T., H. Akimoto, J. Kurokawa, N. Horii, K. Yamaji, X. Yan, and T. Hayasaka (2007), An Asian emission inventory of anthropogenic emission sources for the period 1980? 2020, *Atmospheric Chemistry and Physics Discussions*, 7(3), 6843-6902.
- Olivier, J., and J. Berdowski (2001), Global emission sources and sinks.
- Owen, C. Boissard, and C. N. Hewitt (2001), Volatile organic compounds (vocs) emitted from 40 mediterranean plant species:: Voc speciation and extrapolation to habitat scale, *Atmos Environ*, 35(32), 5393-5409.
- Owen, O. Cooper, A. Stohl, and R. Honrath (2006), An analysis of the mechanisms of North American pollutant transport to the central North Atlantic lower free troposphere, *J. Geophys. Res*, 111, D23S58.
- Piccot, S. D., J. J. Watson, and J. W. Jones (1992), A global inventory of volatile organic compound emissions from anthropogenic sources, *Journal of geophysical research*, 97(D9), 9897-9912.
- Pickering, K. E., E. Bucsela, T. Huntemann, R. Cohen, A. Perring, J. Gleason, R. Blakeslee, D. Navarro, I. Segura, and A. Hernández (2009), Lightning NOx production during the NASA TC4 experiment as observed by Aura/OMI, paper presented at Fourth Conference on the Meteorological Applications of Lightning Data.
- Price, C., J. Penner, and M. Prather (1997), NOx from lightning 1. Global distribution based on lightning physics, *Journal of geophysical research*, 102(D5), 5929-5941.
- Pulles, T., M. van het Bolscher, R. Brand, and A. Visschedijk (2007), Assessment of global emissions from fuel combustion in the final decades of the 20th century, *TNO Rep. 2007-A-R0132B*.
- Ramana, M., and V. Ramanathan (2006), Abrupt transition from natural to anthropogenic aerosol radiative forcing: Observations at the ABC-Maldives Climate Observatory, *Journal of geophysical research*, 111(D20), D20207.

- Ramanathan, V., P. Crutzen, J. Kiehl, and D. Rosenfeld (2001), Aerosols, climate, and the hydrological cycle, *Science*, 294(5549), 2119-2124.
- Sandu, A., and R. Sander (2006), Technical note: Simulating chemical systems in Fortran90 and Matlab with the Kinetic PreProcessor KPP-2.1, *Atmos Chem Phys*, 6(1), 187-195.
- Seinfeld, J. H., and S. N. Pandis (1998), From air pollution to climate change, *Atmospheric Chemistry and Physics*, John Wiley & Sons, New York, 1326.
- Streets, Q. Zhang, L. Wang, K. He, J. Hao, Y. Wu, Y. Tang, and G. R. Carmichael (2006), Revisiting China's CO emissions after the Transport and Chemical Evolution over the Pacific (TRACE-P) mission: Synthesis of inventories, atmospheric modeling, and observations, *Journal of geophysical research*, 111(D14), D14306.
- Streets, T. Bond, G. Carmichael, S. Fernandes, Q. Fu, D. He, Z. Klimont, S. Nelson, N. Tsai, and M. Q. Wang (2003), An inventory of gaseous and primary aerosol emissions in Asia in the year 2000, *Journal of geophysical research*, 108(D21), 8809.
- Suthawaree, J., S. Kato, A. Takami, H. Kadena, M. Toguchi, K. Yogi, S. Hatakeyama, and Y. Kajii (2008), Observation of ozone and carbon monoxide at Cape Hedo, Japan: Seasonal variation and influence of long-range transport, *Atmos Environ*, 42(13), 2971-2981.
- Tiao, G. C., G. E. P. Box, and W. Hamming (1975), A statistical analysis of the Los Angeles ambient carbon monoxide data 1955–1972, *Japca J Air Waste Ma*, 25(11), 1129-1136.
- Val Martin, M., R. Honrath, R. Owen, G. Pfister, P. Fialho, and F. Barata (2006), Significant enhancements of nitrogen oxides, black carbon, and ozone in the North Atlantic lower free troposphere resulting from North American boreal wildfires, *J. Geophys. Res*, 111, D23S60.
- Van Der Werf, G. R., J. T. Randerson, L. Giglio, G. J. Collatz, P. S. Kasibhatla, and A. Arellano Jr (2006), Interannual variability of global biomass burning emissions from 1997 to 2004, *Atmospheric Chemistry and Physics Discussions*, 6(2), 3175-3226.
- Van Der Werf, G. R., J. T. Randerson, L. Giglio, G. Collatz, M. Mu, P. S. Kasibhatla, D. C. Morton, R. DeFries, Y. Jin, and T. T. van Leeuwen (2010), Global fire emissions and the contribution of deforestation, savanna, forest, agricultural, and peat fires (1997–2009), *Atmos. Chem. Phys*, 10(23), 11,707-711,735.
- Vinckier, C., F. Compernelle, A. Saleh, N. Van Hoof, and I. Van Hees (1998), Product yields of the alpha-pinene reaction with hydroxyl radicals and the implication on the global emission of trace compounds in the atmosphere, *Fresen Environ Bull*, 7(5-6), 361-368.
- Wang, D. Jacob, and J. Logan (1998), Global simulation of tropospheric O₃-NO_x-hydrocarbon chemistry. 3. Origin of tropospheric ozone and effects of nonmethane hydrocarbons, *J. Geophys. Res*, 156, 148-227.
- Wang, J. J. Corbett, and J. Firestone (2007), Improving spatial representation of global ship emissions inventories, *Environ Sci Technol*, 42(1), 193-199.
- Wu, N. E. Huang, S. R. Long, and C. K. Peng (2007a), On the trend, detrending, and variability of nonlinear and nonstationary time series, *Proceedings of the National Academy of Sciences*, 104(38), 14889-14894.

Wu, L. J. Mickley, D. J. Jacob, J. A. Logan, R. M. Yantosca, and D. Rind (2007b), Why are there large differences between models in global budgets of tropospheric ozone?, *Journal of geophysical research*, 112(D5), D05302.

Yang, Q., D. M. Cunnold, Y. Choi, Y. Wang, J. Nam, H. J. Wang, L. Froidevaux, A. M. Thompson, and P. Bhartia (2010), A study of tropospheric ozone column enhancements over North America using satellite data and a global chemical transport model, *J. Geophys. Res.*, 115(D08302), D08302.

Yevich, R., and J. A. Logan (2003), An assessment of biofuel use and burning of agricultural waste in the developing world, *Global Biogeochem Cy*, 17(4), 1095.

Yienger, J. J., M. J. Phadnis, S. K. Guttikunda, G. R. Carmichael, M. Galanter, T. A. Holloway, W. J. Moxim, and H. Levy (2000), The episodic nature of air pollution transport from Asia to North America, *Journal of geophysical research*, 105(D22), 26931-26945.

Zhang (2010), Intercontinental transport of air pollution, *Frontiers of Environmental Science & Engineering in China*, 4(1), 20-29.

Zhang, and N. A. McFarlane (1995), Sensitivity of climate simulations to the parameterization of cumulus convection in the Canadian Climate Centre general circulation model, *Atmosphere-Ocean*, 33(3), 407-446.

Zhang, D. G. Streets, G. R. Carmichael, K. He, H. Huo, A. Kannari, Z. Klimont, I. Park, S. Reddy, and J. Fu (2009), Asian emissions in 2006 for the NASA INTEX-B mission, *Atmos. Chem. Phys*, 9(14), 5131-5153.